Master Thesis

Indoor environment conditions and energy performance of a residential building constructed in SIP technology - computer simulations and measured parameters comparison.

Author
Adam Emil Swiniarski

Aalborg University
Idoor Environment and Energy Engineering

Department of Civil Engineering
Aalborg University
www.civil.aau.dk

AALBORG UNIVERSITY

Title:
Indoor environment conditions and energy performance of a residential building constructed in SIP technology - computer simulations and measured parameters comparison.

Theme:
Scientific Theme

Project Period:
Spring Semester 2018

Project Group:
Adam Emil Swiniarski

Participant(s):
Adam Emil Swiniarski

Supervisor(s):
Rasmus Lund Jensen

Copies: 4

Page Numbers: 138

Date of Completion:
June 7, 2018

Abstract:

The main topic of this project is an investigation of correlation between simulations and measurements regarding indoor environment in a house erected in sandwich panels technology. The building under the study is the Test House of DC-System Insulation A/S. The thesis was developed in cooperation with this company.

It includes detailed heat transfer calculations realised with use of COMSOL Multiphysics software with additional analyses of three-dimensional dynamic models (comparison with thermal imaging). Moreover, materials testing and weather conditions measurements have been conducted to provide precise input data for BSim simulations which are the core of this thesis. The values retrieved from the program have been confronted with evaluation of room temperatures and absolute water content inside the wall construction of the actual building. Lastly, input variations and sensitivity analysis of the computational model has been performed to identify the most influential parameters.

Department of Civil Engineering
Aalborg University
www.civil.aau.dk

AALBORG UNIVERSITY

Titel:
Indeklima og energiforbrug i en boligbygning bygget i SIP teknologi - sammenligning af målte parametre og computersimuleringer.

Tema:
Videnskabelig tema

Projektperiode:
Forårssemester 2018

Projektgruppe:
Adam Emil Swiniarski

Deltager(e):
Adam Emil Swiniarski

Vejleder(e):
Rasmus Lund Jensen

Oplagstal: 4

Sidetal: 138

Afleveringsdato:
June 7, 2018

Abstract:

Hovedemnet for dette projekt er en undersøgelse af korrelation mellem simuleringer og målinger af indeklimaet i et hus opført i sandwichpanelteknologi. Bygningen der undersøgelses er Prøve Huset i DC-System Insulation A / S. Afhandlingen er udviklet i samarbejde med dette firma.

Det indeholder detaljerede varmeoverførselsberegninger realiseret ved hjælp af COMSOL Multiphysics software med yderligere analyser af tredimensionelle dynamiske modeller (sammenligning med termisk billeddannelse). Derudover er der foretaget målinger af materialeegenskaber og vejrforhold for at give præcise inputdata til BSim-simuleringer, som er kernen i denne afhandling. De værdier, der hentes fra programmet, er blevet konfronteret med evaluering af rumtemperaturer og absolut vandindhold inde i selve bygningens vægkonstruktion. Endelig er inputvariationer og følsomhedsanalyser af beregningsmodellen blevet udført for at identificere de mest indflydelsesrige parametre.

Contents

Preface

This report has been developed as the master thesis by Adam Emil Swiniarski, student of the 4th semester of the Master's Degree in Indoor Environmental and Energy Engineering at Aalborg University.

I would like to thank DC-System Insulation A/S for the possibility of cooperating during this project. The support of the executives and engineers working at the company has been an immense help during this research. I would also like to thank my supervisor Rasmus Lund Jensen for his guidance in the course of the project.

Last but not least, I would like to thank my parents and my girlfriend for their support and understanding throughout my higher education.

Reading guide

In this report the references are listed through the Harvard-method. The source is noted in square parentheses, wherein the author's surname and the publication date is listed, e.g. [Hyldgaard et al., 1997]. When the author of a publication is a company and not a person, said company will be listed. The reference is placed before the full stop when it refers to the sentence. If the reference is placed after the full stop, it refers to the paragraph. The bibliography is found in the back of the report along with the sources listed in alphabetical order. In the bibliography the remainder of information about the source is listed, such as whether the source is a book, pdf-file, webpage, etc. References to figures and tables occur are made through numerical order in occurrence with the chapter number and placement within the chapter. For example, the first illustration in chapter one is named Figure 1.1, the next illustration Figure 1.2, etc. All figures and tables are provided with explanatory captions; they are placed below the figures and above the tables.

Aalborg University, June 7, 2018

Adam Emil Swiniarski
<aswini16@student.aau.dk>

Chapter 1

Introduction

1.1 Legal basis

This master thesis in Indoor Environment and Energy Engineering at Aalborg University has been developed in cooperation with DC-System Insulation A/S located in Aars, Denmark. The main focus point of this dissertation is the investigation of simulated indoor conditions and energy consumption convergence with real-world, measured values in the DC-System Test House building constructed with load-bearing structural sandwich panels. The project was executed in the final semester of the programme from February 2018 to June 2018 by student Adam Emil Swiniarski.

1.2 Company profile

For more than four decades, DC-System has produced polyurethane insulation panels for national and international markets. Today, the company is considered a world leader in insulation panel production. DC panels are often used in cold storages, freezer storages and food production rooms, but are also suitable for use in livestock buildings, façades, freezing cabinets and ship building. DC Thermopanels are not only ideal for all types of new developments but also for energy renovations in existing buildings. [...] The sandwich panels are CE-certified according to EU standard EN 14509 and have an U-value for efficient control of internal temperatures in buildings equipped with DC-System insulation panels. Approx. 75% of all DC-System panels are exported. Furthermore, the company exports complete cooling solutions for a variety of building types.

DC-System is a global company with production facilities in Denmark and Spain as well as a regional office in Cuba and currently employs 50 people. DC-System is a member of the following organisations: Inno BYG, the Confederation of Danish Industry, the Danish Plastics Federation and the EIB's AAA rating scheme. **[DC-System website (2018)]**

The core areas of the company are cooling and freezing rooms, industry, agriculture and turnkey projects. It provides holistic approach towards projects, offering expertise at all stages of the project - from initial design, through planning and manufacturing to erection and supervision of the construction sites. Its supply does not only include the structural insulated elements but also steel structures, doors, gates, windows, etc. for completing the total project after the foundations have been laid.

1.3 Sandwich panels technology

Sandwich panel is any structure made of at least three layers - external skin layer(s), internal skin layer(s) and a low-density core between them. Sandwich panels are used in applications where a combination of high structural rigidity and low weight is required.

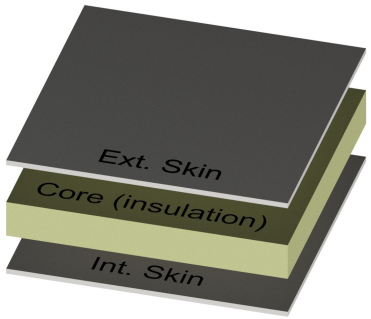

Figure 1.1: The principle of sandwich panels

The given type of sandwich panels is also called Structural Insulated Panel (or SIP for short). SIP is a form of sandwich panel used in the construction industry. Structural insulated panels are often made of skin elements which sandwich a foam core from both sides. The materials used both for the core and skin layers vary and can be applied in many different combinations.

- The most common core materials are: expanded polystyrene (EPS), extruded polystyrene (XPS), polyurethane foam (PUR), mineral wool.
- The most common skin materials are: OSB board, plywood or pressure-treated plywood, steel, aluminum, cement board, stainless steel

The application of structural insulated panels in the building covers the majority of construction elements including floors, main (load-bearing) walls, partition and façade walls, cooling rooms walls, ceilings, façades, and roofs. The limitations and design solutions for sandwich panels depend on their location in the structure, purpose, thermal and sound insulation requirements, acting forces, fire safety, kind of environment (the risk of corrosion, sterility requirements etc.).

1.3.1 Advantages and disadvantages of sandwich panels

As every type of material used in the building industry SIP elements can be preferable in one kind of constructions but their application might prove to be troublesome in others. Here a brief list of the main pros and cons regarding use of sandwich panels has been presented with an indication of possible preferences or limitations.

SIPs advantages

- Mobility and efficiency - SIP is a material that allows disassembling the elements and erecting them somewhere else if designed properly. At the same time, thanks to the light weight, transportation could be relatively cheap and fast. What is more, an increase in the useful area of the building is possible due to the significant decrease in thickness of walls and partitions using SIP technology.

- Erection time - Quick erection is possible as a result of high-quality prefabrication of the elements which are designed and prepared to be mounted in the specific construction. Lightness of the panels and special lifting systems are also beneficial from the efficiency point of view. Furthermore, the application of pre manufactured locks and connection solutions results in easier and quicker erection comparing with for example traditional brick wall. The elements can be delivered all at the same time form one supplier and installed in just couple of days.

- Hygiene - Thanks to application of sterile skin layers such as stainless steel, SIP elements can easily meet the sanitary and environmental standards. The panel construction excludes the appearance of fungus or mould, and panel materials are not attractive to rodents. Sandwich panels cladding perfectly carries detergent treatment. As a result, an increasing number of food and medicine storage cooling rooms realised in SIP technology can be observed.

- Thermal and acoustic insulation - Sandwich panels by definition consist mainly of low-density core material which acts as a thermal and sound insulation. Especially aspect of low U-value can be attractive for the building owner since it can drastically contribute to lower energy demand and reduce operation costs of the building. Moreover, thanks to the simplicity of the installation process and detailed design, the risk of thermal bridges or other unwanted thermal breaks is reduced comparing with the traditional insulation solutions.

- Air tightness - Due to lack of great amount of connections (like in brick or block walls) the number of possible air tightness breaks in the buildings is drastically reduced. Tightness of panels connections can be easily provided by application of special locks, insulation and cladding overlapping or sealants. On top of that, SIP elements grant constant insulation around a building which all in all makes structures realised in SIP technology extremely airtight.

- Pre manufactured elements - If an element is designed, produced and delivered by the producer to the construction site properly, correct parameters of the building part are easier to ensure. Comparing with traditional erection methods, where there are many different elements that need to be produced, stored and mounted correctly to achieve success, SIP technology ensures less potential mistakes that can be made during the erection process.

- Environmental impact (recycling of sandwich panels) - SIP elements are sometimes used in temporary small structures. Providing that specific prerequisites are taken during design and erection precesses, re-installation of the elements is possible. Moreover, even in the end of panel's life cycle, there are some ways of a green disposal or recycling. There are two main possibilities for PU/PIR core which is the essential component of many structural insulated panels - mechanical and chemical recycling. The former comprise material regrind, powdering, or compression moulding, whereas the latter includes use of chemical reactions (hydrolysis, pyrolysis, and glycolysis) to get oil that can be mixed with virgin material to create another polyurethane products.

SIPs considerations

- Fire - One of the major concerns surrounding structural insulated panels is fire safety. Depending on the type of the building, there are different requirements for SIP elements to withstand in case of fire (R- load carrying capacity, E - integrity, I - insulation). This yields a great amount of prerequisites during the design process. The main focus point should be the skin layers of SIP element and panels connection. Reaction to fire certification needs to be performed as even for residential building the requirement for RE parameters is 15 minutes according to [**Bygningsreglementet (2015)**].

- Ventilation - As a result of extreme air tightness (resulting in very low infiltration), buildings constructed in accordance with SIP technology require good mechanical ventilation systems (only small residential buildings can be ventilated naturally).

- Prior prerequisites and know-how - Manufacturers use advanced tools to cut the panels according to the CAD drawings. Nevertheless, it is important to control quality and to minimize waste as SIP elements need to be designed, manufactured and installed precisely in a specific structure. It requires collaboration and an accuracy from building owners, designers or architects, engineers, manufacturers, and contractors. The panels have to be cut to specific sizes and pre-drilled for electric wiring and plumbing, and have to consider doors, windows and other architectural features. One of the advantages - short erection time generates the necessity of heavier workload in the initial project stage. Furthermore, since SIP technology is not as well-known as others commonly used, many builders and their workforce are not familiar with SIP construction. Thus an expertise of the manufacturer or engineers involved in the project might be indispensable at construction sites.

1.4 Test House

1.4.1 General information

The DC-System Test House is a 115 m^2 single-detached dwelling building with a roof terrace, shed and a driveway. It consists almost entirely of load-bearing sandwich panels (285m^2 of DC Thermopanels) and was designed to fulfil energy class 2020 requirements. Its construction was completed in only 7 days in the beginning of 2016. The house is located in Aars, Denmark, next to the headquarters of DC-System on Nordvestvej 8. The building is not inhabited and used only on occasions of conferences and presentations for visitors. The general principle of the project combines the function of a showroom for potential clients with a full-size sample of the company's capabilities in sandwich panels design, manufacturing and construction. Furthermore, the presence of the building has significantly contributed to better understanding of sandwich-panels-constructed building properties (including structural, energy and environmental aspects). Worth mentioning is also the fact that Aalborg University has been cooperating with the company from the very initial design stage up to present when this master thesis project was executed.

1.4.2 Location and geometry

The building is orientated in north-south axis with 24° deviation towards east (from north direction) - see figure 1.2. Its surroundings can be considered as open flat country with no trees or other buildings (apart from the manufacturing facility in the east - see figure 2.7) obstructing the view, solar operation or other external conditions.

The house consists of 2 levels (each of approximately 2.5m in net height) with the total height of 6.14m. There are 4 closed rooms on the ground floor which are accessible from the common foyer (where the main entrance is located). The foyer leads also to the staircase connecting the two levels. The first floor comprises mainly of the big open space of the conference room. There is also a kitchen and doors to the open-air terrace. In front of the main entrance there is a driveway covered by the 1st floor of the building. The shed is a separate space that has no direct connection with other rooms. Apart from the conference room the building is not furnished and remains closed for the majority of time being.

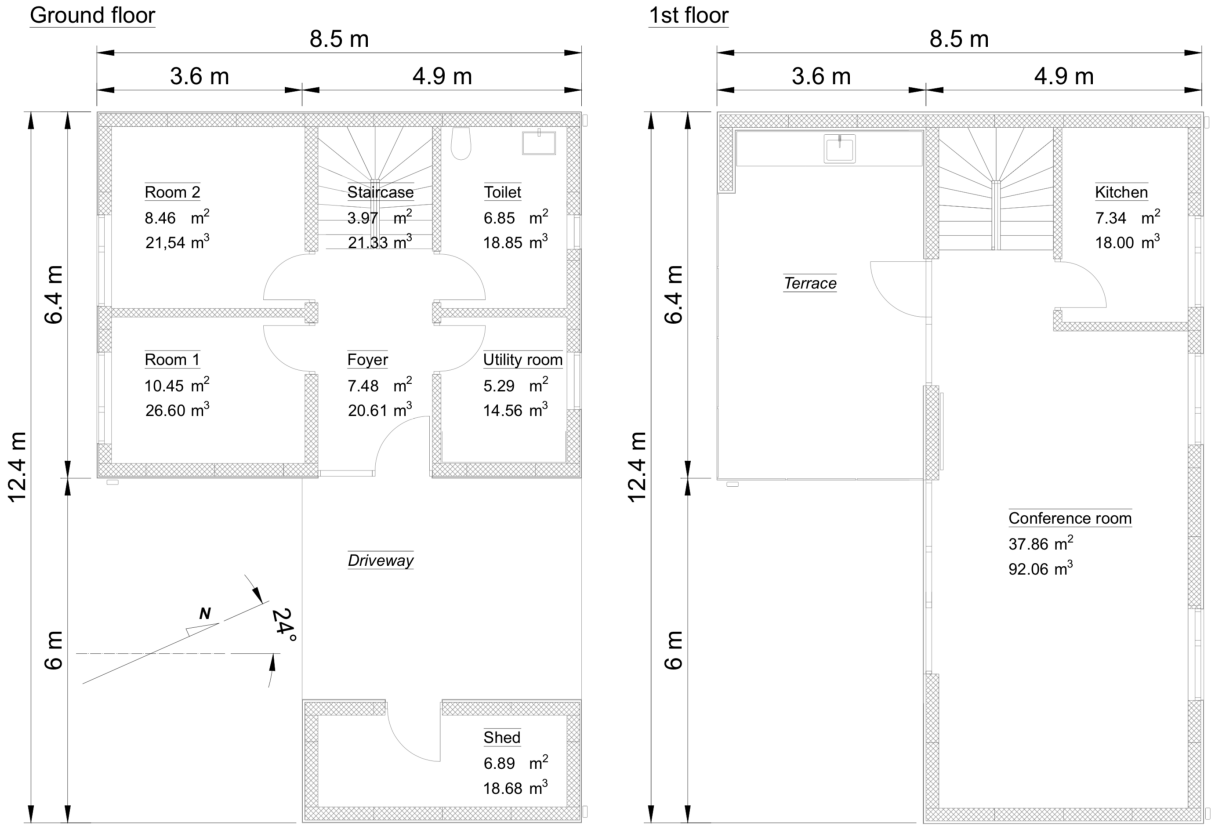

Figure 1.2: Test house floor plans - net floor areas and net room volumes.

More drawings of the building have been presented in appendix A. Placement of the windows together with their size and properties can be found in the same section.

1.4.3 Materials

Since the basic principle of the building was to demonstrate the wide range of sandwich panels application, most of its structure is made of those composite elements. This includes partition walls, ground floor, and parts of the roof and slab structures. Due to structural restrictions and limitations, in some places of long slab/roof span, metal C-profiles were used to provide high rigidity construction. DC Thermopanels (225 mm) have been used in the highest proportion of all sandwich elements in the house. They consist of the polyurethane core in-between two fibre-cement boards from both sides. Another variation of this element (DC Thermopanel - Roof Panel) with additional steel sheet in the bottom (structural reinforcement) has been used in roof and slab. DC-Panel Type EI30 has been used in carport slab (over the driveway). All properties of these elements can be found in the producers' catalogue. More detailed breakdown of building elements will be presented in the following pages of this report in the section devoted to BSim computational model (see section 2.5.2 and appendix D).

1.4.4 Technologies

One of the most important DC-System's trademarks is the tongue and groove connection with cast-in cam locks. This solution combined with application of sealant delivers highly resistant and airtight joint. Furthermore, all other connections are designed not only to transfer loads but also prevent any sort of leakages and cold bridges (construction details in A.2). Thanks to that, the result of blower door test in accordance with DS/EN 13829 gave very low infiltration rate of $q_{50} = 0,066$ L/s/m^2 [**AAU Klimalab (2016)**] ($q_{50,max} = 0,5$ L/s/m^2 according to BK20 [**Bygningsreglementet (2018)**]).

The envelope of the building is compatible with additional structural elements such as wooden beams embedded in the external wall panels to support roof construction. This solution does not cause thermal breaks or influence tightness of the building. However, since wood is an organic material prone to mould, pests and other type of biocorrosion, special precautions including proper moisture isolation should be executed. One of the investigations in this report includes moisture content of the wooden beam (2.3.2).

1.4.5 Systems

Due to the fact that the house is not inhabited and is in fact used only in short time periods (1 to 3 hours) once or twice per month, there is no need for complex systems in the building. Furthermore, there is no access to any sort of district heating in the house vicinity since it is not residential area of the town. As a result the Test House has been equipped with 0.4kW electric heaters with thermostat range from 15 to 28°C. They have been installed one in each room (apart from the staircase) and two of them in the conference room due to its large floor area.

The domestic hot water is provided by an electrical boiler located in the toilet and distributed also to the kitchen upstairs.

Most of the lighting in the building is controlled automatically by infrared sensors located in the lamps.

Figure 1.3: DC Thermopanels wall with glued laminated timber beam. [**DC-System catalogue (2018)**]

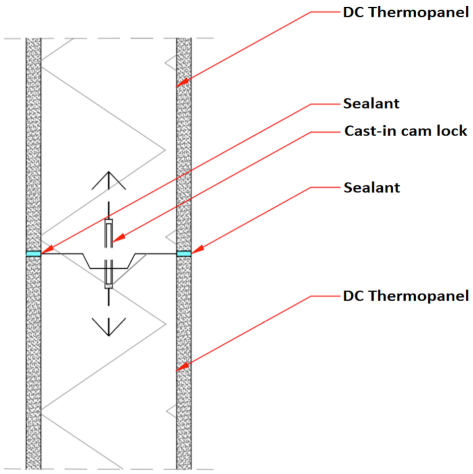

Figure 1.4: Typical wall panels joint with sealants and cast-in cam lock. [**DC-System catalogue (2018)**]

There is no shading system installed in the house (apart from the matte glazing in the toilet window) and there are not any adjustable internal shading elements such as curtains or window blinds.

Natural ventilation can be executed by the use of manually operated vents mounted in most of the windows. Moreover, apart from three windows on the southern facade on the first floor (conference room), all the others are openable with possibility of tilting or fully opening. Thanks to the building's layout (open foyer connected with the staircase and the conference room), buoyancy-driven natural ventilation can be implemented.

Lastly, two data loggers and a desktop PC (which record signals from all the temperature and humidity sensors installed in the house as well as energy consumption from the electrical pulse meters) are located in the utility room on the first floor. What is worth mentioning, they work non-stop which produces substantial amounts of heat in this small, closed space.

Chapter 2

Methods

In this chapter tools and techniques leading to the execution of the experiments, measurements, and simulations will be presented. The sections should be regarded either as source of input data for computational models (for example Weather station setup and Materials testing sections) or measured values to be compared with those models (Test house measurements setup and Thermal imaging sections). Furthermore, an introduction to the input variations will be performed to indicate possible methods of models' sensitivity investigation. Thereby, the chapter illustrates the full scope of actions to be taken to achieve results for analyses.

2.1 Materials testing

The purpose of this stage is to obtain precise input data regarding materials properties for the indoor climate, energy consumption, and heat transfer simulations. Parameters have been chosen according to the nature of the calculations, boundary conditions, and the type of software used. They cover not only heat transfer aspects of the structure elements but also moisture transport in the materials. However, not all of the materials used in the construction of the house under the study have been tested. Due to the time limitation and lack of some of the samples or difficulty to test some of the materials the following plan of measurements has been applied.

Thermal properties

The thermal measurements are deemed to be the core of the entire materials testing stage. Materials present in the main structure as well in the partitions of the building were tested with high precision. However, some other parts were excluded from the measurements.

External façade elements have been disregarded as it has been decided that they do not influence thermal insulation as the façade plasterboards are mounted on the steel substructure with strongly ventilated air gap in between (no air-tightness).

Due to the little share in the construction and difficulty to prepare required samples, sealants were disregarded and modelled as PUR foam in the simulations.

Bitumen felt on the roof has been disregarded due to its low thickness and difficulty to test thermal properties. Its impact on the thermal performance of the building is expected to be negligible. Nevertheless, it was modelled in the simulations as a black layer to account for the high heat absorption of this element.

Moisture properties

Materials located inwards from the PUR foam core of the external walls and other partitions were tested since the foam is regarded as quasi-barrier for moisture transport, thus examination of the external elements is deemed to be redundant.

2.1.1 Thermal conductivity

Theoretical background

Thermal conductivity (often denoted k, λ, or κ) is the property of a material describing its ability to conduct heat. It is expressed in (W/mK) unit, indicating how much energy (heat) is conducted through 1m thick material sample under 1K of temperature difference between its two surfaces. It is the primary property used in building thermal analysis - to calculate thermal resistance and thermal transmittance of construction's elements.

Applied tool

The measurements have been realised with use of *λ-Meter EP500* by *Lambda-Meßtechnik GmbH*. This tool consists of two parallel plates between which the test specimen is to be placed. The device measures precisely the thickness d of the sample at given pressure and then applies set temperatures for the upper and lower plates creating temperature difference dT. It is critical to measure the area A of the sample's surface accurately. As a result of the experiment input and measured value of the energy Q used to set maintain the temperatures of top and bottom surfaces of the sample, the thermal conductivity can be calculated from formula 2.1.

$$\lambda = \frac{Q \cdot d}{dT \cdot A} \tag{2.1}$$

Key specification

- Measuring range from λ=0.002 W/mK to λ=3 W/mK;
- Temperature range from -10°C to 50°C with 1°C increment;
- Temperature resolution 1mK, thickness resolution 0.1mm;
- Measurements at predefined test pressure from 50 to 2500 Pa;
- Sample size 500mm x 500mm or smaller.

Experiment presets

Each sample has been examined at three different temperatures to obtain more data points for analysis. Duration of the experiment varied between tested materials due to their thickness and structural layout from 200 to 3500 minutes. Experiment presets were defined as follows:

- Plate pressure 500 Pa for hard and 2500 Pa for soft materials;
- Test temperatures of 40°C, 25°C, and 10°C with 15°C between plates at each test;
- Stability criteria - maximum lambda fluctuation of 0.5% over 200 minutes.

The device is used, maintained, and periodically calibrated by the Indoor Climate laboratory of Aalborg University personnel as stated in the producer's technical manual. The measurements have been conducted in accordance with *Thermal Conductivity Measurement with the Guarded Hot Plate Apparatus, Step by Step Guide* **[Johra, Hicham (2015)]**.

2.1.2 Thermal diffusivity and specific heat

Theoretical background

Thermal diffusivity α (mm^2/s) is a measure of thermal inertia of a material. It gives an insight of how fast heat is propagated through the medium. The flash method was primarily developed to measure this value. Figure 2.1 shows the principle of how α is determined. The front side of the investigated material sample is heated up by a high intensity, short duration light (laser) pulse. The resulting change of temperature with time on the back side of the sample is recorded by an infrared camera. A typical curve of temperature rise vs. time is shown on figure 2.2. A mathematical analysis of this graph allows for the determination of the thermal diffusivity. For ideal, adiabatic conditions, the thermal diffusivity is described by equation2.2.

$$\alpha = \frac{0.1388 \cdot l}{t_{50}} \tag{2.2}$$

Where l is the thickness of the sample and t_{50} is the time in which the temperature rise on the back side of the sample reaches half of its maximum value (see figure 2.2).

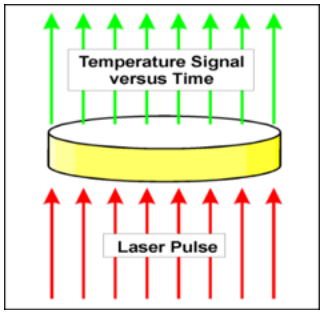

Figure 2.1: Principle of the laser flash method.

[Zajas, Jan; Heiselberg, Per (2013)]

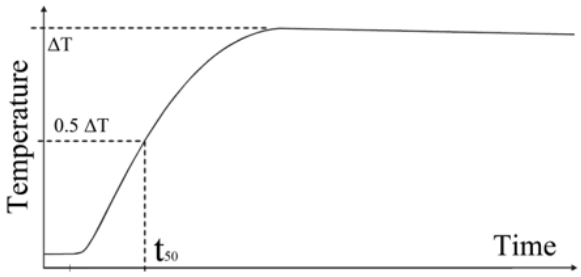

Figure 2.2: Typical curve of temperature vs. time.

[Zajas, Jan; Heiselberg, Per (2013)]

Equation 2.2 is only valid if adiabatic conditions are achieved, i.e. no heat loss from the sample occurs during the measurement. Such assumption can be made when the measured sample is very thin and has a large thermal diffusivity. In that case the measurement duration is very short (approximately 100 milliseconds) and the heat losses can be neglected. In most cases however, the measurement will last much longer and a correction for heat losses from the sample needs to be included. Various mathematical models exist that are capable of estimating that effect and are included in the analysis software. Another assumption made in equation 2.2 is that the duration of the heat pulse is negligibly short in comparison to the heat diffusion time. If that is not the case, this effect should also be accounted for, with the use of another mathematical model.

Specific heat can be obtained by a comparative method, where two samples are measured subsequently under the same conditions: a test sample under investigation, and a reference sample with previously determined properties. By comparing the maximum temperatures obtained on both of the samples and their respective properties the c_p of the test sample can be calculated:

$$c_p^{test} = \frac{T_{max}^{ref}}{T_{max}^{test}} \cdot \frac{(\rho \cdot l)^{ref}}{(\rho \cdot l)^{test}} \cdot c_p^{ref} \tag{2.3}$$

Where T_{max} is the maximum temperature recorded on a sample, ρ is the density and the superscripts ref and test refer to the reference sample and the test sample respectively.

Having determined the thermal diffusivity and the specific heat capacity, it is possible to derive the thermal conductivity of the samples (equation 2.4). [**Zajas, Jan; Heiselberg, Per (2013)**]

$$\lambda = \alpha \cdot c_p \cdot \rho \tag{2.4}$$

Applied tool

The *LFA 447* by *Netzsch Geratebau GmbH* is shown in the figure below. The sample changer, which can hold up to 4 samples, is located in the middle of the apparatus. The heat source, which in this case is a xenon lamp, is placed underneath. The infrared detector is located above the sample changer. The temperature in the sample holder is controlled by a furnace and can be set between the room temperature and 300°C. To prevent the overheating of IR detector, it needs to be cooled down with liquid nitrogen, which should be supplied into the tank located above it.

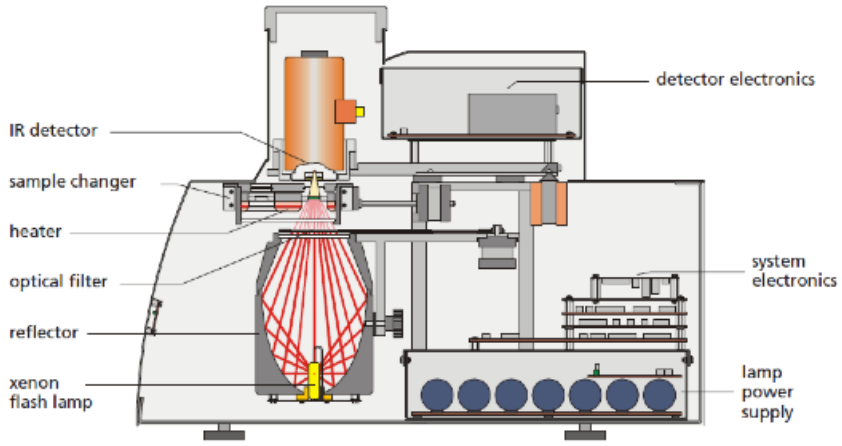

Figure 2.3: Overview of the LFA 447 apparatus [**Netzsch Geratebau GmbH (2001)**]

The sample holders used in the apparatus are suitable for round samples with 12.7 mm diameter. The thickness of the samples can be in the range of 1 - 3 mm. It is however strongly recommended that the test sample has the same thickness as reference samples (2 mm). If both samples are not of the same thickness, it is important to maintain the same distance between surfaces of the samples and the IR detector. [...] The reference samples provided with

the instrument are: Pyroceram, Pyrex, Alumina and Graphite. Their properties can be found in the device manual. When choosing the reference sample it is important to select one that has similar diffusion time as the test sample so that the heat losses during the measurement time, i.e. by radiation from the specimen surface or by lateral heat flow, are comparable in both cases. The samples need to be coated with graphite spray. The procedure is explained in the device manual. [**Zajas, Jan; Heiselberg, Per (2013)**]

Key specification

- Standard sample size up to 25.4 mm (1“) diameter, or 6 mm / 8 mm / 10 mm / 12.7 mm square, up to 3 mm (0.12“) thick;
- Temperature range - ambient to 300°C;
- Thermal diffusivity range from 0.01 mm^2/s to 1000 mm^2/s;
- Thermal conductivity range from 0.1 W/(m·K) to 2000 W/(m·K);
- Accuracy - Thermal Diffusivity ±2%, Specific Heat ±3%.

Experiment presets

Two samples of each material have been formed in circular shape of 12.7 mm in diameter and 2mm in thickness. All measurements were conducted with Pyrex reference sample as its thermal diffusivity is closest to all of the test samples (see table 2.1).

Table 2.1: Properties of the reference samples at the temperature of 25°C. [**Netzsch Geratebau GmbH (2001)**]

Reference sample	Thickness (mm)	Diameter (mm)	Density (kg/m3)	alfa (mm2/s)	C_p (J/g/K)	lambda (W/mK)
Pyroceram	1.990	12.65	2600	1.926	0.800	4.009
Pyrex	1.992	12.67	2210	0.650	0.761	1.098
Alumina	1.994	12.69	3860	10.230	0.775	30.920
Graphite	1.964	12.68	1740	76.200	0.700	91.700

Measurements have been taken at three stages (temperatures): 20°C, 25°C, 30°C. Three pulses ("shots") were performed at each stage. Materials density used as input for this experiment was calculated as average of ρ from Hot Plate tests (SARTORIUS GP3202 Toploading Balance laboratory scale and ruler were used) since size and weight of that samples yielded lower inaccuracy than estimation of density of ϕ12.7x2.0mm sample which weights ±0.50 g. After obtaining the data, Cowan + pulse correction recalculation model was used for all materials.

The device is used, maintained, and periodically calibrated by the Indoor Climate laboratory of Aalborg University personnel as stated in the producer's technical manual. The measurements have been conducted in accordance with *Thermal Conductivity Measurement with the Laser Flash Method, Step by Step Guide* [**Johra, Hicham (2015)**].

2.1.3 Water content

Theoretical background

The water content of a material can be described by e.g. water to dry mass ratio, the water content per m^3, the capilary degree of saturation, and the vacuum degree of saturation. The ratio (u) is determined by weighing a material sample (m_1 kg) and drying at 105°C until the mass is constant (m_2 kg). u can be calculated as:

$$u = \frac{m_1 - m_2}{m_2} \tag{2.5}$$

In air with a certain relative humidity and temperature a porous building material after a while will reach a state of equilibrium with the environment, i.e. the partial vapour pressure and the temperature of the water vapour in the pores of the material will be quite the same as in ambient air. The porous material will exchange water with the ambient air until the point of equilibrium is reached. [...] Equilibrium established during drying gives a desorption isotherm, and equilibrium established during wetting gives adsorption isotherm. Two boundary curves show a hysteresis loop. The desorption isotherm always lies above the adsorption isotherm at the same temperature. **[Hansen, Kurt Kielsgaard (1986)]**

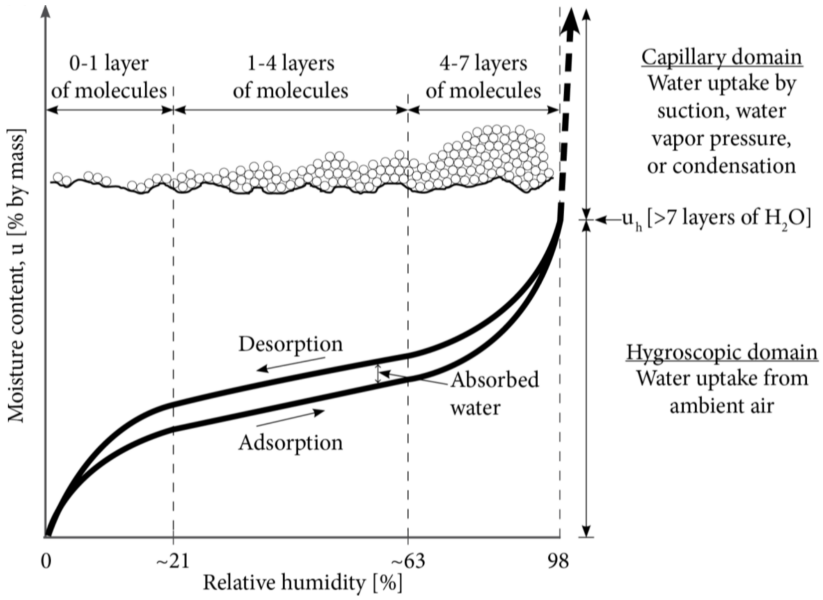

Figure 2.4: Typical adsorption and desorption isotherms showing hysteresis **[Ivanov Antonov, Yovko (2018)]**

Applied tool

For the water content measurements in this project, the *Vapor Sorpion Analyzer* by *Decagon Devices, Inc.* has been used. The device has the possibility of performing two different methods:

- Dynamic Vapor Sorption (DVS) - generates equilibrium isotherms. Equilibrium between sample weight and relative humidity is assumed when the weight of the sample under given water activity (relative humidity) stops changing.

- Dynamic Dew point Isotherm (DDI) - generates dynamic isotherms. This method directly measures water activity while gravimetrically tracking weight, so there is no dependence on equilibration to known water activity levels to determine water content. Adsorption occurs as saturated wet air passes over the sample. Desorption happens as desiccated air passes over the sample. After a short period of time, the VSA halts airflow and takes a snapshot of the sorption process by directly measuring the water activity and weight. [**Decagon Devices, Inc. (2016)**]

During the experiment the sample is placed in a stainless steel cup in a sealed chamber where relative humidity and sample weight are precisely recorded throughout the process (by the optical sensor and weighing pan respectively). Uniform air distribution is provided by a fan in the top of the testing chamber. The air flowing through the capacitance filter is pre-wetted with water stored in the water tank or pre-dried in the desiccant cartridges. The device should be placed on a flat, leveled surface and protected from any vibrations.

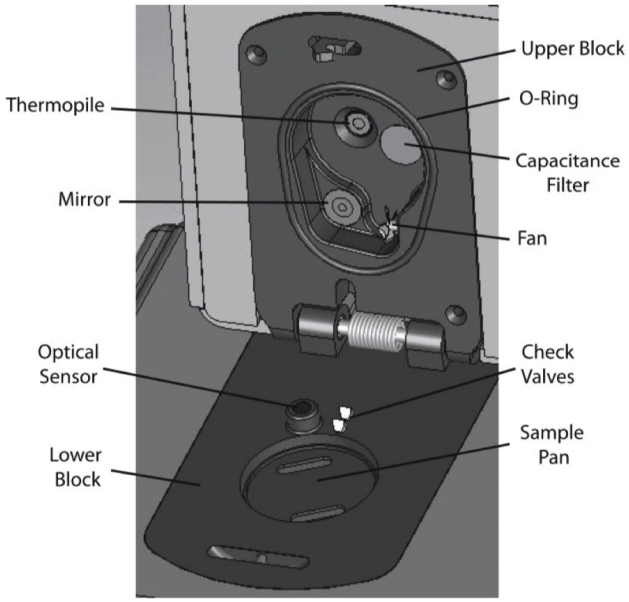

Figure 2.5: Testing chamber breakdown [**Decagon Devices, Inc. (2016)**]

Key specification

- Temperature operating range from 15 to 40°C;
- Humidity operating range 3.5-93%;
- Sample weight range 500-5000 mg;
- Sample cup volume 10 cc;
- Weight accuracy $\pm$ 0.1 mg.

Experiment presets

The most significant advantage of the DDI method is increased analysis speed which proved to be the decisive factor in method choice for this project. Nevertheless, the experiment preset has been specified according to [**DS/EN ISO 12571 (2013)**], meaning that:

- The drying process has been done with use of a drying oven (in 105°C), in accordance with ISO 12571;
- Adsorption and desorption curves have been made of at least four measurements points each, in evenly spread relative humidity intervals;
- The starting point for desorption curve has been relative humidity of 93% (95% recommended by the standard exceeds device's capabilities);
- The experiment has been conducted at constant temperature of 23°C $\pm$ 0.5°C.
- Relative humidity resolution has been set to 7%;

The device is used, maintained, and periodically calibrated by the Indoor Climate laboratory of Aalborg University personnel as stated in the producer's technical manual. The measurements have been conducted in accordance with user's guide and [**DS/EN ISO 12571 (2013)**].

2.2 Weather station

2.2.1 Setup

A set of sensors together with data loggers and computers storing the weather data (called weather station later in the report) were installed to gather information needed as an input for the dynamic simulations of indoor environment and energy consumption in BSim software. Measured values have been also used as boundary conditions for thermal simulations in COMSOL Multiphysics program.

The following external environment conditions have been registered:

- Air temperature at 2m height (PT100 sensor protected from direct solar radiation and moisture in an "English cage");
- Wind speed and direction (FT702 ultrasonic anemometer placed on a mast at 10m height oriented towards north);
- Direct and diffuse solar radiation (SPN1 and CMP22 pyranometers placed on the roof of the factory building at height of approximately 7m with unobstructed view towards sun).
- Relative humidity of air (Honeywell HIH4000 sensor placed also at 2m height in the "English cage");

2.2.2 Location

The weather station was located in Aars, Denmark, next to the manufacturing facility of DC-System just few meters away from the Test House (see figure 2.7). This position combined precision of collected data (measurements were gathered in the vicinity of the building under the study) and did not have any impact on the indoor environment and tightness of the house (no additional devices were placed in the house and the envelope was not punctured by wholes for wiring).

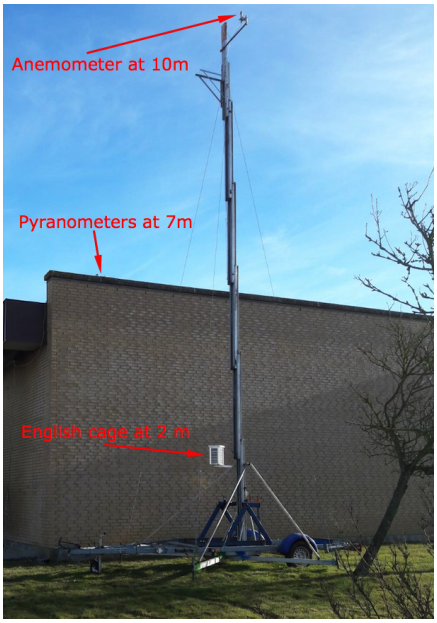

Figure 2.6: The weather station mast.

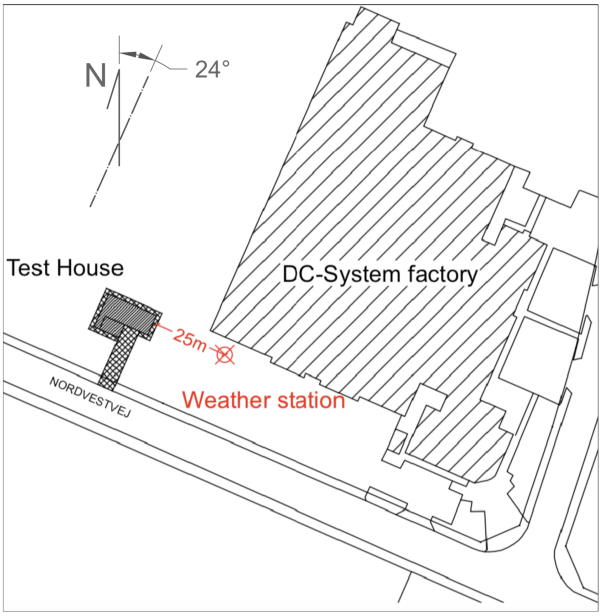

Figure 2.7: The weather station location.

2.2.3 Calibration

Used sensors and data loggers are maintained, and periodically calibrated by the personnel of Indoor Climate laboratory. Nevertheless, due to the natural wear of the devices and their unique properties and imperfections, instruments should be calibrated in the given sensor-data logger setup. It is critical especially for sensors with low voltage output since the impact of the noise on the results can be significant. The main goal of the calibration phase is to obtain recalculation (conversion) formula to translate voltage output of a sensor recorded by a data logger into actual values describing given phenomena i.e. air temperature expressed in Celsius degrees or wind speed in metres per second. Manuals and technical reports were used to calibrate the devices. The procedures have been presented in appendices B.1, B.2, B.3.

2.2.4 Data logging

Sensors outputs were registered by the following dataloggers:

- Fluke Helios Plus 2287A – for sensors with very low and medium voltage output (Helios measuring range $\pm$ 64mV to $\pm$ 64V) and logging interval of 60 seconds: SPN1, CMP22, HIH4000;
- National Instruments USB-6009 – for a sensor with voltage output of 0-3.6V and frequency of 10Hz: FT702 ultrasonic anemometer;
- National Instruments cDAQ-9174 – for resistance sensor with logging interval of 60 seconds: PT100.

Additionally, each datalogger was connected to a different computer to reduce risk of all measurements loss due to hard drive, operating memory, and CPU capacity shortage or other technical malfunctions. The full scheme of the sensors, dataloggers, and computers arrangement has been illustrated in B.3.

2.2.5 Measurements

Weather conditions have been recorded over the same time as the measurements in the Test House took place (see the phases of the experiment in 2.3). Voltage outputs from the sensors were converted into actual values of the given parameters using formulas obtained in the calibration stage. Unfortunately, due to malfunction of the humidity sensor and incorrectly recorded solar data (LabView script ignored decimals and rounded all the values), these parameters for the phase 2 of the experiment were taken from internet weather archive [**meteoblue.com (2018)**]. Validation of the webpage data has been presented in appendix B.5.

Gathered information has been post processed by use of moving average to obtain input expressed hourly over the period under the study. Then the log files were combined and transformed into BSim weather file. As a result, the software has performed calculations based on the actual external environment conditions for the given period (see appendix E).

2.3 Test House measurements

The experiment can be divided into two main phases (1 and 2) which were conducted from 23.04.18 (08:00) to 30.04.18 (08:00) and from 01.05.18 (23:00) to 08.05.18 (17:30), respectively.

- Phase 1 - No heating, temperatures in the house are being recorded. The aim of this stage is to investigate the correlation between simulated air temperature distribution in the house with values measured in the actual building. During this phase, the structure is exposed only to the external conditions variation which influence internal climate. Influence of the heat capacity and thermal inertia are tested. This stage can be also used as validation of the geometry and materials input of the computational models.
- Phase 2 - Heating is turned on, the energy consumption is being recorded. The aim of this stage is to investigate the correlation between dynamic energy consumption simulations and values measured in the actual building. During this phase heating setpoint is fixed at one value and electric energy is used to maintain the given temperature. Influence of the thermal insulation and airtightness are tested. This stage can be also used as additional validation of the systems settings of the computational models.

Moreover, a set of sensors has been mounted inside one of the external walls of the building to investigate the temperature and humidity gradient (and their product - absolute water content) across the envelope (see 2.3.2). This experiment is meant to demonstrate the material properties of the building elements. It has been also used to illustrate correlation between moisture and heat transport calculations with the actual measurements inside the wall.

2.3.1 Experiment presets

- During the experiments, the house was closed for any admittance with all windows and doors locked.
- Windows and glass doors remained unshaded with unobstructed view towards outside.
- No ventilation (either natural or mechanical) was applied during the experiment. The window vents remained closed.

- Lighting was turned off, however domestic hot water boiler tank (in the toilet), a fridge (in the kitchen) and a desktop computer with 2 data loggers (in the utility room) were working during the experiment which might have impact on the temperature distribution.
- During the second phase of the experiment heating setpoint has been fixed at 20°C in each room. The maximum power of each electric radiator is 0.4 kW.

2.3.2 Measuring setup

The measuring setup present in the test house can be divided into three separate systems. The most extensive one is the set of Pt-100 sensors located in the building. There is 1 temperature sensor in each room, 2 temperature sensors in the conference room on the 1st floor, and 7 sensors in the staircase to calculate the vertical temperature gradient (figure 2.10). Their precise locations have been indicated in the figure 2.8. Measured temperatures are recorded by National Instruments NI cDAQ-9174 data logger and can be accessed by the LabView program. The sensors are protected from direct solar radiation and minor mechanical damages by plastic spheres which cover the entire fragile probe (figure 2.9).

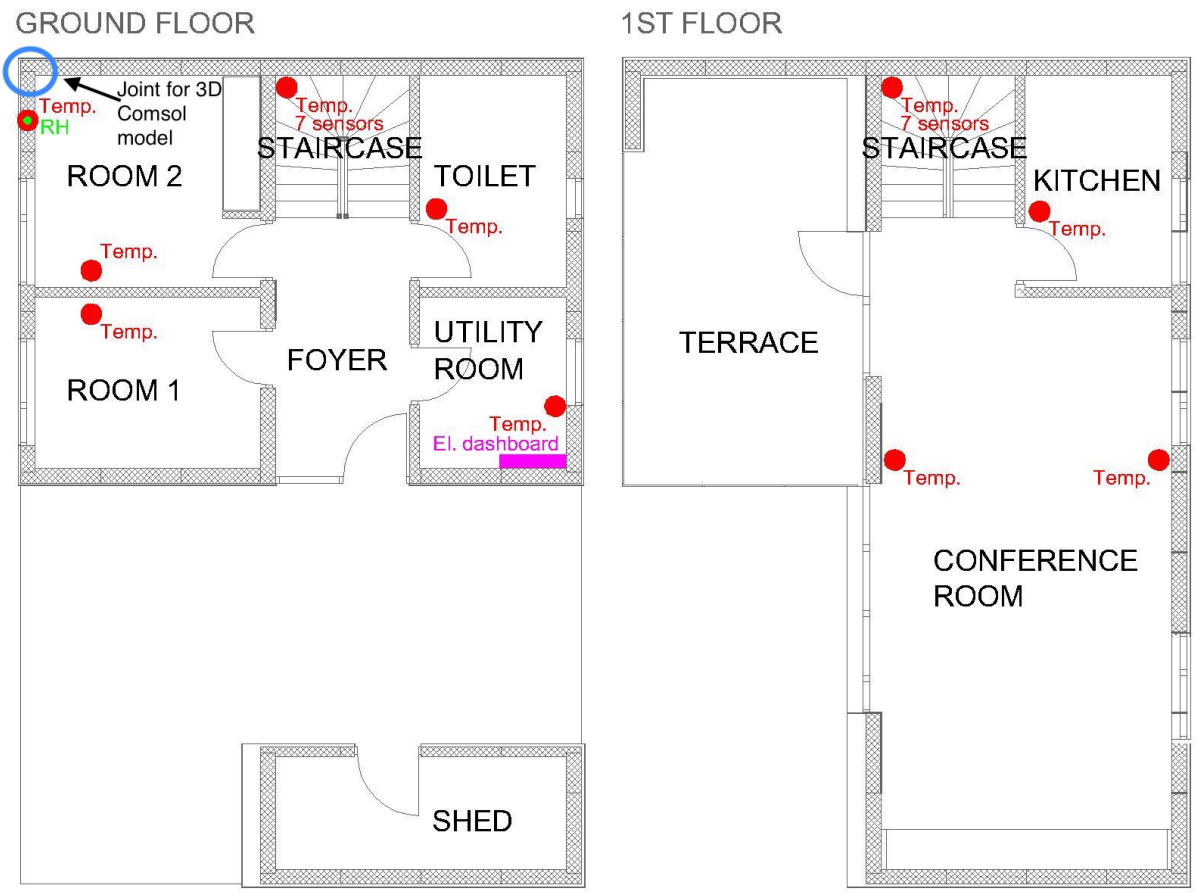

Figure 2.8: Sensors in the test house.

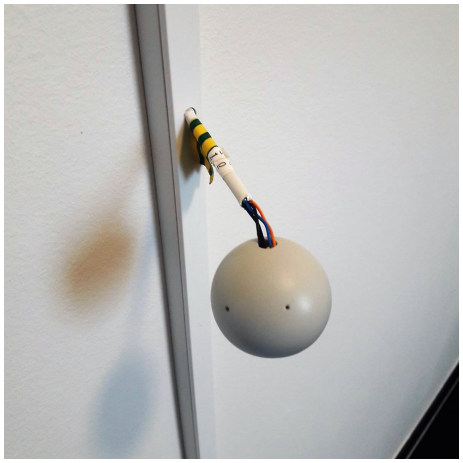

Figure 2.9: Temperature sensor in protection sphere.

Figure 2.10: Sensors in the staircase.

Another set of measurements covers energy consumption of the building. The entire electricity usage is logged (including electrical heaters and all other plugs for appliances) thanks to the connection between the electricity meters on dashboard with the data logger. Since the heating, lightning, and socket power are recorded separately it is easy to track the proportion of the given component in the total energy consumption of the building. In this project, investigation of the heating share has been targeted.

Last but not least, 4 SHT71 sensors (accuracy: $\pm 3\%$ RH, $\pm 0.4^{\circ}$C temp.) which register both relative humidity and temperature have been placed inside the external wall of the room 2 in pre-drilled, sealed cavities (figures 2.11 and 2.12). As it can be seen in the figure 2.11, the construction of the wall includes a wooden beam which is used as linear reinforcement and support for the roof structure above. The element is located outside (close to the external environment conditions), protected by the fibre-cement board of the sandwich panel. The humidity and temperature distribution in this joint is to be logged in order to see if the solution yields moisture condensation or thermal bridge problems. It is especially vital since the beam is the only organic material in the envelope of the building thus it is prone to degradation due to biocorrosion caused by moisture presence and significant temperature fluctuations.

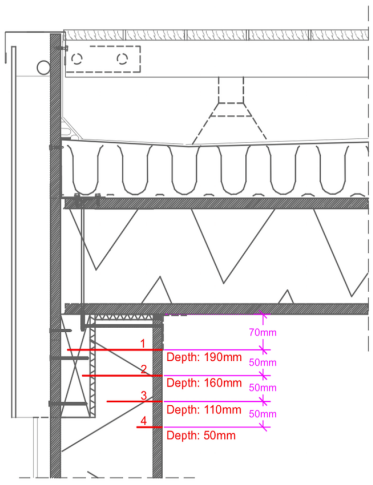

Figure 2.11: Wall - roof joint. Room 2, south facade.

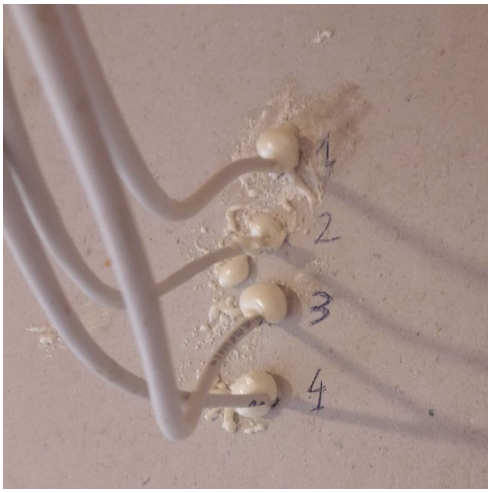

Figure 2.12: Sealed cavities for sensors inside the wall.

2.4 Thermal imaging

The purpose of this experiment is to analyse joints in the actual building regarding cold bridges. It can demonstrate the impact of mechanical connectors, linear reinforcement and other structural elements on the thermal performance of a house constructed in sandwich panels technology. Furthermore, it gives a source of data to confront with computational model results obtained with Comsol Multiphysics software.

Theoretical background

Thermography (or thermal imaging) is the science of detecting and measuring variations in heat emitted by an object and transforming them into visible images. All objects radiate infrared energy in proportion to their temperature and emissivity. The Stefan-Boltzmann equation 2.6 quantifies that relationship. Infrared radiation is typically described as wavelength between 2-15μm. These waves are shorter than radio waves. They are longer than visual light, so infrared radiation is invisible to our eyes. Thermal infrared waves, which are used for thermography, are also longer than the wavelengths captured on infrared film. Infrared imaging systems use a lens to focus the infrared radiation given off by a surface onto a detector. An electrical response results either from the photon or thermal effect. For imaging systems, this signal is converted into an electronic picture that shows the relative temperature differences in a range of grey tones or a series of colours. **[Eads, Lowry (2000)]**

$$Q = \sigma \cdot \varepsilon \cdot T^4 \tag{2.6}$$

Where

Q	Heat energy (W)
σ	Stefan-Boltzmann constant $\sigma = 5.669 \cdot 10^{-8}$ W/m^2
ε	Emissivity value 0<ε<1
T	Temperature (K)

Applied tool

The device used in this experiment was Testo 875-2 infrared camera by *Testo SE & Co.*. Gathered data has been then post-processed in IRSoft program. The sensor can operate in ambient temperature range from -15 to +40°C within air humidity from 20 to 80%. The measuring temperature range spans from -30 to +350°C with accuracy of ±2°C and 50mK resolution. **[Testo (2018)]**

Experiment presets

The measurements were taken on a cloudy day (30.04.18, 15:30) with no direct solar radiation (figure B.10) to prevent envelope surfaces from excessive solar heating and reduce signal noise recorded by the camera due to intensive solar operation. Indoor air temperature and relative humidity values will be indicated for the measurement in the results section of this project. Images have been captured inside the building in structural joints with some sort of structural interference in elements uniformity (plasterboard substructure, wooden support beam inside the wall, corners etc.).

2.5 Computational models

2.5.1 Comsol Multiphysics - heat transfer simulations

Heat transfer in solid module of *Comsol Multiphysics* software has been used to perform simulations in 2D and 3D joint models of the building under the study. There have been three different simulation cases:

- Case A - Heat transfer in the structural joints of the building (2D static and time-dependant simulations). The goal is to obtain line integration of the normal total heat flux along external edges of a model. The normal total heat flux can be then recalculated into linear heat loss ψ which is to be used as input for BSim simulations. Most of the connections are to be calculated as steady state cases but the wall-foundation joint needs to be modelled and solved as a time-dependant simulation according to annex D of [**DS 418 (2011)**].

  Stationary simulations:

  - A.1 Wall-wall (corner) , *according to detail A.5;*
  - A.2 Wall-wall corner (utility room), *analogical to detail A.5 with additional 45mm layer of mineral wool and gypsum plasterboard inside*;
  - A.3 Wall-roof (beam), *according to detail A.6;*
  - A.4 Wall-roof (gable), *according to detail A.7;*
  - A.5 Wall-roof (Room 1), *according to detail A.8;*
  - A.6 Wall-roof (Room 1 - gable), *analogical to detail A.7 without ceiling layers*;
  - A.7 Room 1 roof-building, *according to detail A.11;*
  - A.8 Wall-slab (Conference room), *according to detail A.9;*
  - A.9 Wall-window, *according to detail A.10;*.

  Time dependant simulations:

  - A.10 Wall-foundation, *according to detail A.12 and annex D of* [**DS 418 (2011)**].

- Case B - Heat transfer in a series of structural joints (modelled as one 3D element of the building). The goal is to obtain surface integration of the normal total heat flux on the external surfaces of the model. The investigation is to be performed for the top joint (walls with the roof), bottom (walls with the foundation), and for the entire geometry. An additional simulation including metal connectors (screws and bolts) should be executed in order to set a benchmark (most realistic geometry). The subcases have been presented in figure 2.13. This investigation aims at confronting the total heat flux calculated as stationary problems.

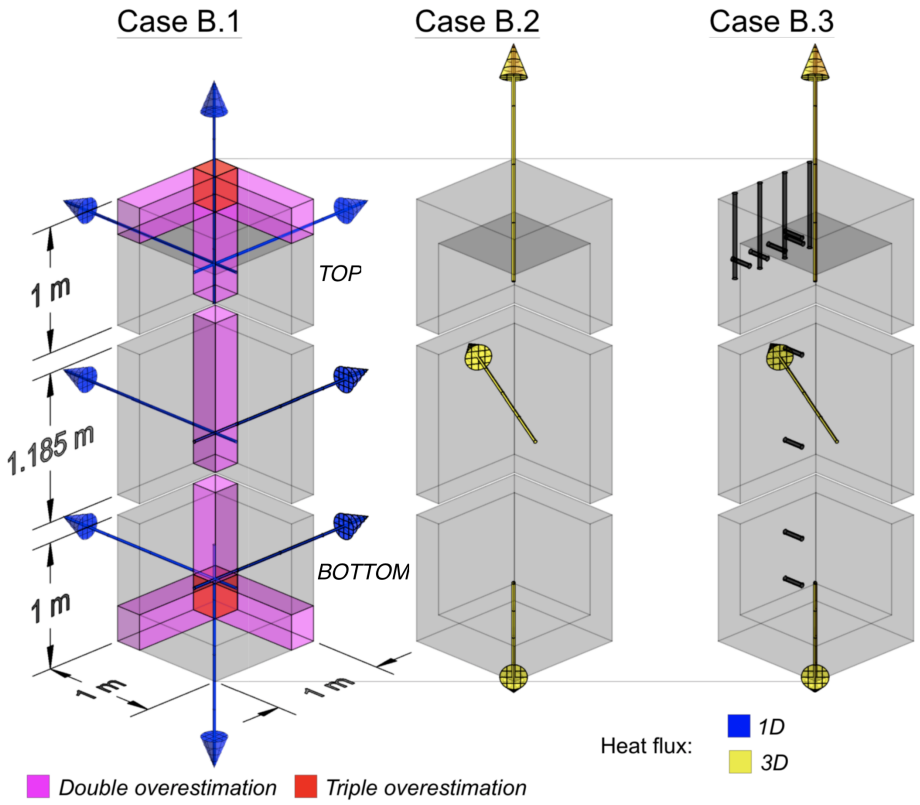

Figure 2.13: B-subcases.

- Case C - Heat transfer in a series of structural joints (modelled as one 3D element of the building). The goal is to obtain surface temperature plot to compare it with thermal imaging (section 2.4). Weather and indoor climate data are to be used as the input for this time-dependant case to reflect the real-world temperature fluctuations.

Theoretical background

Comsol Multiphisics is an advanced engineering tool solving complex mathematical problems using finite element method. Full description of its capabilities and theory behind it can be found in the official data sheets and the help file of the program. It can be however assumed that the basic principle of the heat transfer simulations can be described by the heat transfer equation 2.7.

$$\rho \cdot C_p \cdot \frac{\partial T}{\partial t} + \rho \cdot C_p \cdot u \cdot \nabla T + \nabla \left(-k \cdot \Delta T\right) = Q \tag{2.7}$$

For a steady-state problem the temperature does not change with time and the first term disappears. The equation includes the following material properties: density ρ, heat capacity C_p, and thermal conductivity k (a scalar or a tensor when the thermal conductivity is anisotropic). It also includes the velocity field u and a heat source (or sink) Q-one or more heat sources can be added separately. Apart from the temperature distribution, the total normal heat flux is to be calculated. Flux refers to the area density of any quantity that flows through a well-defined

boundary of a domain. The domain could be a volume (in 3D), surface (in 2D), or edge (in 1D). Correspondingly, the boundary through which we compute the flux would be surface (in 3D), edge (in 2D), and point (in 1D), respectively. The total flux through the cross section is then the sum total of flux coming out of that boundary.

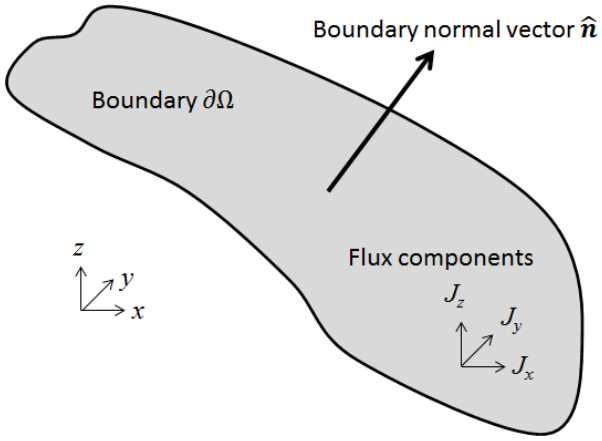

Figure 2.14: An arbitrary boundary ($\partial\Omega$) in 3D space whose normal vector is $\hat{n} = [n_x; n_y; n_z]$. The flux through this boundary is specified by the vector, $\vec{J} = [J_x; J_y; J_z]$. **[Comsol Multiphysics (2018)]**

To find the total normal flux through an arbitrary boundary, denoted by , we first need to find the normal flux through that boundary. This can be obtained from the dot product of the normal vector of the boundary and the flux vector . The total normal flux can then be obtained by integrating this quantity over the boundary. The final expression used for computing the total normal flux has been presented below. **[Comsol Multiphysics (2018)]**

$$I = \int_{\partial\Omega} \hat{n} \cdot \vec{J} = \int_{\partial\Omega} \left(n_x J_x + n_y J_y + n_z J_z\right) \tag{2.8}$$

Geometry

Case A Two-dimensional geometries used in these simulations were converted directly from .dwg files (detail drawings from DC-System) into Comsol Multiphysics geometry instances. This ensures high level of quality and detailed definition of the problem to be solved. It has been assumed however, that the external cladding (facade elements and their substructure) should not be included in the simulations as they do not influence the insulation properties of the envelope but increase complexity, thus computation time. Furthermore, simulations of geometries with point connectors (screws or bolts) are deemed to be unreliable since such a fragment of a joint represents only a minor areal fraction of the entire connection. However, the influence of the screws and associated cold bridges is to be investigated in case B. Tapes, bands, and sealants mounted inside (indoors) have been used to increase airtightness and make finishing of the joint smoother. Their influence on the heat transfer calculations is negligible just like the external cladding. Each model has been converted and simplified in the same manner as the principle shown in figure 2.15.

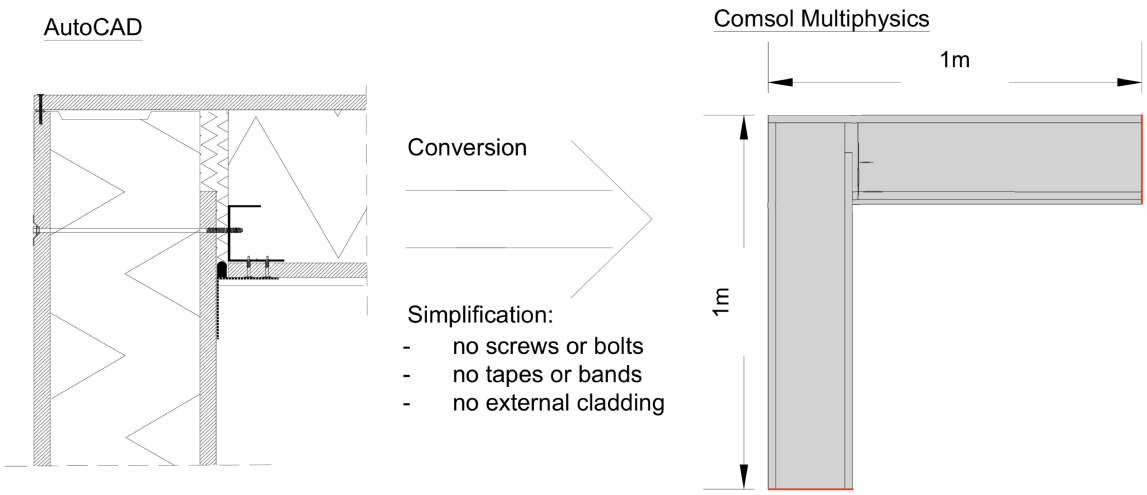

Figure 2.15: Geometry conversion principle.

Case B+C For these studies a 3D model of the entire external joint of the building (from the foundation up to the roof) in the corner of Room 2 has been created. Its precise dimensions are based on the details A.5, A.7, A.8, and A.12 and correspond with those in figure 2.13. Three-dimensional dwg-format geometry (shown below) has been directly loaded into Comsol geometry module.

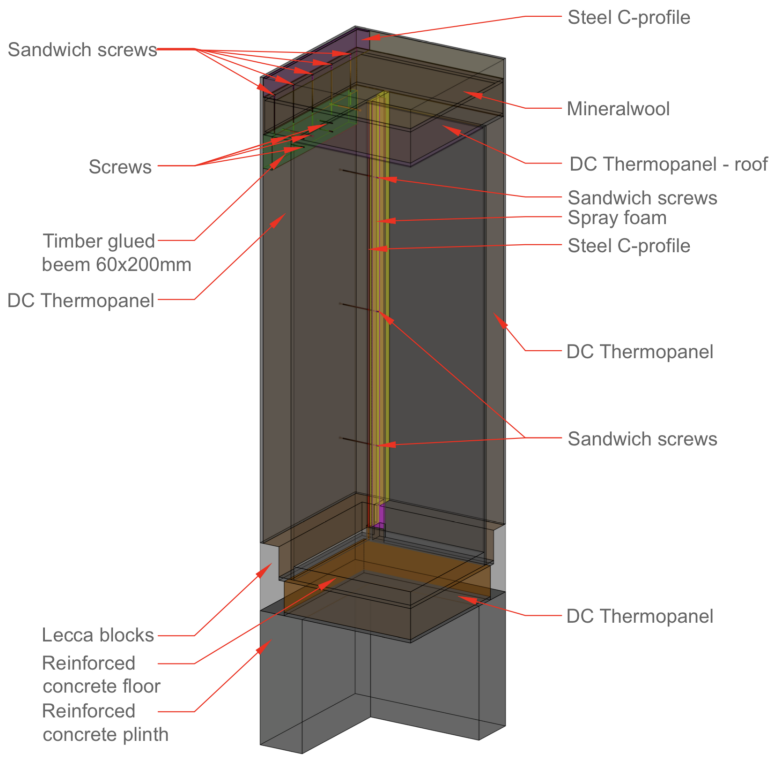

Figure 2.16: Case B.4 - geometry. Location of this joint has been presented in figure 2.8.

Materials

To deliver highest quality of the computational models, material properties obtained from experimental research described in section 2.1 are to be used in this investigation. The key characteristics for steady-state simulations are components dimensions, density and thermal conductivity (equation 2.8). On top of that, the heat capacity C_p values are to be assigned especially for time-dependant problems. Final results - the input for thermal calculations - will be presented in section 3.1.

Boundary conditions

Case A+B For these steady state problems, fixed ambient temperatures have been set. To simplify later calculations of the linear heat losses, the difference of 1°C has been chosen. Thus fixed ambient air temperature of 0°C has been applied along models' edges facing outdoors and 1°C along those facing indoors. Another important parameter is the surface resistance. The values for normal emissivity materials are given in Table 1 of EN ISO 6946 : 2007 *Building components and building elements - Thermal resistance and thermal transmittance - Calculation method*.

Table 2.2: Surface resistance boundary conditions [**EN ISO 6946 (2007)**].

Surface resistance	Direction of heat low		
(m^2K/W)	Upwards	Horizontal	Downwards
Rsi	0.10	0.13	0.17
Rse	0.04	0.04	0.04

Lastly, thermal insulation has been applied on the short edges (surfaces in case B) - see red lines on Comsol model in figure 2.15. The Thermal Insulation node is the default boundary condition for all Heat Transfer interfaces. This boundary condition means that there is no heat flux across the boundary:

$$n \cdot (k \cdot \nabla T) = 0 \tag{2.9}$$

and hence specifies where the domain is well insulated. Intuitively, this equation says that the temperature gradient across the boundary is zero. For this to be true, the temperature on one side of the boundary must equal the temperature on the other side. Because there is no temperature difference across the boundary, heat cannot transfer across it [**Comsol Multiphysics (2018)**]. For time-dependant wall-foundation study, waveform function formula describing external temperature fluctuations has been assigned according to annex D of [**DS 418 (2011)**]. Computation time step is 15 days and the simulation period is 10 years, like the standards indicates.

Case C Boundary conditions are analogical to the previous case B. The only differences are the simulation time step and range. The time step is to be set as 1h whereas the range is to be defined according to the weather conditions indicated in figure B.10. Indoor and outdoor temperature input will be realised as direct import form the Test House and weather station temperature sensors respectively.

Mesh

There are two different types of meshing schemes in Comsol Multiphysics software: physics-controlled mesh and user-controlled mesh. While the latter gives opportunity to design and fit the mesh precisely for the given problem, the former is less time consuming, easy to use and satisfactory quality tool. Due to time and computation power resources limitation, the physics-controlled automatic meshing has been chosen. Its precise description is accessible through Comsol help guide. There are 9 size presets for physics-controlled mesh, from extremely coarse, through normal up to extremely fine.

Case A For these two-dimensional models, extremely fine triangular mesh has been chosen since the computation time does not exceed 10 seconds. Mesh properties have been presented in appendix C.1. Furthermore, mesh independence test have been conducted in appendix C.2.

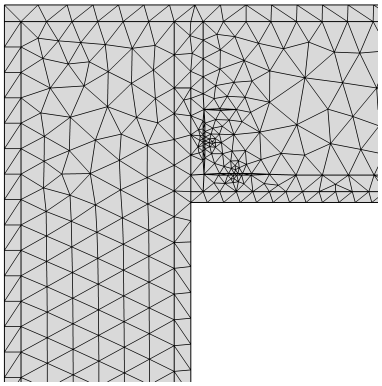

Figure 2.17: Extremely coarse physics-controlled mesh. 1134 elements in wall-wall (corner) 2D model.

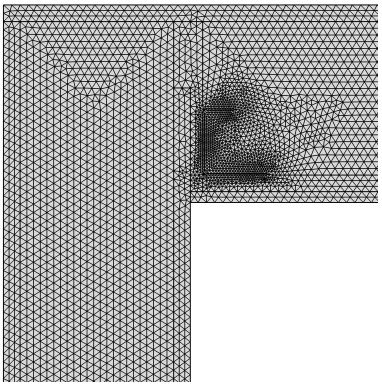

Figure 2.18: Extremely fine physics-controlled mesh. 12595 elements in wall-wall (corner) 2D model.

Case B+C For these three-dimensional models, extra fine tetrahedra mesh has been chosen due to computational power limitation. Mesh properties have been presented in appendix C.1. Furthermore, mesh independence test have been conducted in appendix C.2.

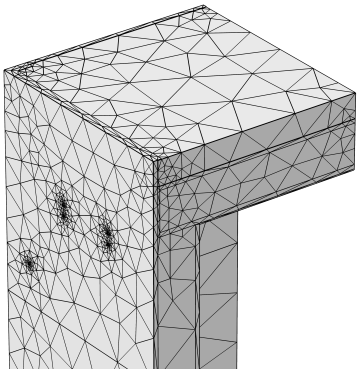

Figure 2.19: Extremely coarse physics-controlled mesh. 38859 elements in 3D model.

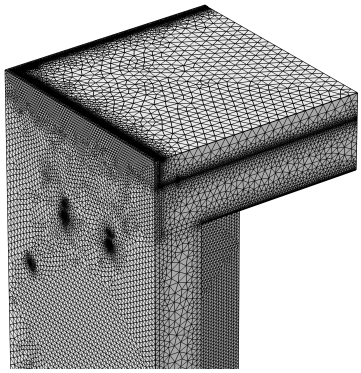

Figure 2.20: Extra fine physics-controlled mesh. 3396549 elements in 3D model.

2.5.2 BSim - Indoor climate and energy consumption simulations

This part of the simulations can be assumed as the most important culmination which incorporates most of previously used methods to deliver indoor environment and energy consumption data that will be confronted against measured values. Generally speaking, this model is meant to reflect the actual building with highest degree of details. Only simplifications concern geometry which will be discussed further in this chapter. Information presented in this section consider the baseline model that will be then subjected to input variation and sensitivity analysis (more in the next section 2.5.3). The simulations can be divided into 2 phases (like in Test House measurements section 2.3).

- Phase 1 [*from 23.04.18 (08:00) to 30.04.18 (08:00)*] - Temperatures in the house (rooms)are simulated. The aim of this stage is to investigate the correlation between simulated air temperature distribution in the house with values measured in the actual building. This stage (combined with input variation) can be regarded as a validation of the construction model since no heating is simulated. The only variables influencing the temperature distribution are geometry of the building, material properties, and weather conditions.
- Phase 2 [*from 01.05.18 (17:30) to 08.05.18 (23:00)*] - Heating is included in the model, the energy consumption is simulated. The aim of this stage is to investigate the correlation between dynamic energy consumption simulations and values measured in the actual building. This stage (combined with input variation) can be regarded as a validation of the heating system. During this phase heating setpoint is fixed at one value.
- Phase 3 [*from 22.04.18 (01:00) to 08.05.18 (18:00)*] - Moisture transport in the construction is simulated to calculate the absolute water content in the wooden beam and in the PUR foam insulation. The results are to be confronted with the measured values (see 2.3.2).

Theoretical background

A building is understood by BSim as being a number of zones, separated from each other and from outside air or from possible virtual zones by constructions of different kinds. In a numerical model such as the one used in BSim, every continuous event of the real world is described in a discrete time steps. This means that the temporal sequence of the various processes, which in reality are modified continuously, are described in the program as changes from one time-step to the next, where the time-steps are of a finite size. The program assumes quasi-stationary conditions, that is to say that for the length of time which a time-step lasts, the conditions (for example, the temperatures of the individual components in the building) are assumed to be constant. By using suitably small time-steps this gives a reasonable approximation of reality.

In a corresponding manner, the building materials are divided into control volumes, which are each represented by a nodal point (or node). In each control volume, the alterations in the nodes' thermal condition are enumerated as a function of the heat flows in and out of the volume and of the material's thermal capacity. Even though a control volume has a certain extent, the conditions in the nodal point are assumed to be valid for the whole control volume. The nodes are thus central elements in the description of the building. The air in the zones is also described as nodes, but no heat or moisture capacity is attributed and the condition of which

is therefore altered momentarily according to influences from the surroundings. [**BSim (2013)**]

Detailed explanations to how the stationary balances for heat and moisture are arranged for each individual zone and how the non-stationary thermal transmission through constructions is calculated are given in the following chapters of the BSim help file:

- The heat balance for the zone air;
- Heat transmission in the constructions;
- Detailed simulation of moisture transport;
- Longwave radiant heat exchange between surfaces in a thermal zone.

Geometry

Technical drawings presented in appendix A.1 were used as basic source of information for the BSim geometry creation. However, it should be pointed out that some assumptions have been made to simplify the geometry in order make it compatible with the program and convenient to use.

- *Location:* The model has been placed in the correct position of 56'82"N and 9'50" with 24 degrees deviation from north towards east. The terrain type has been set to open flat country with ground properties of 9 to 12°C;
- *Rooms:* All rooms (cells) have been modelled as separate but neighbouring (facing each other) instances. Cell faces can face other cells and either indoors or outdoors. There are no virtual cells and none of them faces itself. The rooms were created by merging or splitting box-shaped instances into desired cells. Shed has been included in the geometry to account for its influence on the heat transfer but will not be investigated in terms of temperature distribution or moisture analysis;
- *Walls:* The walls have been modelled according to the user guide recommendations. External elements are created from the external line of the building inwards whereas internal walls are modelled along central axis of the partition. Taking into consideration internal wall layers asymmetry, the BSim models axes are shifted from the construction axes by this asymmetry offset;
- *Floors:* The ground floor level has been set the same for the entire geometry. Due to different materials layers layout, storeys heights differ. The definition principle is the same like for walls. The ground floor and roof from external line (minimum and maximum level of the building) inwards, whereas the internal floors from the central axis outwards. Once again, this convention yields axes deviation from the construction drawings (see drawing D.1 for visual explanation);
- *Roofs:* There are two types of roof in the model - one over room 1 and room 2 (under the terrace) and the main roof over the kitchen and conference room. Both of them are constructed with slope of 2° realised by changing thickness of the top mineral wool layer. Due to software limitations this geometry has been simplified to average height of the building (average roof level) - see drawing D.1 for visual explanation. The roofing felt

has not been included in the model due to its low thickness resulting in problems with time step definition for moisture balance and its low impact on the thermal insulations properties. Yet, to account for heat absorption, the top roof faces have been assigned black colour;

- *Windows, doors and openings:* External doors and windows size and positions have been modelled according to figures A.13 and A.14. No internal doors have been included in the geometry due to separate thermal zones of each room. It has been assumed that because of relatively low temperature differences, lack of forced air movement and minimal air leakages around doors which remained closed for the entire measurements period (in the real house), their influence on the virtual model can be neglected.

  There are two openings present in the geometry. The first one on the ground floor, between foyer and lower part of the staircase, and the second one on the first floor ,between upper part of the staircase and the conference room. There are not any elements (obstacles) in this places in the real building. However, since the stairs are not included in the model as such, an equivalent volume of spruce timber have been assigned around these openings (0.10m x 0.10m band around each opening).

Thermal zones

To represent the real case (all doors in the building closed), the baseline model has been defined with 9 separate thermal zones with no mixing between them. This assumption enables to assign individual systems and then investigate thermal and moisture parameters of each cell separately. Such convention seems to be a reasonable solution for the rooms on the ground floor and the kitchen upstairs. However, the quality of this representation might be questioned with regard to the foyer, the staircase, and the conference room. This is why, alterations of this scheme will be realised in section 2.5.3.

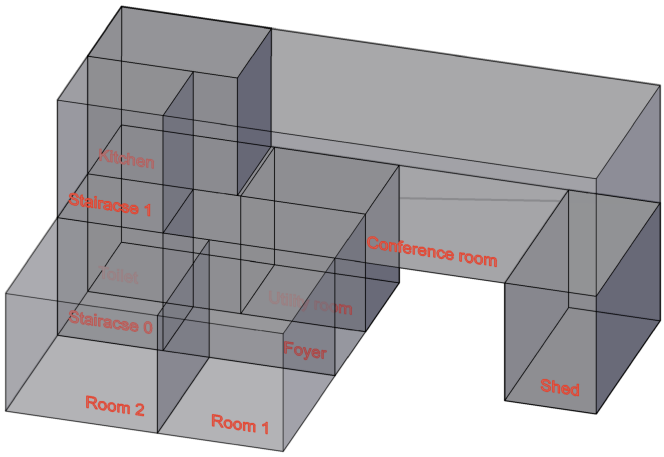

Figure 2.21: Baseline model - thermal zones layout.

Materials

Based on the Test House drawing documentation (A.1), model's elements have been divided into groups of the same materials layout (figures 2.22 and D.1). The elements comprise numbers of materials that have been listed in tables D.1 and D.2. The material properties are among the most important input data for the model since they describe the properties of building's envelope. This is why, material testing has played substantial role in the input preparation. Obtained values are to be presented in a separate chapter (3.1). These numbers (including density, thermal conductivity, heat capacity, ad/desorption curves) will be used directly as materials properties in the BSim simulations.

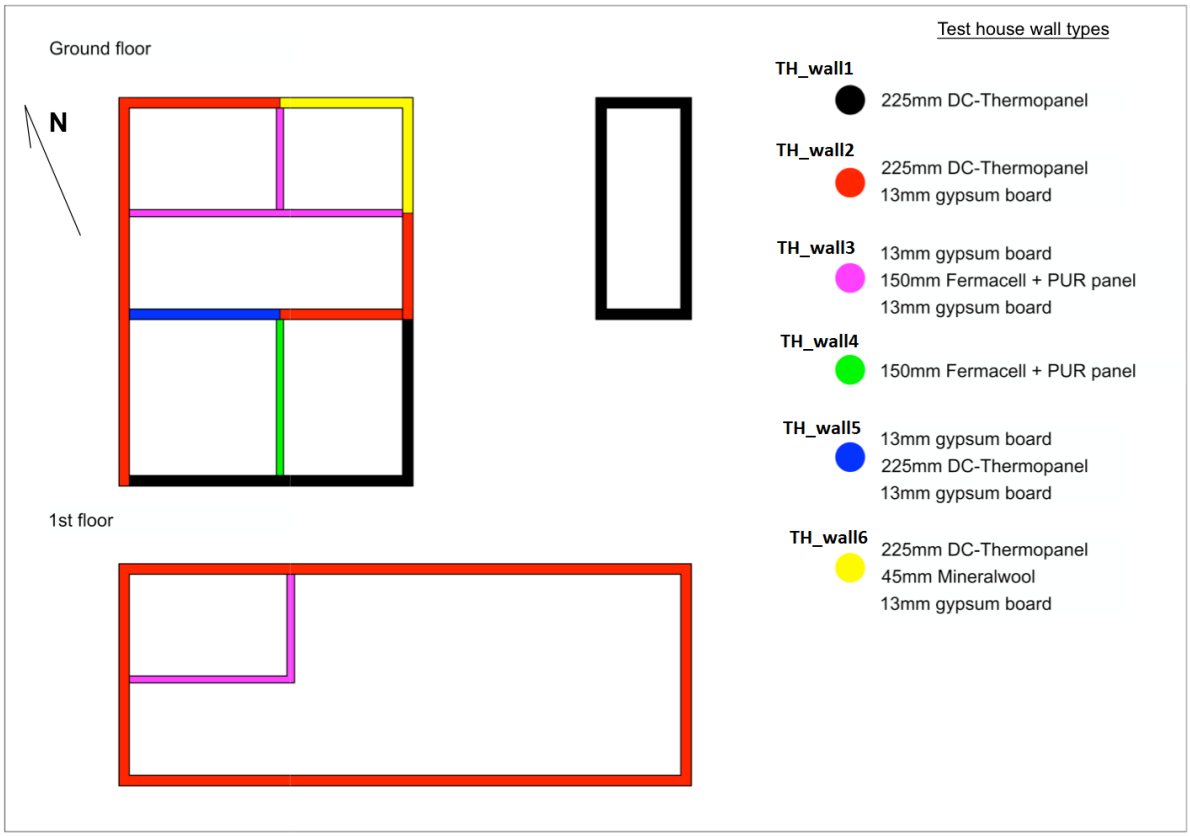

Figure 2.22: Baseline model - walls layout.

Systems

Since each room has been modelled as a separate thermal zone, the systems can be assigned accurately to a specific cell. The systems and their settings are listed in table D.3 and reflect the actual building systems, presented in 1.4.5. There are three main groups that have been considered in this model:

- *Infiltration*: The infiltration rates have been assigned to each thermal zone according to the results of blower door test conducted by Aalborg University Indoor Climate Laboratory. The experiment, carried out in accordance with DS/EN 13829, gave very

low infiltration rate of $q_{50} = 0,066$ L/s/m^2 for the entire house[**AAU Klimalab (2016)**] ($q_{50,max} = 0,5$ L/s/m^2 according to Bygningsreglementet 2020). This value has been then broke down into infiltration rates for each room by weighing over their net volumes;

- *Heating*: This system has been assigned to the rooms with electrical heaters to simulate their impact on the temperature distribution and energy consumption of the building. The presets are the same for each of that spaces, however since in the conference room there are two heaters, the maximum power output for this thermal zone has been doubled. For more information see table D.3;

- *Equipment*: The devices within this system have not been modelled in order to measure their energy consumption but to account for their heat emission. This includes computer and data loggers working non-stop in the smallest room in the house - the utility room on the ground floor, a domestic hot water tank in the toilet, and a fridge in the kitchen. For more information see table D.3.

Simulation presets

The simulation presets have remained fixed for all three phases of the experiment (the moisture transport was enabled only for phase 3). Because the computation time did not exceed 1 minute, the maximum number of time steps (256 per hour) was chosen to deliver highest available quality of the simulations. Solar radiation model has been set to Perez, and the layers thickness left as default value - 0.05m. Longwave Radiation and Thermal Bridge have been enabled.

2.5.3 BSim input variation

The primary goal of the simulations described in the previous section is to convert real building into accurate computation model which is to be solved. Nevertheless, due to precision limitations for the materials testing, weather data collection, construction joints heat transfer simulations, or even the BSim geometry definition, the baseline model should not be considered as definite. This is why the input variation needs to be implemented to examine the accuracy of the model and perform simple sensitivity analysis. It can also prevent the study from failure due to badly stated assumptions.

Input variation has been realised as change of one at a time of the baseline model properties in accordance with table 2.3. All other parameters and simulation presets remain fixed (and the same as in baseline model), while the influence of the investigated characteristic is studied. Due to time limitation, the variations have been set as discrete values rather than global, uniformly distributed modifications. The choice and range of these variations addresses the inaccuracies and assumptions described in the preceding paragraph.

The expected outcome of this stage is the deviation of each variation from the baseline model, indicating what is its importance in the overall model definition. Possibility of the model adjustments according to this sensitivity analysis will be developed in the next chapter.

Table 2.3: BSim input variation

No.	Variable	Variations	Details
1	Weather input	Solar radiation +10%; Solar radiation -10%	-
2	Material properties	λ+10% ; λ-10%; c_p+10%; c_p-10%	-
3	Thermal zones	Conference room + staircase 1 and foyer + staircase 0 ; conference room + staircase + foyer; Conference room and staircase 1 + 0 and foyer	-
4	Cold bridges	-10% ; +10%	Construction joints, around foudation, around openings
5	Window properties	-10% ; +10%	Heat transmittance, U-value

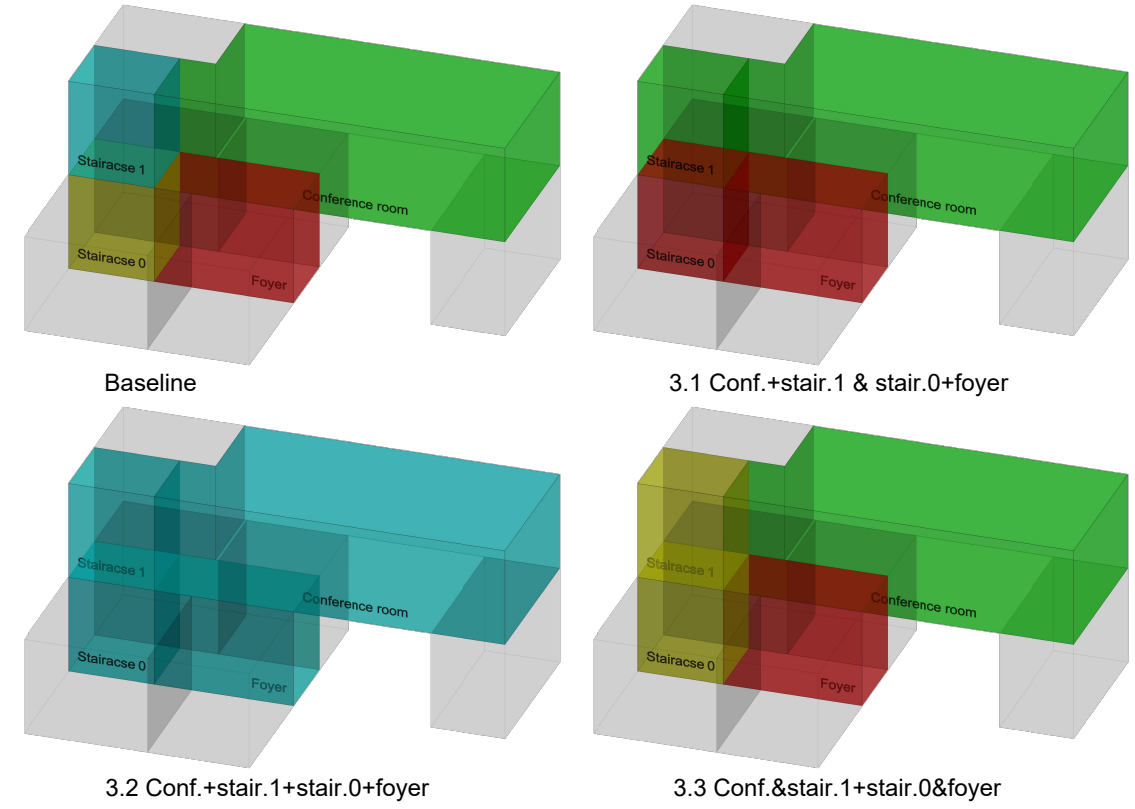

Figure 2.23: Different thermal zones layouts for input variation.

Chapter 3

Results

3.1 Materials properties

3.1.1 Thermal conductivity

During the experimental examination of materials thermal conductivity, three values of this property have been obtained, one for each temperature. This discrete set of data (for 40°C, 25°C, and 10°C) has been then subjected to linear interpolation to get polynomial describing the relation between the test temperature and thermal conductivity of the material. Mentioned plots and formulas can be found in appendix F.1, where test reports for examined materials are presented. An example of result plot and function is shown below in figure

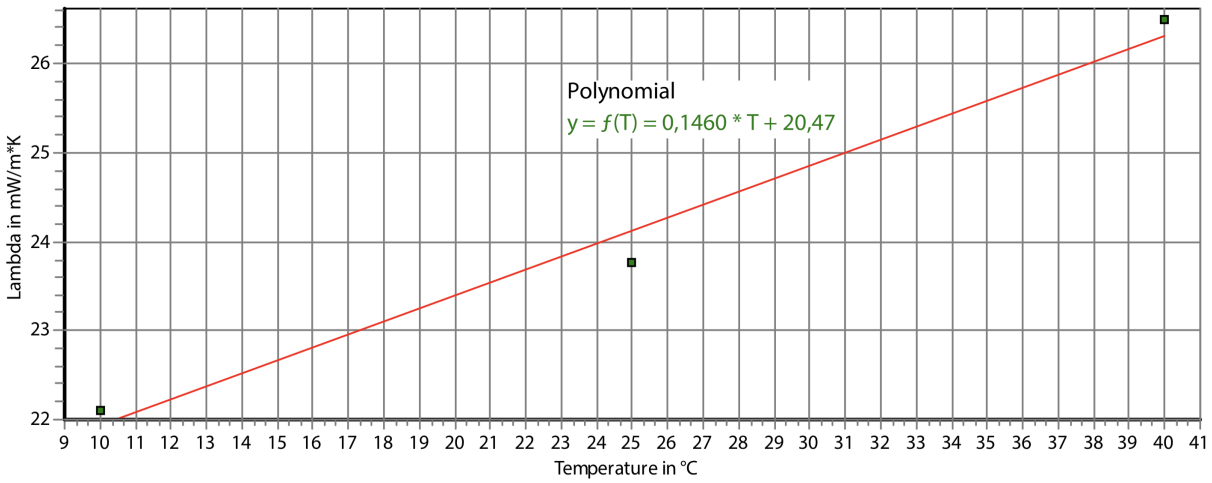

Figure 3.1: PUR foam - thermal conductivity vs test temperature relation.

"Procedure for determining declared and design thermal values" standard allows to define material's λ in two temperatures, 10°C and 23°C, depending on the expected thermal conditions. Due to relatively high outdoor and indoor temperatures during the experiment period, it has been assumed that use of λ_{23} value is more accurate and representative. To derive its value, the polynomial equations for each material were used. Thermal conductivity of each sample is listed in the table 3.1. The last column of the table is denoted as λ_{dec} which stands for the declared thermal conductivity value. These numbers have been collected from data sheets and technical reports provided by materials' producers.

Table 3.1: Measured thermal conductivity. Valid results in **bold**.

No.	Material	λ_{40}	λ_{25}	λ_{10}	λ_{23}	λ_{dec}
		(mW/mK)				
1	PUR foam	26.49	23.77	22.11	**23.83**	23.00
2	AMROC board	242.21	236.52	232.31	**236.35**	230.00
3	Fermacell board	291.33	293.09	294.69	**293.27**	320.00
4	Rockwool A-Batts, 45mm	37.91	35.12	33.04	**35.03**	37.00
5	Flexi-batts 37, 145mm	42.75	38.04	35.34	**38.22**	37.00
6	Gypsum plasterboard	150.34	146.84	144.66	**146.90**	250.00
7	Glued timber GL30C	123.38	99.86	93.15	**103.45**	120.00
8	Plywood	97.14	93.50	91.69	**94.05**	90.00

The comparison of experimentally defined λ_{23} with the value declared by a producer can be treated as quasi-validation of the measurements. It can help to identify gross errors but minor deviation is acceptable and in fact expected. Moreover, producers rarely share information about the lambda test temperature. It should be borne in mind that thermal conductivity tends to decrease in lower temperatures. Thus the differences between these two numbers, visible in table 3.1 for the listed materials are deemed reliable especially since most of them present deviation around 3-5% whereas, the accuracy of measurements is 1%.

Apparently, the highest inconsistency can be observed in gypsum plasterboard results. The relative error between measured and declared λ reaches 41%. Likewise, glued timber results differ albeit by much lower proportion of 14%. There are several possible sources of these variations.

Firstly, it should be pointed out that not only producers' experiment presets (temperature) are unknown but also samples conditions. According to **[DS/EN ISO 10456 (2010)]**, ageing and moisture content factors should be included in declared thermal conductivity definition. Furthermore, the standard describes two different sets of conditions for testing - one with dry sample and the second one with moisture content when in equilibrium with air at 23°C and relative humidity of 50%. These inconsistencies combined with unknown age of samples used in this project might cause results deviation. These problems could be solved by measurements in the same conditions and with use of analogical correction factors as producers.

Secondly, the amount of results obtained for this project is significantly lower than required minimum for official product declaration. Due to time limitation (one data point takes up to 15 hours) the polynomials used to define λ_{23} are based only on three measurements. Furthermore, an evaluation directly at 23°C could be performed to find explicit results. Values declared by producers are also recalculated as 50% (mean) or 90% fractiles. This leaves the possibility of examining samples that are out of these confidence ranges.

Lastly, thermal conductivity of all materials have been subjected to input variation for the core simulations which provides information about its importance for the model which is expected to be relatively little in case of non-insulation materials.

3.1.2 Heat capacity

Laser flash experiment produced thermal diffusivity, conductivity and heat capacity results for 2 samples of each material at 3 different temperatures. There were three "shots" (laser impulses) per sample per temperature, thus the values presented in table 3.2 should be considered as average of three single measurements. As a result a complex set of values for each material has been obtained.

Since thermal conductivity has been already defined in guarded hot plate experiment 3.1.1 which is assumed to be a more robust method, λ_{23} was used as criterion for heat capacity results choice (validated measurements denoted in bold in table 3.2). This convention is based on equation 2.4 which indicates direct relation between thermal diffusivity, conductivity and heat capacity. Thus, it can be assumed that if λ evaluated by flash method corresponds with the one obtained in guarded hot plate (with the same ρ), α and Cp are correct as well. Nonetheless it should be kept in mind that this hypothesis neglects the possibility of diffusivity-heat capacity discrepancy at the same relative ratio. To check if the final results are representative, [**Thermal properties database (2017)**] was used to confront them with average properties of given material. All measurements listed below fall into expected range.

Table 3.2: LFA measurements. Valid results in **bold**.

Material	Sample	T	Diffusivity α	Conductivity λ	Cp-calc.
		(°C)	(mm^2/s)	(W/(mK))	(J/g/K)
Amroc fibre-cement board	1	20	0.354	0.407	1.445
	2	20	0.269	0.309	1.324
	1	25	0.351	0.404	1.660
	2	25	0.269	0.310	1.463
	1	30	0.334	0.384	1.485
	2	**30**	**0.220**	**0.253**	**1.031**
Fermacell fibre-gypsum board	**1**	**20**	**0.239**	**0.330**	**0.930**
	2	20	0.346	0.477	1.002
	1	25	0.262	0.361	1.093
	2	25	0.329	0.454	0.967
	1	30	0.267	0.368	1.256
	2	30	0.320	0.442	1.083
Gypsum plasterboard	**1**	**20**	**0.170**	**0.148**	**0.983**
	2	20	0.367	0.319	1.053
	1	25	0.220	0.191	1.522
	2	25	0.356	0.309	1.077
	1	30	0.214	0.186	1.518
	2	30	0.360	0.313	1.102
Plywood	1	20	0.201	0.161	1.567
	2	**20**	**0.159**	**0.127**	**1.358**
	1	25	0.206	0.165	1.626
	2	25	0.206	0.165	2.013
	1	30	0.203	0.163	1.767
	2	30	0.207	0.166	2.271

Values presented in table 3.2 indicate significant differences between the measurements, in particular for distinct samples. The divergence can be also observed among various test temperatures. The most likely explanation of this phenomenon is based on the condition of samples and their quality. As mentioned in 2.1.2, each specimen was to be in size of the reference Pyrex sample (ϕ12.7mm x 2.0mm). However, because of the structure of some materials, this little dimensions proved to be troublesome to realise in the lab. Although the specimens in desired size have been acquired, their quality (especially surface smoothness) was low. As a result, the laser pulses were shot at spots with different angles and of varying specimen thickness. It is also likely, that because of the roughness, the graphite paint did not penetrate and cover samples uniformly, thus some portion of the laser pulse might have been reflected. Specimen quality problem caused complete failure of some experiments (figure 3.2).

Figure 3.2: Floor laminate sample for LFA.

There are several materials used in the house construction which are missing in table 3.2. The problem which prevents from thermal properties collection lies in data post-processing. As a result of badly prepared specimens and quasi-transparent material such as PUR foam, the software used to operate laser flash apparatus and recalculate raw measurements, could not manage recorded temperature vs time signal (fig. 3.3). Precisely, the shape of the plot diverged from the typical pattern by substantial factor making it impossible to apply Cowan + pulse correction or any other interpolation - see figure 3.3.

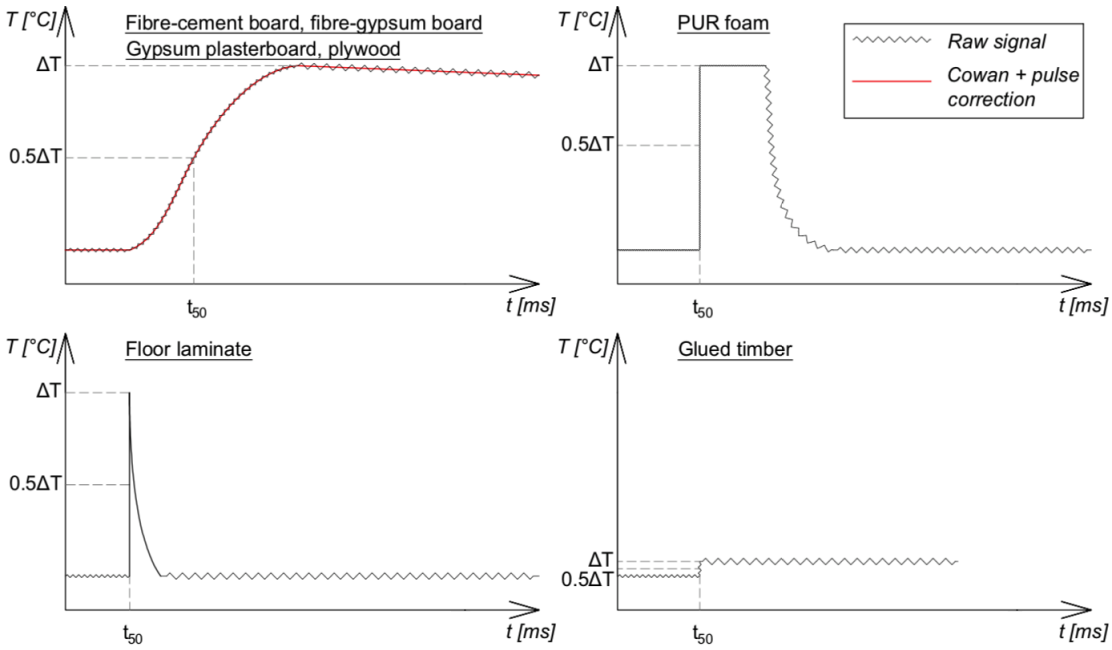

Figure 3.3: Laser flash temperature vs time result plots principle.

Even though the measurement presets were changed (pulse width, duration, delay) and the experiment was conducted many times with different samples, the results have not been obtained. Last but not least, some of the materials could not be prepared to maintain required size of the sample (i.e. mineral wool).

3.1.3 Sorption isotherms

As an outcome of VSA experiment, sorption isotherms for most of the construction materials used in the house have been gathered. Plots presented in appendix F.2 demonstrate different humidity-moisture content relations, meaning that the influence of hysteresis, minimum and maximum u, curves shape and angle differ among materials. Note that due to time limitation, pine wood isotherm was used instead of glued timber built in the wall panels of the Test House construction.

The vast majority of the isotherms fall into Type II and III curves, typical for building materials. This includes gypsum plasterboard (fig. F.12), fibre-cement (fig. F.10) and fibre-gyspum boards (fig. F.11), plywood (fig. F.14) and pine wood (fig. F.13). Generally, the adsorption and desorption processes follow the patterns illustrated in figure 2.4. At low RH the water molecules are bound in one layer to the surface of the pores by hydrogen bond or van der Waal forces. When all surfaces of the pores are covered with one layer of molecules, the building of the next layer starts. The transition is marked by the fact that the curve is straight. The thickness of the adsorbed water layer increases to a third or possibly a fourth layer with an increasing pore humidity. Capillary condensation is the last mechanism that takes place. **[Hansen, Kurt Kielsgaard (1986)]**

However, the two insulation materials - polyurethane foam (3.4) and mineral wool (3.5) - present different sorption mechanisms. Firstly, both samples present relatively high (comparing with previously mentioned materials) level of hysteresis. This phenomenon combined with the fact that desorption curves end above and do not reach the adsorption start point (within measuring range $\phi = 3.5\% \div 93\%$) indicate that some proportion of moisture remains absorbed. Another tendency involves lack of vivid capillary condensation segment. After building the initial layer of water molecules, the straight part of the curve can be observed meaning that consistent increase of particles number (water uptake from ambient air) takes place. Then, the mineral wool line angle decreases at approximately $\phi = 65\%$ which expresses lower condensation rate due to maximum molecules concentration on the surface. On the other hand, PUR isotherm stops at around 38%. Although the experiment with polyurethane foam lasted 235h, this limit could not be surpassed. All the measurements were clustered around the last point of adsorption curve shown in figure F.8. Basing on the evidence that the polyurethane foam is a lightweight material with extraordinary insulation properties a hypothesis that its capillaries are mostly closed or of shapes difficult to penetrate (very thin capillaries). Lastly, winding desorption curve for PUR foam, and nearly flat one for mineral wool, both with moderately decreasing tendency, show that dehumidification of the samples is rather slow which might be cause by above mentioned capillary closure/ molecules penetration resistance.

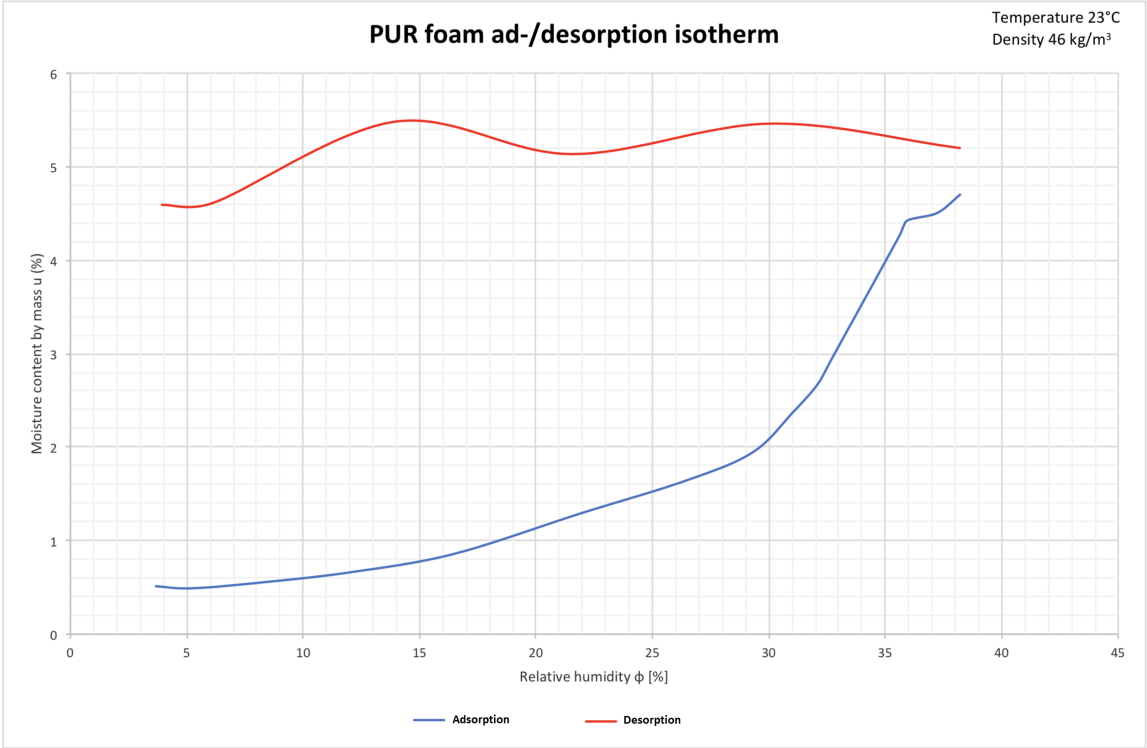

Figure 3.4: PUR foam isotherm.

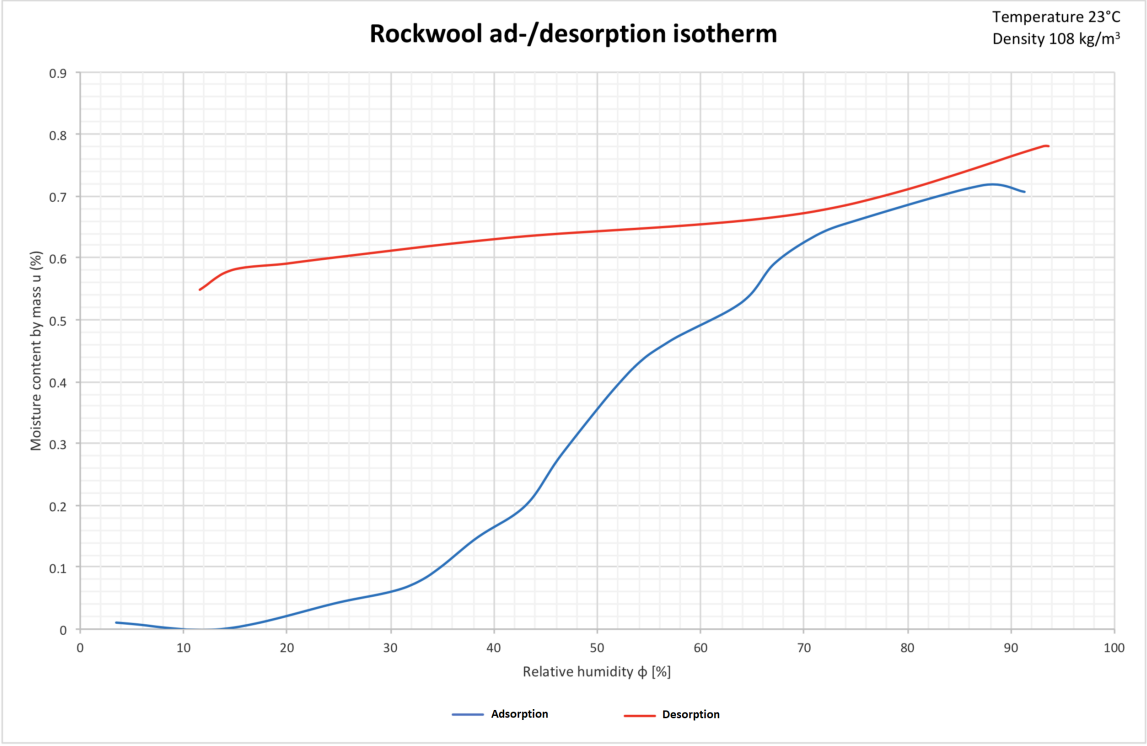

Figure 3.5: Rockwool isotherm.

3.1.4 Conclusion

The results listed and depicted in entire section 3.1 are meant to be used mainly as input for further stages (Comsol and BSim simulations) but they can be also treated as separate material physics study. Although obtained data is deemed satisfactory and representative, some materials are missing certain (or all) properties. The reason for that is either complete lack of samples or impossibility of performing measurements on the samples (i.e. thermal properties of floor laminate). Due to time constraint it has been decided that the parameters which have not been evaluated will be substituted by values acquired form external sources. Therefore, missing heat capacities have been gathered from [**Thermal properties database (2017)**], whereas thermal conductivity and volumetric mass density values have been retrieved from producers resources - for floor laminate [**PERGO laminate (2013)**] and for ceiling sound dampening panels [**Troldekt akustik (2011)**]. Please note that Heradesign plano 25mm was used as sound dampening element in the test house construction, however due to lack of technical data available on producer's website, an analogical (similar) product has been adopted. Lastly, all reinforced concrete parameters have been acquired from [**BSim database (2011)**].

Table 3.3: Final material properties. Numbers in **bold** have been collected from external sources.

No.	Material	λ_{23}	C_p	ρ
		(W/mK)	(J/kg/K)	kg/m^3
1	TH_PUR	0.0238	**1400**	46
2	TH_AMROC	0.2364	1031	1452
3	TH_FERMACELL	0.2933	930	1257
4	TH_Limtrae	0.1035	**1600**	451
5	TH_Gypsum board	0.1469	983	695
6	TH_Plywood 22 mm WBP P-30	0.9405	1358	473
7	TH_Stone wool 36	0.0350	**840**	49
8	Concrete reinforced v/c 0.4 C420	**1.6000**	**800**	**2385**
9	TH_Floor laminate	**0.1400**	**1800**	**1150**
10	TH_SoundDampeningBoard	**0.0800**	**1100**	**390**

Hereby, the values listed in table 3.3 are the final results of materials testing phase and are valid to use in the subsequent stages of the project as input data for computational models.

3.2 Comsol Multiphysics

3.2.1 Cold bridges

Comsol Multiphysics computations gave outcome of normal total heat fluxes along external edges of the two-dimensional models. These values, however, had to be recalculated to get comprehensive information about linear heat loss in given joint. Although a complete explanation of the data treatment have been presented in appendix G.1, it can be summarized that two different methods for computation of BSim cold bridge input have been applied.

The former (denoted as ψ_{BSim} in table 3.4) is established as correction factor for simplified BSim linear heat loss calculation whereas the latter (denoted as ψ in table 3.4) is the explicit value found according to [**DS 418 (2011)**]. All in all, numbers listed below stand for precise heat loss estimation (in one form or another) and are to be used in indoor climate and energy consumption computations.

Table 3.4: Linear heat loss input for BSim simulations.

No.	**Joint**	ψ_{BSim} **(W/mK)**
A.1	Wall-wall (corner)	-0.021
A.2	Wall-wall corner (utility room)	-0.029
A.3	Wall-roof (beam)	-0.005
A.4	Wall-roof (gable)	-0.037
A.5	Wall-roof (Room 1)	-0.023
A.6	Wall-roof (Room 1 - gable)	-0.034
A.7	Room 1 roof-building	-0.032
A.8	Wall-slab (Conference room)	-0.011
No.	**Joint**	ψ **(W/mK)**
A.9	Wall-window	0.095
A.10	Wall-foundation	0.097

The first (upper) part of table 3.4 indicates negative values of all ψ_{BSim}. It should be understood as reduction of cold bridge assumed by BSim. In other words, the software overestimates linear heat losses in the joints. It can be easily noticed that the lowest reduction coefficient has been obtained for the wall - roof joint with embedded glued timber beam as support for the roof. This indicates that double 1D heat flow assumption made by the software is nearly true. It also expresses that the energy loss in this joint is relatively higher than among other due to presence of substantial heterogeneity in its structure. This should be treated as one of the reasons why this structural detail is to be thoroughly examined in subsequent stages of the project. What is more, based on the data A.1 and A.2 it can be concluded that increase of insulation proportion (additional 45mm mineral wool layer in A.2 relative to A.1) reduces accuracy of the above mentioned assumption (see also temperature plots in figure fig:PSI1). It can be concluded that for joints with large presence of additional elements (beams, profiles etc.) the cold bridge calculated with simplified method (presented in G.1) converges with precise thermal simulations. On the other hand, for uniform structural solutions, the overestimation is brought out more vividly.

The second (lower) part of the table includes linear heat losses computed in accordance with annex C.1 for wall-window joint and D.1 for wall-foundation [**DS 418 (2011)**]. These explicit values have also been used directly as input for BSim simulations. Nonetheless, they can be confronted with default values for traditional construction joints presented in standard *Thermal bridges in building construction – Linear thermal transmittance* [**ISO 14683 (2017)**]. And so, the heat loss around window frame installed in lightweight wall (example W4, table C.2 of the standard) equals 0.150 W/mK, while ψ for lightweight wall - foundation (example GF4, table C.2 of the standard) is imposed as 0.500 W/mK. In both cases, values obtained from precise thermal simulations are significantly lower than the ones declared by the standard (by 158% and 515%, respectively). There are several possible explanations of this divergence. Firstly, sandwich panels and structural solutions connected with their technology have not been included in arbitrary tables of the standard. Therefore, comparison with lightweight building elements is a similarity assumption which involves significant error space. Secondly, the cases depicted in ISO 14683 are wildly simplified and do not account for any distinctive characteristics of a joint. Lastly, the values declared by the standard include safety factors to prevent users from underestimating cold bridges in buildings. Thus, the results of Comsol Multiphysics linear heat loss calculations should be treated as more accurate and representative of the actual building under the study.

3.2.2 Interdimensional calculations

As an outcome of series of three-dimensional heat transfer simulations, surface integration of normal total heat flux values have been obtained. These numbers are treated as reference for simplified one-dimensional hand calculations which are performed using U-values of the elements (see table G.1), surface area A shown in figure 2.13, under dT=20°C difference between indoor and outdoor environment. Therefore, 1D heat flow can be expressed as:

$$Q_{1D} = U \cdot A \cdot dT \tag{3.1}$$

Table 3.5: Interdimensional simulations results. All cases have been depicted in 2.13.

Joint part	**Q (W) - surface integration of normal total heat flux**					
	Without screws			**With screws**		
	1D (B.1)	**3D (B.2)**	**Relative deviation**	**1D (B.1)**	**3D (B.3)**	**Relative deviation**
Top	6.4526	5.1430	20%	6.4526	5.1994	19%
Bottom	7.1334	7.4071	-4%	7.1334	7.4301	-4%
Whole	19.1958	17.6190	8%	19.1958	17.7530	8%

Positive relative deviation expresses overestimation of the heat loss calculated with use of 1D heat flux through the elements (i.e. upper part of the joint and the whole geometry). Contrary, the negative value indicates that the simplified 1D calculation is subjected to underestimation (i.e. bottom of the joint). Retrieved data show that one-dimensional study results are on the safe side of the evaluation for most of the cases. Nonetheless, it should be pointed out that due to complexity of the wall - foundation connection, the simplified method fails as it produces results which are misjudged on the unsafe side. The most likely reason of this divergence is the simplification of the placement in the ground. In this case, uniform ambient temperature

of 0 °C has been applied on the entire surface of the geometry. This assumption neglects the thermal properties of the ground, thus exposes this part of the joint on somewhat unrealistic boundary conditions. This yields also decreased level of assurance for correct hear loss of the whole geometry. Secondly, it can be concluded that the influence of the screw presence in the model is negligible. While it increases the complexity of the geometry, thus computation time, by substantial proportion, it does not deliver significantly different results. In this case, the variation is observable only in the top of the joint. This is caused by the fact that most of the mechanical connectors are located in this area. In the bottom, there are not so many of them, therefore in this part as well as generally for the entire geometry, the difference is minimal.

To summarize, this brief investigation demonstrates that even though the simplified method of heat loss calculation is not perfectly accurate, it delivers fairly close results to much more complex three-dimensional simulation. Thanks to safe of time and computation power, and most importantly its simplicity, it can be successfully used as initial estimation even in advanced cases. Moreover, presence of screws, which might seem to be thermal breaks of the envelope, has hardly any impact on the final results.

3.2.3 Dynamic heat transfer simulation and thermal imaging comparison

In this section a brief comparison of measured and simulated temperature surface distribution in wall-roof (Room 1) joint will be illustrated (discussed figures 3.6 and 3.7 are depicted on the next page). Due to weather conditions it has been decided that thermal imaging/ heat transfer simulations should take place on a day without direct solar radiation to reduce error caused by heating of building's envelope (for outdoors conditions see figure B.10). In order to account for temperature fluctuation inside and outside, the dynamic simulations were performed with actual indoors and outdoors temperatures recorded by sensors of the weather station and the one installed in the house (Room 2). The computation has been realised over period of 48h - from the day preceding thermal imaging till the end of the day when it took place (29.04.18, 00:00 - 01.05.18, 00:00). This should, in theory, include by some proportion thermal inertia aspects due to relatively high heat capacity of sandwich panels. Longer simulation period has been dismissed because of extensive solar operation during several days prior to the experiment and substantially increased computation time of the model. However, the initial temperature of the structure (in the simulation) have been set to the wall core temperature (18 °C) measured by the sensors inside. Obviously, figures 3.6 and 3.7 depict the same point in time.

Although the deviation between simulated and measured surface temperatures does not exceed 5%, it should be pointed out that this investigation should be treated as rough estimation of correlation between thermal imaging and dynamic 3D simulation of heat transport. First and foremost it should be noted that measurement points location might differ, thus the comparison is approximate. Secondly, thanks to the design of the joint, the cold bridge presence is hardly observed. The difference between highest and lowest record is only 1.4°C. Furthermore, the indoor and outdoor temperatures should be at least 10°C apart during thermography test to see an actual impact of thermal bridging [**Eads**, **Lowry (2000)**]. In this case, the minimum has been barely achieved.

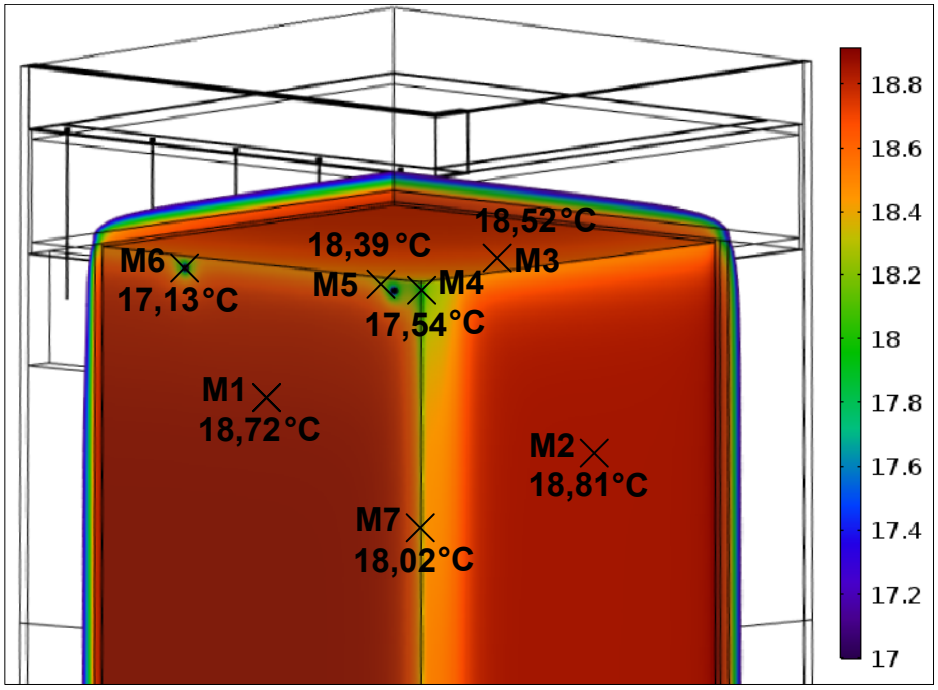

Figure 3.6: Comsol multiphysics time-dependant simulation result.

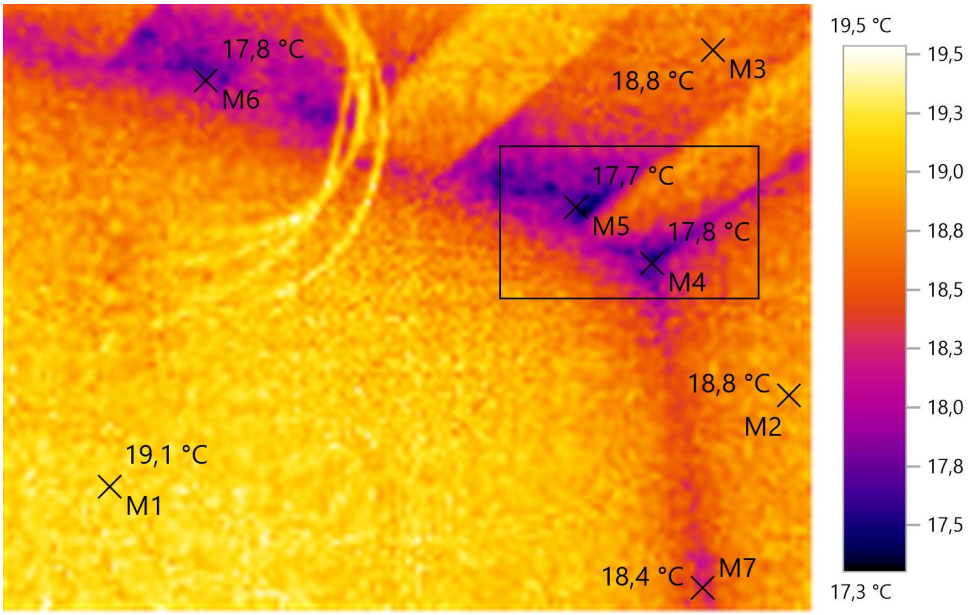

Figure 3.7: Thermal imaging - Wall-roof (Room 1) joint. Date: 30.04.18, time: 15:30. T_e=13.0°C, ϕ_e=66%; T_i=23.6°C, ϕ_e=37%.

More thermal images of the Test House, together with comprehensive analysis can be found in project report *PUR-paneler som fremtidens klimaskærm* [**AAU group B148 (2017)**].

3.3 BSim simulations and measurements comparison

3.3.1 Baseline model

In the following sections the outcomes of the core computations of this project will be presented. References to appendix H, which contains information about data post processing and raw results, will be often made as it is meant to be database of the simulations' output. On the following pages, the results of all three phases of indoor climate and energy consumption calculations will be depicted and discussed.

Room temperature distribution

General information Graphs and values illustrated in this section are products of raw results which have been included in appendix H.2. Temperatures recorded by sensors in the Test House are treated as benchmark for comparison with the simulated values. Nonetheless, their accuracy and level of reliability will be also reviewed on the following pages of this segment. Deviation distribution presented in the charts indicates whether simulated values are underestimated (negative), overestimated (positive) or completely converged (zero) with corresponding benchmark.

Trends Although the results vary wildly among studied rooms (thermal zones), some trends in figure 3.8 can be observed. First and foremost, repeating fluctuations of all lines are the effect of daily temperature amplitude and solar operation. Maximum deviation (point farthest from the horizontal axis) in each case is recorded in afternoons (from around 1 pm to 6 pm) while minimum in mornings (from around 6 am to 10 am).

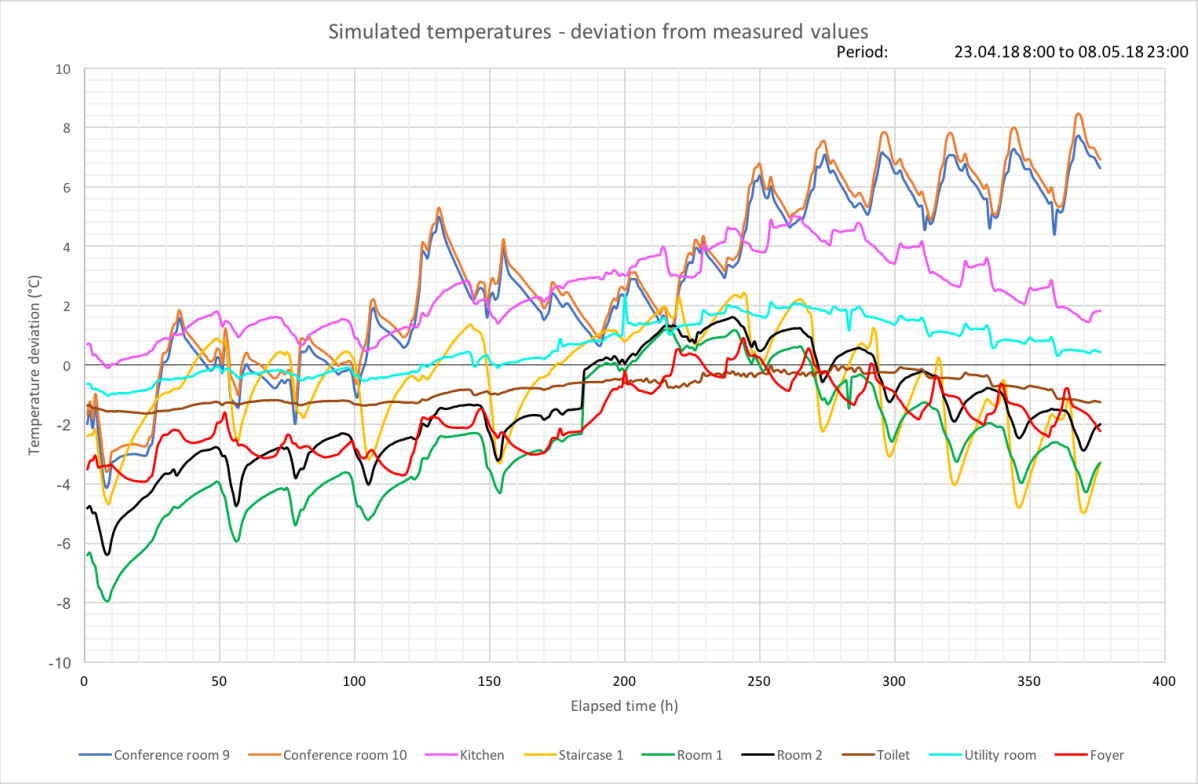

Figure 3.8: Baseline model - temperature deviation.

Furthermore, it can be globally observed that deviations are negative (underestimation) and aggregated together in the beginning of the experiment whilst diverged and stretched in the end. The distributions have similar course, they increase moderately towards positive part of the plot, reach the peak around 2nd / 3rd of May (elapsed time 240-270h), and decline afterwards. However, this tendency does not apply to conference room results as they steadily increase throughout study period (with slight recession after 200h). Temperature deviation of the kitchen seems to follow the one of the conference room, albeit after climaxing in previously mentioned point in time (2nd/3rd of May) it decreases just like other distributions.

Moreover, rooms located on the ground floor are mainly underestimated. Contrary, upstairs spaces are generally overestimated (positive deviation). Similarly, patters regarding windows orientation and size can be recognized. Namely, temperature divergence of areas situated along southern façade (i.e. Room 1, Room 2, Conference room) is significantly greater (farther from the horizontal axis) than those on the opposite (northern) side of the building - i.e. Toilet, Utility room. The highest deviation has been recorded for the room with the largest glazed surface - the Conference Room. Rooms 1 and 2 which have also relatively large windows (see figures A.13 and A.14).

Problem recognition It can be argued what are the reasons of mentioned discrepancies. Here some hypotheses explaining these phenomena will be stated.

Essentially, based on the data depicted before and its breakdown to single comparisons (appendix H.2), as well as recorded weather parameters and the room layout in the house, presumable relations are distinguished. Firstly, the external environment conditions are unarguably the major factor of deviation fluctuations as they are the only variables in the experiment period (the construction of the house and systems settings do not change). Examination of weather charts (appendix E) indicates that in the beginning of the test (when the temperatures are mainly underestimated by the software), the air temperature fluctuated steadily around 10°C whilst the wind speed was rather high (10-12 m/s on average with gusts up to nearly 20 m/s, mainly from west). The direct solar radiation was low due to complete cloud coverage. The weather changed drastically, from May 1st (elapsed time $\approx$ 220h). Considerable, steady growth of air temperature (exceeding 25 degrees) and direct solar radiation (up to 600 W/m^2), combined with minimal wind speed (approximately 4 m/s, mainly from west) has been recorded.

It should be pointed out that the main wind direction did not change during the experiment so its decreased velocity should influence all zones evenly (note that there are no windows on the western façade). Likewise, the outdoor air temperature should affect the rooms regardless of their orientation. Therefore, direct solar radiation should be suspected as the major factor influencing the readings since its availability varies among studied room. Although it was also present in the initial stage of the experiment, its magnitude and frequency was not as high as after May 1st. The correlation between temperatures deviations and direct solar radiation has been depicted in figure 3.9. Note that to clarify the results moving average of 20h period has been applied. Thermal zones have been grouped according to their location in the house.

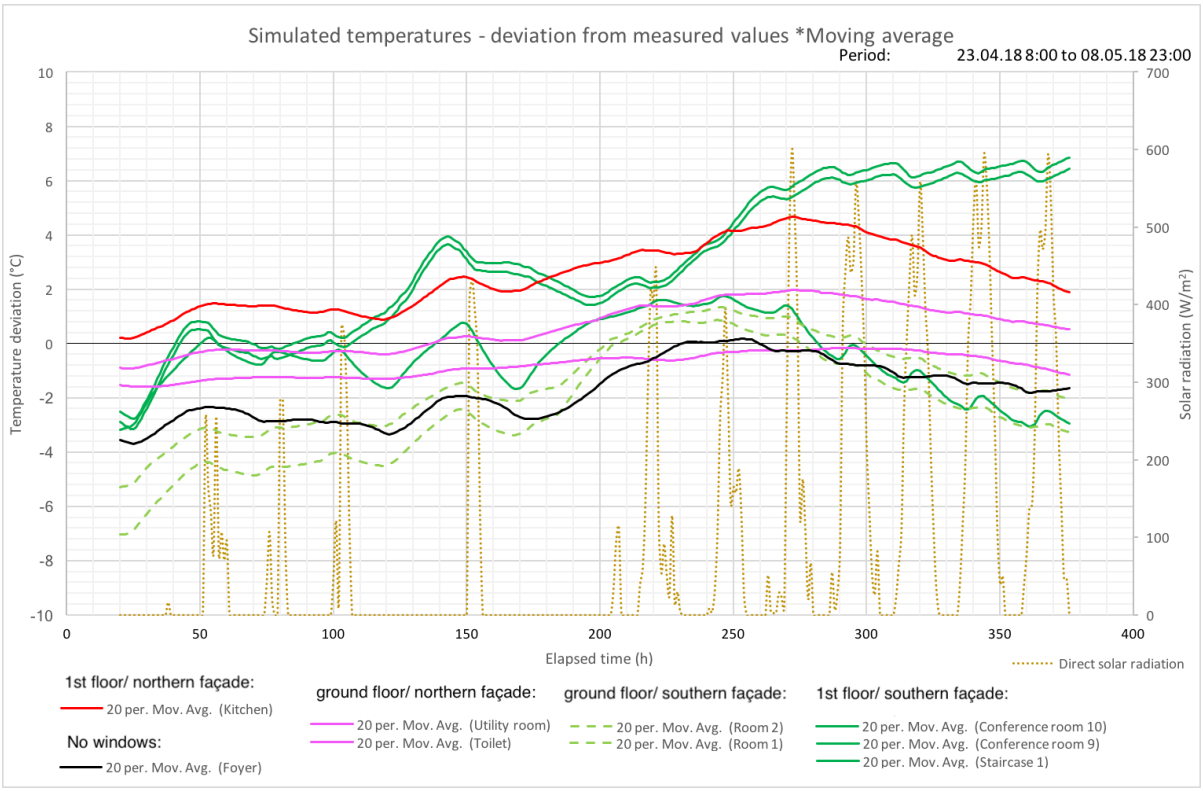

Figure 3.9: Baseline model - temperature deviation (20 period moving average) confronted with direct solar radiation.

It can be argued that overestimated temperatures on the first floor can be caused not only by intensive direct solar operation but also by excessive heat convection. Despite modelling simplified equivalent of the stairs (wooden band around the opening between the Staircase 1 and the Conference room), it does not reflect the reality of this element as it does not influence the hot air flow. Moreover, the baseline model comprises of separate thermal zones for Foyer, staircase (lower part), staircase (upper part), and the Conference room. This assumption might be questioned, thus it will be examined in input variations 2.5.3 and sensitivity analysis 3.3.2.

Last but not least, sensors location in the house should be discussed. TopMean which is the value obtained form the simulations is the operative (experienced) indoor temperature mean over the hour. It is calculated as average of mean radiant (area weighted surface temperature) and indoor air temperature. This seems to be a good approximation of the related readings in the actual house. However, it can be observed that rooms in which sensors were exposed to the sunlight (located close to the windows or just with a view to the sun) are subjected to considerably higher deviations than those in which the probes were hidden (i.e. Toilet - northern façade, small window with matte pane). Apparently, the spheres put on the devices do not protect from overheating due to sun operation. Therefore, level of confidence of some of the measured temperatures can be lower. This applies to the Conference room (the largest glazed surface and two sensors exposed to the direct sunlight), both rooms on the ground floor, and perhaps top of the staircase (if the radiation comes with low angle from south-east (see figure 2.8). It should be mentioned that the sensor in the kitchen is located right next to the door leading to the conference room on which sun shines for most of the day.

Conclusion To sum up, there is a number of aspects to consider and, perhaps, to improve regarding this investigation. As mentioned before the thermal zones layout will be subjected to input variation and examined in the sensitivity analysis. Besides, the properties of windows will be also analysed in 3.3.2 as they might have direct influence on the results. Taking into consideration the daily fluctuation of the deviations and the fact that the divergence increases in higher temperatures and excessive solar radiation, the material properties of the structure (including the heat capacity) are to be examined as well. On top of that, the placement of sensors in the actual building could be changed or at least the probes should be properly protected from the direct sunlight. In addition, the BSim model does not recognize the equipment (pieces of furniture) present for example in the Conference room. Also, the type (colour) of the room surfaces is not included. These might be yet another sources of the discrepancy between the simulated and measured values since they affect the longwave radiation calculations (emissivity and the view factors). This theory is backed up by the fact that the room with highest temperature divergence (the Conference room) is the only space with complex geometry (not one box-shaped cell like the other thermal zones), with large glazing area, and furniture in the middle.

Energy consumption

Unfortunately due to high temperatures in the Test House the set point for heating (20°C) was not reached in any room. Therefore, no energy consumption (apart from the use of electrical power to run the equipment) was recorded by the pulse meters connected with the data logger. Likewise, BSim simulation result indicates that the heaters did not turn on during the experiment period. This is why it has been decided to prolong the first phase of the experiment till 08.05.18, 23:00.

While it can be concluded that the dynamic simulations for the energy consumption should be repeated with either higher set point or in colder period of the year, the general overview of energy consumption can be made thanks to the *Documentation of the energy frame* for the Test House [**MOE (2016)**]. Generally, the building satisfies energy frame BK2020 with primary energy consumption of 19.7 kWh/m^2 per year (the limit is 20 kWh/m^2 per year).
[**Bygningsreglementet (2018)**]

Wall structure - absolute water content

General information The raw data - temperature and relative humidity at each sensor - and its treatment principles have been listed and depicted i appendices H.3, H.4, H.1, respectively. Measured parameters have been recalculated to absolute water content W and compared with values retrieved from simulations. This property expresses the mass of water (in kilograms) contained in 1 kg of substance (i.e. air). Furthermore, the breakdown into plots and group graphs have been included in appendix H.5.

Trends During nearly 18 days of the measurements (400h), the results from four sensors located at different depths inside the wall structure have been collected. The measurements are fixed as a benchmark for comparing simulations. It can be recognized, that the raw data as well as recalculated absolute water content and its deviations demonstrate the main trend of grouping sensors (simulation nodes) 1,2 (glued timber beam) and 3,4 (PUR foam) together

(very close). Although slight differences both in magnitude and shape among point 1 and 2 or 3 and 4 can be observed (figure 3.10), they tend to follow the same course. Like in the thermal zones temperatures discussed previously, the daily fluctuation of the deviation have been recorded. The positive peaks (overestimation) repeat from 9 am to 1 pm, whereas the negative peaks (underestimation) happen from 4 pm to 8 pm. Throughout the experiment period, the deviation of absolute water contents calculated in points 1,2 is larger (further from the horizontal, "zero" axis) than in points 3,4. Nodes 1 and 2 exhibit also significantly higher amplitude of fluctuations. The least fluctuating deviation is the one in point 4.

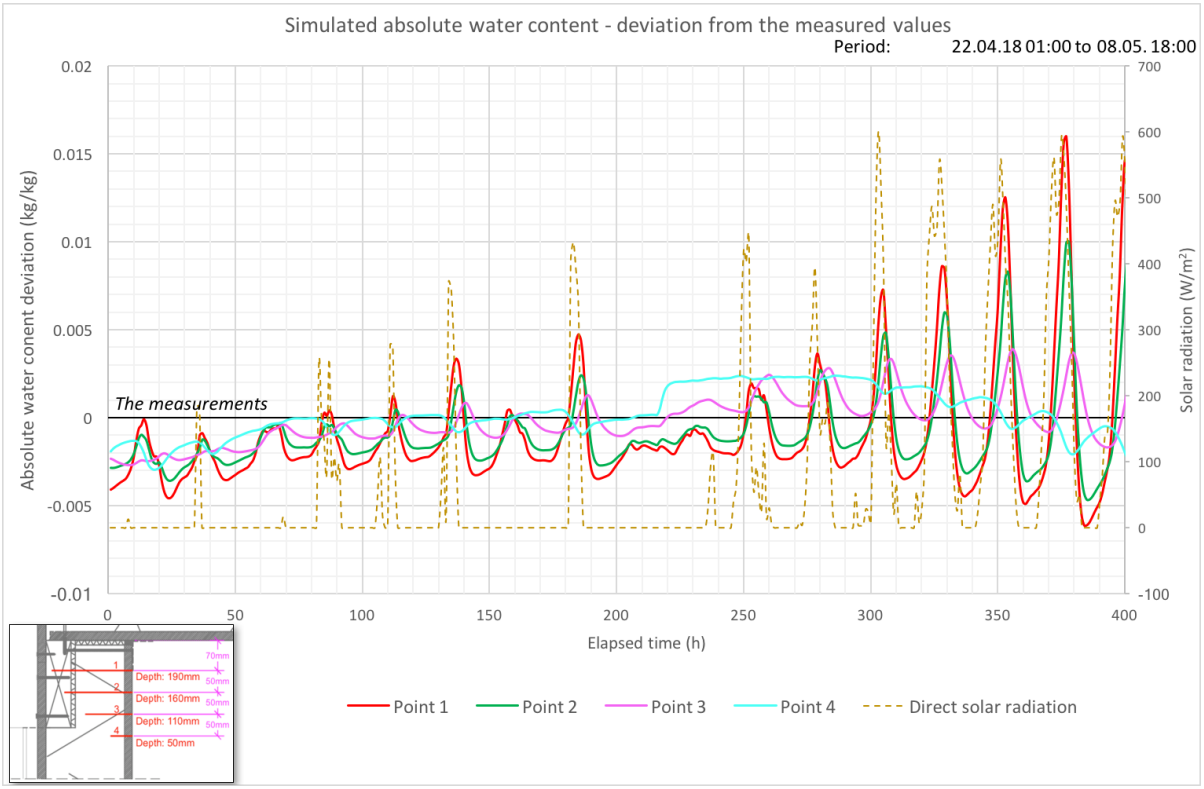

Figure 3.10: Wall structure - absolute water content deviation.

It can be clearly observed that in the beginning (up to around 220h - 250h, so 2nd/3rd of May) the deviation for all points remains rather low with underestimation trend. Then it rapidly increases for each sensor, however the highest amplitude of fluctuations (spanning through both negative and positive part of the plot) have been recorded for probes located in the glued timber beam. At the same time, values simulated for sensors placed in the PUR foam are mainly positively deviated (point 3 more than point 4). The course of these distributions is similar to the one discussed in the thermal zones temperature investigation. The graph appears to be influenced by analogical external factors, albeit by different form and proportion. Furthermore, an insight into relative humidity graphs (appendix H.4) shows that the simulated parameters tend to fluctuate wildly (especially in PUR foam - overestimated) while the measured values are almost fixed throughout the experiment period. On top of that, the temperatures recorded in sensors 3,4 are higher in the beginning (before 250h) than those in 1,2 in both cases (simulated - figure 3.12 and measured - figure 3.11). Subsequently, BSim temperatures in the timber beam (which is closer to the external environment) become significantly greater than related measurements.

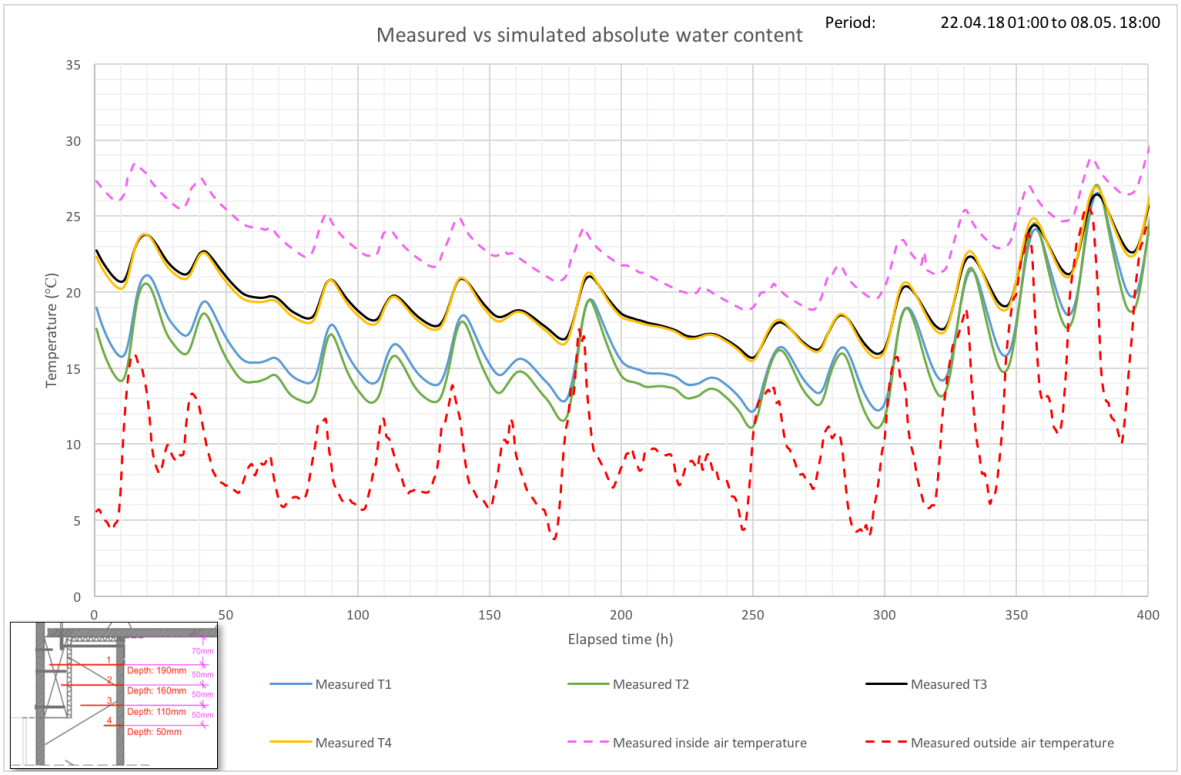

Figure 3.11: Measured temperatures inside the wall.

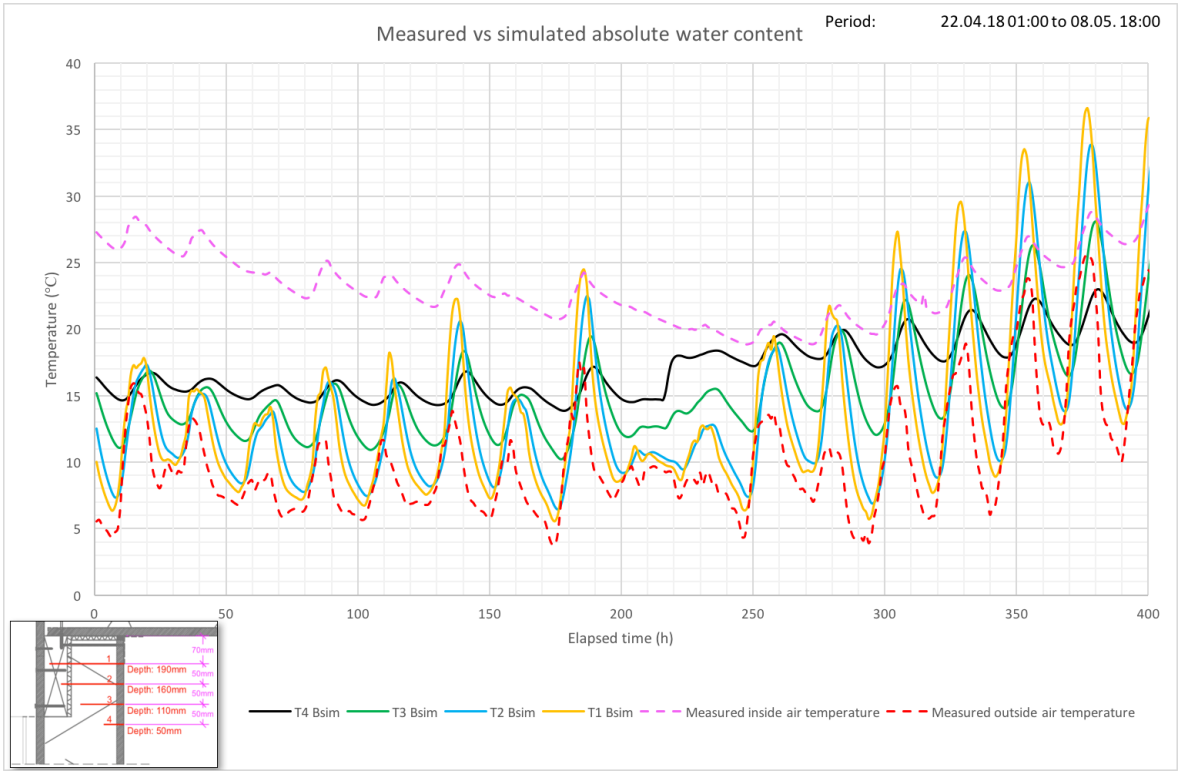

Figure 3.12: Simulated temperatures inside the wall.

Problem recognition There are three main sources of the discrepancy between simulations and measurements which can be identified based on the evidences mentioned in the previous paragraph.

Firstly, the divergence of relative humidity calculation indicates that the software fails to model material properties accurately. Since higher mean absolute errors have been recorded for the points inside the PUR core and the sorption isotherm of this material has been questioned before, it can be argued that this may have direct impact on the results in this part. This hypothesis is backed up by the fact that even though the beam is placed right next to the external environment, the relative humidities for this element are simulated more accurately as its isotherm is more reliable.

Secondly, it should be pointed out that the BSim model does not include façade cladding which is present in the actual building. Therefore, the virtual reproduction of the construction misses a layer which acts like a screen, blocking the direct solar radiation. As a result, the simulated beam is covered only by thin (2 cm) layer of fibre-cement board, thus it is heated by the sun almost directly. For that reason, the beam temperatures retrieved from the software are considerably higher during solar operation (and are even greater than those in the PUR foam). In reality, façade elements absorb thermal energy from the sun and then re-radiate to the main wall structure (Thermopanel). It is also expected that some of the heat dissipates as the space between the cladding and the panel is strongly ventilated.

Last but not least the quality of measurements should be discussed. It has been assumed in the beginning that the experimental values give the reference for comparison with the simulations. Nevertheless, an evidence of badly-installed sensor is undeniable. As figure 2.11 shows, there are multiple screws in the vicinity of points 1 and 2. Presumably, the second sensor has been placed too close to one of them since its readings remain lower than those of the first sensor throughout the experiment. This opposes the normal temperature distribution across an external wall. As an outcome, the absolute water content in point 2 is also lower than in the other point inside the beam.

Conclusion This case delivers information regarding the relations between computations of virtual models and real-life constructions. Nevertheless, there is a pool of aspects that should be taken into consideration when studying or developing this research. Primarily, to provide solid benchmark for the investigation, sensor number 2 should be reinstalled to eliminate the cold bridge which most likely occurred. Looking from the perspective of model definition, it should be borne in mind that in case of structural parts located close to the surface, it is vital to represent all layers which may seem to be redundant, considering their little influence on heat and moisture transport, but can impact other aspects in given study - i.e. direct solar radiation on the wall surface. Lastly, the material properties play a great role in such studies which examine structural characteristics. In this example, doubtful sorption isotherm of PUR foam might have changed the results by meaningful factor. Most importantly water permeability ought to be evaluated to check the ability of this porous material to allow fluids to pass through it.

3.3.2 Sensitivity analysis

Study presented in this section is based on the input variation explained in 2.5.3. Cases listed in table 2.3 have been realised as single models and the results of their computation have been demonstrated below. It should be borne in mind that the sensitivity analysis takes into consideration the temperatures in the thermal zones (not energy consumption or absolute water content inside the structure). Chart 3.13 indicates mean absolute errors for each case. Since the baseline model is used as a reference, all negative values (depicted in green, on the left) indicate that the error between this simulation and the measured values is lower than in the baseline model. On the other hand, the red bars (positive, on the right) indicate that given variation yields increased deviation from the measured temperatures with reference to the baseline model. What is more, the magnitude (length of the bars) demonstrates how sensitive is the model regarding studied property. The higher mean absolute error is, the sensitivity is more significant and vice versa. Please note that presented numbers are average values (over all rooms) for the entire house.

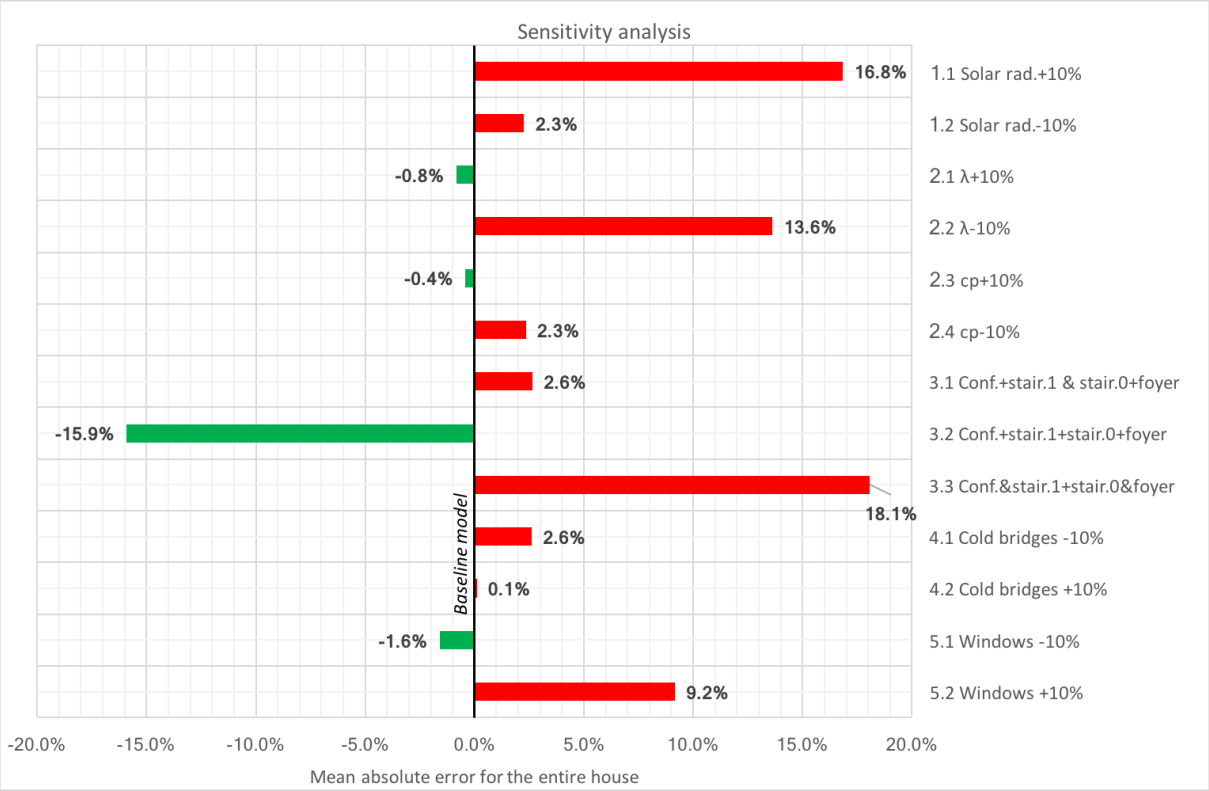

Figure 3.13: Sensitivity analysis results.

Each group of modifications exhibit significant impact on model's sensitivity by at least one of its cases. The only exception are the variations of cold bridges which seem to have minimal importance. It could be then speculated if simplified linear heat losses calculation scheme used by BSim is accurate enough, thus complex thermal simulations could be abandoned. At the same time, solar radiation input and thermal zones layout prove to be the most influential features of the computational model. Surprisingly however, even reduced proportion of solar radiation gives increased absolute mean error. Clearly, the model sensitivity is highest considering thermal zones design (both positively and negatively). The merge of conference

room, staircase and the foyer is undoubtedly beneficial for simulations accuracy and in fact, it reflects the real rooms layout fairly precisely. Contrastingly, modelling the staircase as one zone whereas the foyer and conference room are two separate ones yields vast increase of the error (the simulated temperatures are further apart from the measured). Another notable outcome is the fact that increase of materials thermal conductivity and decrease of windows U and g values, so in logical sense worsening their properties, gives positive result on the accuracy (increased comparing with the baseline model). Lastly, a slight favourable trend in case of increased heat capacity can be observed, albeit by marginal proportion.

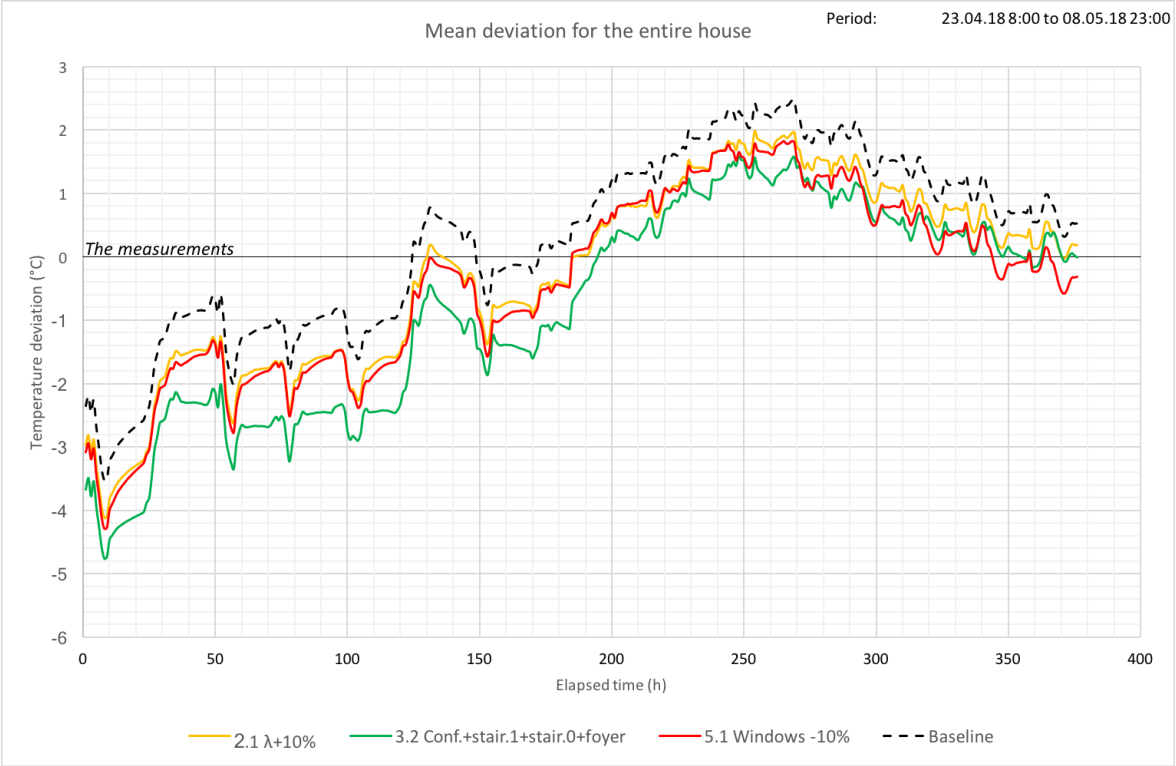

Figure 3.14: Modified models - deviation.

It can be concluded that the variations that give drop in the divergence between simulations and measurements are in fact underestimating the temperatures in the house. It is beneficial in the second part of the experiment (after 180h) but not in the initial phase (see figure 3.14). Nevertheless, it should be expected since all of them promote heat dissipation (by infinite mixing between cells in the same thermal zone) or heat transfer through partitions and windows as a result of increased thermal conductivities. Cases 2.1 and 5.1 seem to follow the same course and be close in terms of values up till 250h of elapsed time of the experiment. Nevertheless beyond this point it is decreased window properties variation that demonstrates lower deviation. It should be prompted that in this period, high solar operation occurs. Therefore it can be assumed that not the solar radiation input in the weather file is the reason of the deviation (even though it is the cause of the problem) but the window properties as they define the proportion of the heat that is allowed into the house. Definition of one thermal zone for the conference room, entire staircase and the foyer results in highly decreased temperatures, thus

the deviation distribution is moved downwards in the graph. It is suspected that the reason of this phenomena is the fact that the excessive heat accumulated mainly in the conference room is then dissipated and mixed among all the cells comprising the thermal zone. Therefore, even though the temperature in that space remains relatively high, the average of all spaces is decreased, resulting in significantly lower absolute mean error and deviation in this case.

All in all, the overheating is the most likely cause of the divergence between simulations and the measurements. Therefore any means which help to cool down the building bring positive change in computations accuracy. The thermal zones layout and solar radiation magnitude prove to have highest impact on the models output.

3.4 Summary

The last pages of this chapter should be considered as the culmination of the entire project. Most of the actions taken throughout this research were meant to enable or facilitate highly precise simulations presented here. It can be undoubtedly concluded that all pieces of this project successfully produced computational models which were then compared with the measurements from the real-size building. Besides, some additional cases with use of those data have been performed.

Materials testing phase has been beneficial not only due to collection of input data for simulations but also as an empirical evaluation of the physical properties. It gives an insight into how the characteristics are defined and gives possibility to confront them with the values declared by producers. Unfortunately, because of the time constraint and limited access to material samples (or difficulty in specimens' preparation), some of the values describing given components were retrieved from declarations of performance or other reliable resources. Therefore, the quality of the computational models has not been hindered.

Basic heat transfer simulations gave the correction factors or explicit values of linear heat losses required by BSim software in the subsequent stage of the project. Apparently, the program overestimates the cold bridges in all cases. On top of that, series of additional investigations have been performed to examine the correlation of thermal imaging with three-dimensional, time-dependant virtual studies and relations between simplified 1D and detailed 3D calculations. The former presented high level of convergence whereas the latter indicated that the basic estimations are reasonable and in most of the cases safe to use.

Ultimately, indoor climate simulations produced the outcome of temperatures in thermal zones. These values have been carefully compared with the measurements over 18 days of the experiment. The deviation of computed distributions proved to increase in the second part of the research, during high solar operation and increased temperatures. Similar tendency has been observed for absolute water contents inside the external wall. Unfortunately, due to relatively high outdoor and indoor temperatures, the set point for heating has not been reached, thus the energy consumption for heating could not be investigated. On top of the baseline model studies, the sensitivity analysis has been performed to capture importance of the input parameters on the results. Thermal zones layout, solar radiation and material properties proved to be highly influential factors while cold bridges the least.

Although the main cases have been accomplished and the project is deemed successful, some of its objectives could not be fully realised. Therefore, the following extension advice need to be outlined:

- Missing materials should be collected and examined in terms of their thermal and moisture properties. The water permeability test should be performed on the PUR foam sample. Specimens for the LFA method need to be prepared with precision due to high sensitivity of this method.
- Absolute water content evaluation could be performed for other elements of the building including the external wall in the utility room, roof under the terrace, and the slab over the driveway. Unfortunately, this yields the necessity of interference in the structure and architecture of the building. This might be troublesome since the house is used by the company as a showroom and should demonstrate high architectural quality.
- The vertical temperatures gradient measured by the set of Pt100 sensors should be examined over the experimental period and compared with simulations with use of Kappa model. The value of κ=0,5 is recommended for cases when there are no strong point heat sources (like in case of this project). However, this value can be reduced if the heating will be turned on, since an electric heater is in close vicinity of the sensors setup in the staircase.

Chapter 4

Discussion

Complexity and scope of this project led to some compromises due to time and workforce constraints. Since many of the presented methods require time-consuming advanced actions, a single researcher might find it troublesome to execute all studies within assigned period. This is why some assumptions and shortcuts were made to deliver the investigation in given time schedule. Although the general performance of this study is regarded successful, some of the cases and stated hypotheses could be examined thoroughly to produce deep analyses. Alternative experimental methods should be discussed as well.

Lack of energy consumption investigation is a major issue since it was meant to be one of the core parts of the entire research but there was no way to overcome it. Warm weather caused that the set point was not reached thus the heating did not turn on and therefore no data have been collected or retrieved from simulations. Although there are some energy consumption calculations available (study performed by MOE in Be10 software), they prove to be incomprehensive since were obtained as monthly average values. As a result, they indicate the yearly demand on energy (which describes the building and enables to assign it to building standards) but do not capture the dynamic changes that occur in the course of experimental period. For that reason, use of that data is deemed inadequate. The only option is to incorporate the values recorded by the electrical dashboard to compare with the dynamic simulations. Though such data is available from the last year (until the end of September) it faces the same problem of high temperatures. On top of that the heaters settings, doors and windows positions, number of people and time of their admittance, and most importantly the precise weather conditions are unknown. These are the factors which prevent from performing correct simulations to compare with that data. Therefore, the only possibility of executing this study is to realise all the steps described in this project (monitor all the essential parameters including weather) in colder period (heating season) or increase the set points drastically higher but it is unwanted by the company due to excessive overheating of the house.

Besides problems with PUR foam regarding sorption isotherms, other materials-related matters could be also executed in alternative ways. Firstly, it would be beneficial to conduct λ measurements directly in 23°C and 10°C, as the standard says, to obtain explicit values along the ones calculated from polynomial interpolation. On top of that the number of measurements should be increased to apply correction coefficients for tolerance interval from table C.1 [**DS/EN ISO 10456 (2008)**] to define declared values. Moreover, the moisture and ageing factors should be taken into consideration since even the PUR foam producer (DC-System In-

sulation A/S) states that it has an impact on the final results. Specific heat capacity evaluation is yet another crucial issue. The LFA method is of course accurate, quick and reliable but at the same time extremely sensitive and prone to errors if the specimens are not prepared with high precision. The samples made in the lab were unfortunately far from perfection. This is why the best recommendation is to repeat (or conduct for the first time) measurements with new specimens with exact size and with properly smooth surfaces covered completely with graphite paint. In addition, utilization of alternative, more robust method could be considered, for example electrical calorimeters. Lastly, the assumption of high similarity between the pinewood and glued timber (regarding their sorption properties) ought to be investigated. In other words, their isotherms should be compared, and the actual distribution for glued timber should be used in the absolute water content analysis as it is the core element of this study. Apart from that, another way of isotherms definition could be incorporated at least for the main materials (important regarding moisture transport) to validate VSA results, for example the experiment with use of ambient air.

Heat transfer simulations have been another interesting part of the project which could be extended. First and foremost, it would be undoubtedly valuable to confront the explicit values of ψ factor in the Test House joints with the corresponding, default ones listed in **[ISO 14683 (2017)]** and compare by how much the SIP solutions are lower than the "traditional" ones. Regarding the interdimensional investigation, examination of combined 2D and 1D estimations and their different variations could be performed and confronted with complex three-dimensional benchmark. An attempt for 2D calculation of the heat loss in case B was made but due to multiple overlapping of the models and geometrical difficulties the results proved to be inadequate and produce more than double overestimation. Nonetheless, further analysis might be performed. Besides, there is a possibility of more thermal imaging executions to create larger sample pool to contrast them with virtual Comsol models. The measurements need to be done in different weather and indoor climate conditions with different structural joints. Only then the real correlation between reality and simulations could be captured. Last but not least, the 3D models themselves and their meshes in particular could be improved.

All in all, this study gives experimental data together with its analysis and reflections on the trends with explanations of possible sources of the differences between measurements and simulations. Nonetheless, each of the cases (materials testing, heat transfer calculations etc.) can be treated as separate study and possibly expanded according to the recommendations stated in the summary and discussion parts of this report.

Bibliography

[1] [**BSim (2013)**] - BSim User's Guide, Danish Building Research Institute, Aalborg University, Copenhagen, Denmark, 2013

[2] [**BSim database (2011)**] - BSim2011 materials database, Danish Building Research Institute, Aalborg University, Copenhagen, Denmark, 2011

[3] [**Bygningsreglementet (2015)**] – Danish Building Regulations 2015, Trafik-, Bygge- og Boligstyrelsen, Copenhagen, Denmark, 2015

[4] [**Bygningsreglementet (2018)**] – Danish Building Regulations 2018, Trafik-, Bygge- og Boligstyrelsen, Copenhagen, Denmark, 2018

[5] [**Comsol Multiphysics (2018)**] - User's Guide, COMSOL INC., 2018

[6] [**DC-System catalogue (2018)**] – Official catalogue of products, DC-System Insulation A/S, Aars, Denmark, 2018

[7] [**DC-System website (2018)**] – Official company website, http://www.dc- system.dk, DC-System Insulation A/S, Aars, Denmark, 2018

[8] [**DC-System**, **Test House (2015)**] - Technical documentation (drawings) of the Test House, DC-System Insulation A/S, Aars, Denmark, 2015

[9] [**Decagon Devices**, **Inc. (2016)**] – Vapor Sorption Analyzer - Operator's Manual, Decagon Devices, Inc., Pullman, USA, 2016

[10] [**DS 418 (2011)**] - Calculation of heat loss from buildings, Danish Standards, Copenhagen, Denmark, 2013

[11] [**DS/EN ISO 10456 (2010)**] - Building materials and products - Procedure for determining declared and design thermal values, Danish Standards, Copenhagen, Denmark, 2010

[12] [**DS/EN ISO 12571 (2013)**] – Hygrothermal performance of building materials and products – Determination of hygroscopic sorption properties, Danish Standards, Copenhagen, Denmark, 2013

[13] [**Eads**, **Lowry (2000)**] - Thermography: Practical Guide, ASHRAE Journal's, Lowry G. Eads, Richard A. Epperly, John Snell Jr., 2000

[14] [**EN ISO 6946 (2007)**] - Building components and building elements - Thermal resistance and thermal transmittance - Calculation method, European Standards, Brussels, Belgium, 2007

[15] [**engineeringtoolbox.com (2018)**] - Engineering ToolBox - Resources, Tools and Basic Information for Engineering and Design of Technical Applications, website, 2018

[16] [**Hansen**, **Kurt Kielsgaard (1986)**] – Sorption isotherms - A catalogue, Building Materials Laboratory at The Technical University of Denmark, Copenhagen, Denmark, 1986

[17] [**ISO 14683 (2011)**] - Thermal bridges in building construction – Linear thermal transmittance – Simplified methods and default values, Danish Standards, Copenhagen, Denmark, 2011

[18] [**Ivanov Antonov**, **Yovko (2018)**] – Introduction to measurement methods for water vapor sorption in building materials - lecture slides, Indoor Environmental Engineering at Aalborg University, Aalborg, Denmark, 2018

[19] [**Johra**, **Hicham (2015)**] – Thermal Conductivity Measurement with the Guarded Hot Plate Apparatus, Step by Step Guide, Indoor Environmental Engineering at Aalborg University, Aalborg, Denmark, 2015

[20] [**Johra**, **Hicham (2015)**] – Thermal Conductivity Measurement with the Laser Flash Method, Step by Step Guide, Indoor Environmental Engineering at Aalborg University, Aalborg, Denmark, 2015

[21] [**meteoblue.com (2018)**] - Online weather database, meteoblue AG, Basel, Switzerland, 2018

[22] [**MOE (2016)**] - DC Provehus - Endelig energiberegning, Dokumentation af energirammen, Aarhus, Denmark, 2016

[23] [**Netzsch Geratebau GmbH (2011)**] - Operating Instructions Nano-Flash-Apparatus LFA 447, Netzsch Geratebau GmbH, Selb, Germany, 2001

[24] [**PERGO laminate (2013)**] - Declaration of performance, Laminate floorcoverings, Wielsbeke, Belgium, 2013

[25] [**PXL HVAC (2016)**] - New Mollier diagram, spreadsheet, PXL High school, Diepenbeek, Belgium, 2016

[26] [**Reissmann (2018)**] - Pt100, Pt500, Pt1000 Product Information, Manual, Rosengarten-Uttenhofen, Germany, 2018

[27] [**Testo (2018)**] - testo 875 Thermal imager - Instruction manual, Testo SE Co. KGaA, Lenzkirch, Germany, 2018

[28] [**Thermal properties database (2017)**] - Thermal properties database, Hicham Johra, Indoor Environmental Engineering at Aalborg University, Aalborg, Denmark, 2017

[29] [**Troldekt akustik (2011)**] - Declaration of performance, Troldtekt akustik, Troldtekt agro og Troldtekt ventilation (aktiv), Bureau Veritas Certification Denmark A/S, Fredericia, Denmark, 2011

[30] [**VELFAC**, **Test House (2015)**] - Technical documentation of the Test House, VELFAC A/S, Horsens, Denmark, 2015

[31] [**Zajas, Jan; Heiselberg, Per (2013)**] - Measurements of thermal diffusivity, specific heat capacity and thermal conductivity with LFA 447 apparatus, DCE Technical Report No. 144, Department of Civil Engineering, Architectural Engineering at Aalborg University, Aalborg, Denmark 2013

[32] [**AAU group B148 (2017)**] - PUR-paneler som fremtidens klimaskaerm, student report, group B148, Department of Civil Engineering at Aalborg University, Aalborg, Denmark, 2017

[33] [**AAU Klimalab (2016)**] – Air leakage analyse for DS/EN 13829 - experiment report, Indoor Environmental Engineering Laboratory at Aalborg University, Aalborg, Denmark, 2016

Appendix A

Test house documentation

A.1 Construction drawings

This section includes plan drawings and cross-sections of the Test House construction:

- Figure A.1 - Wall panels plan;
- Figure A.2 - Cross-section A-A;
- Figure A.3 - Cross-section B-B;
- Figure A.4 - Slab construction.

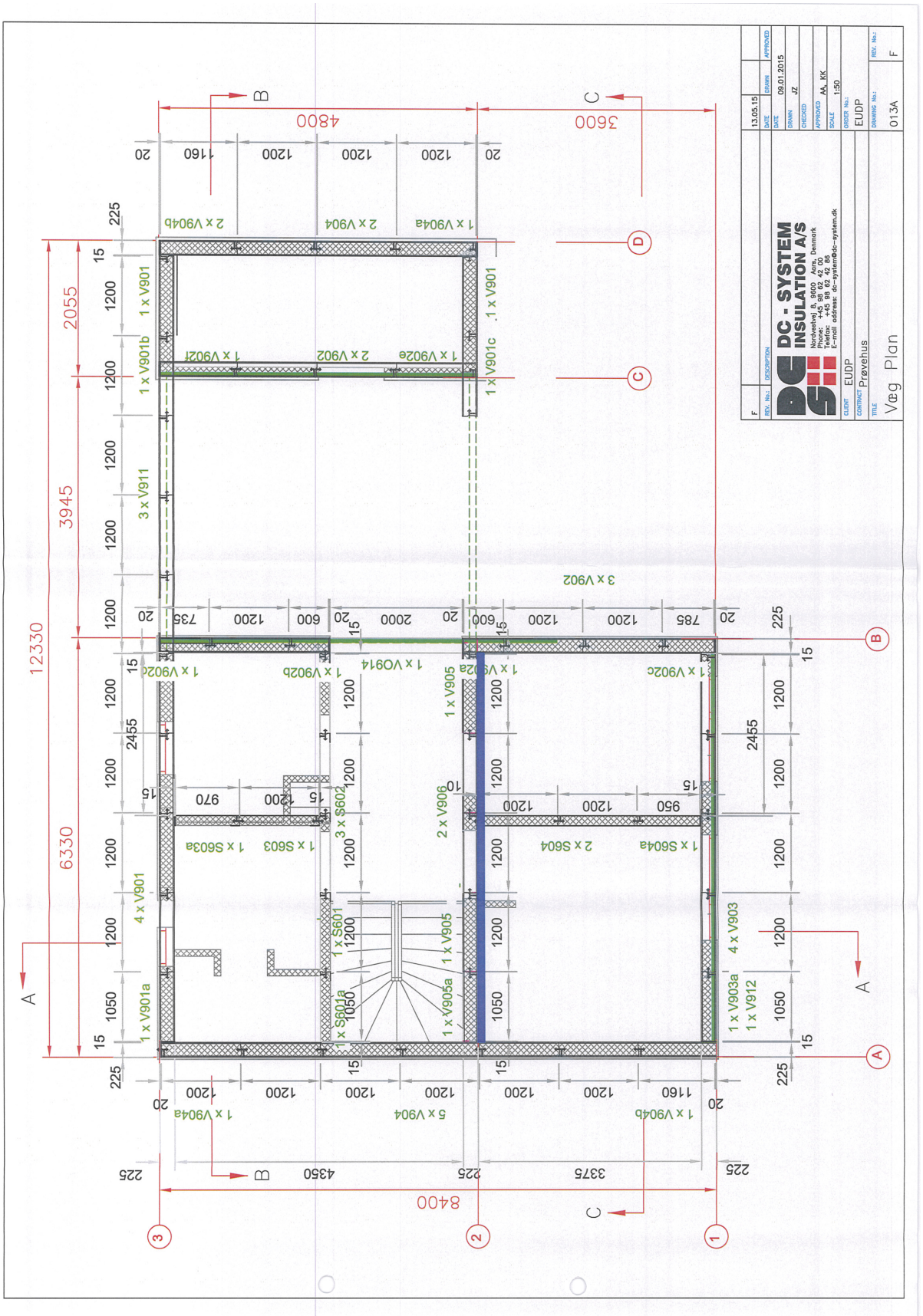

Figure A.1: Wall panels plan. **[DC-System, Test House (2015)]**

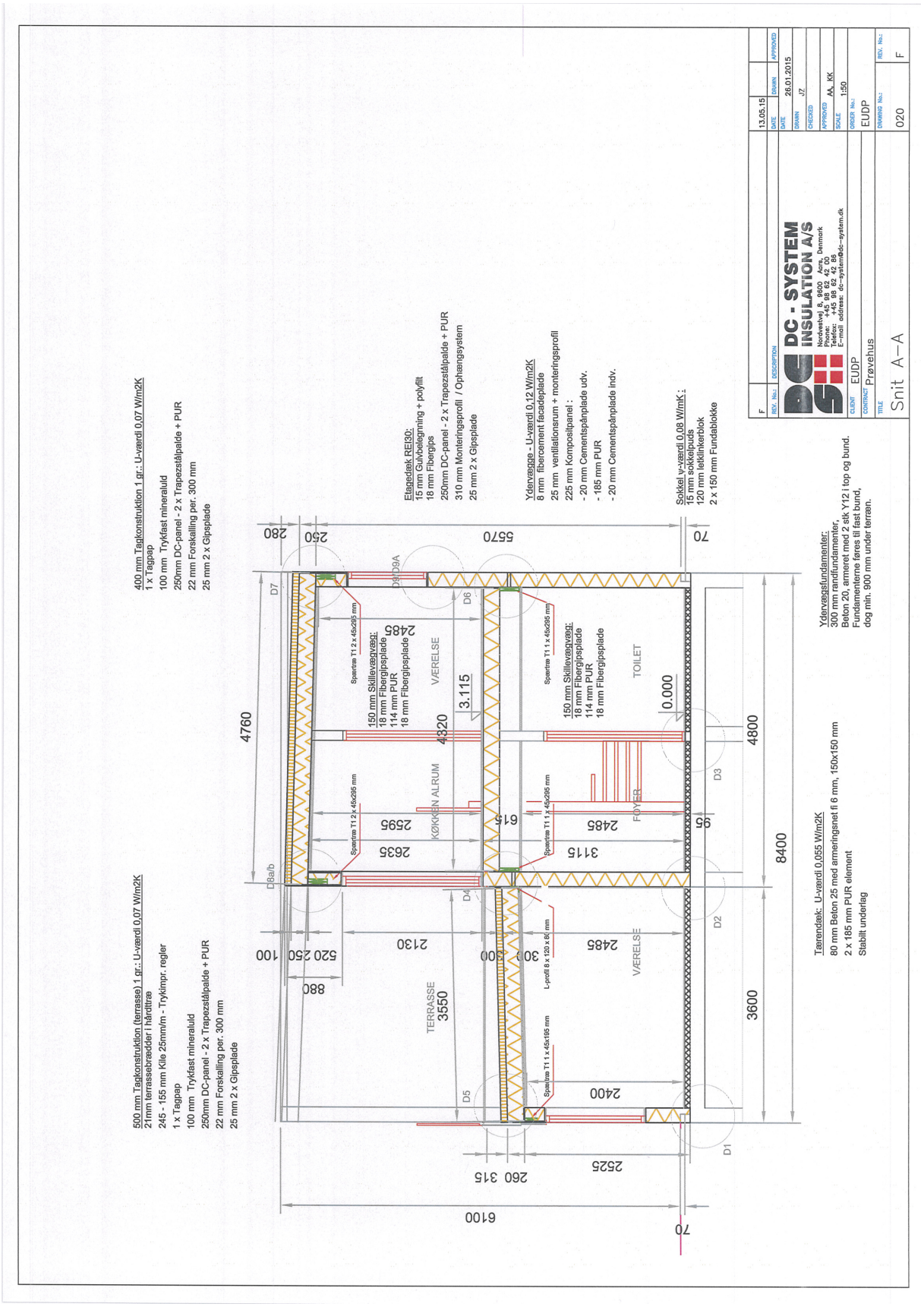

Figure A.2: Cross-section A-A.[**DC-System, Test House (2015)**]

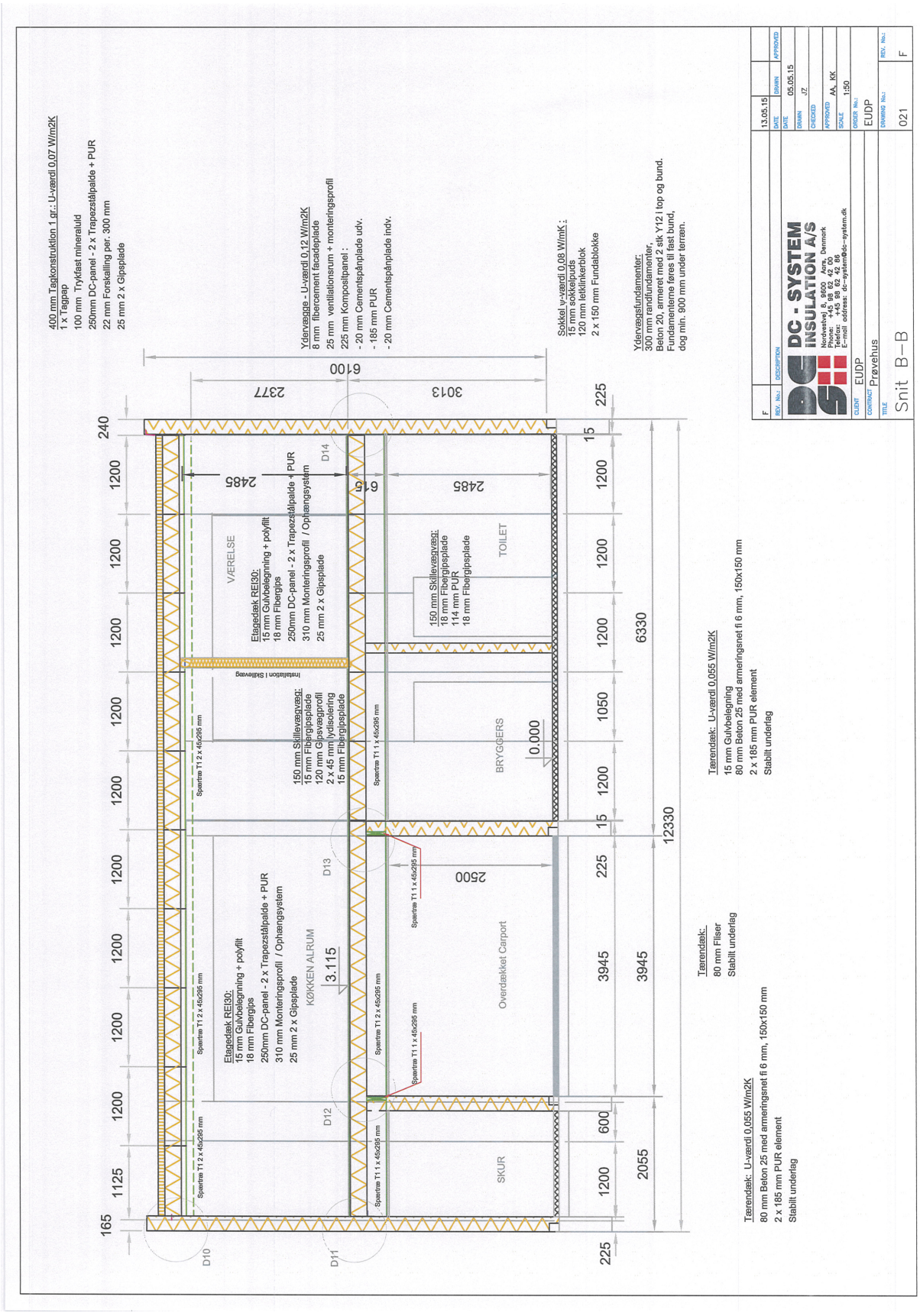

Figure A.3: Cross-section B-B.**[DC-System, Test House (2015)]**

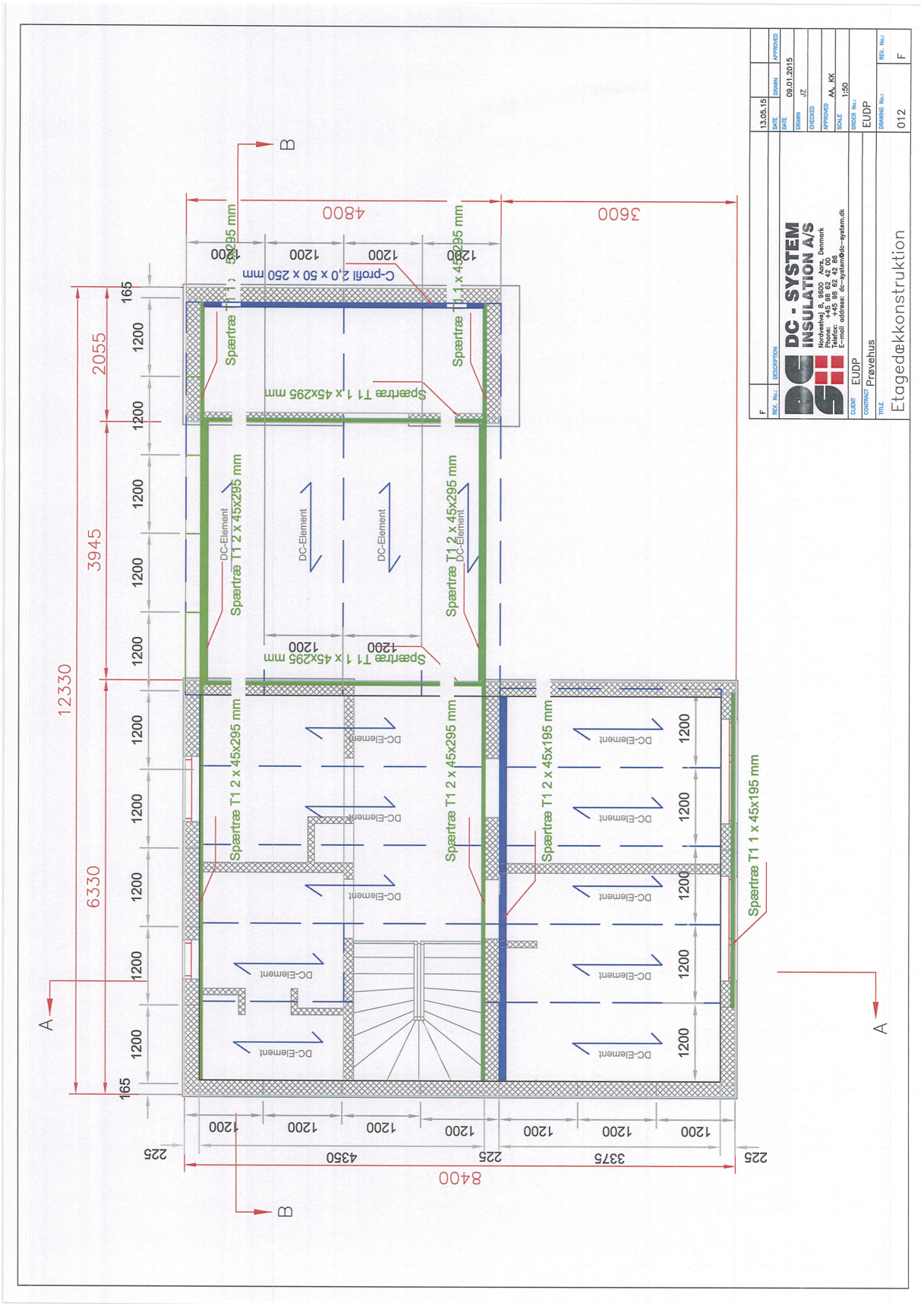

Figure A.4: Slab construction.[**DC-System, Test House (2015)**]

A.2 Details

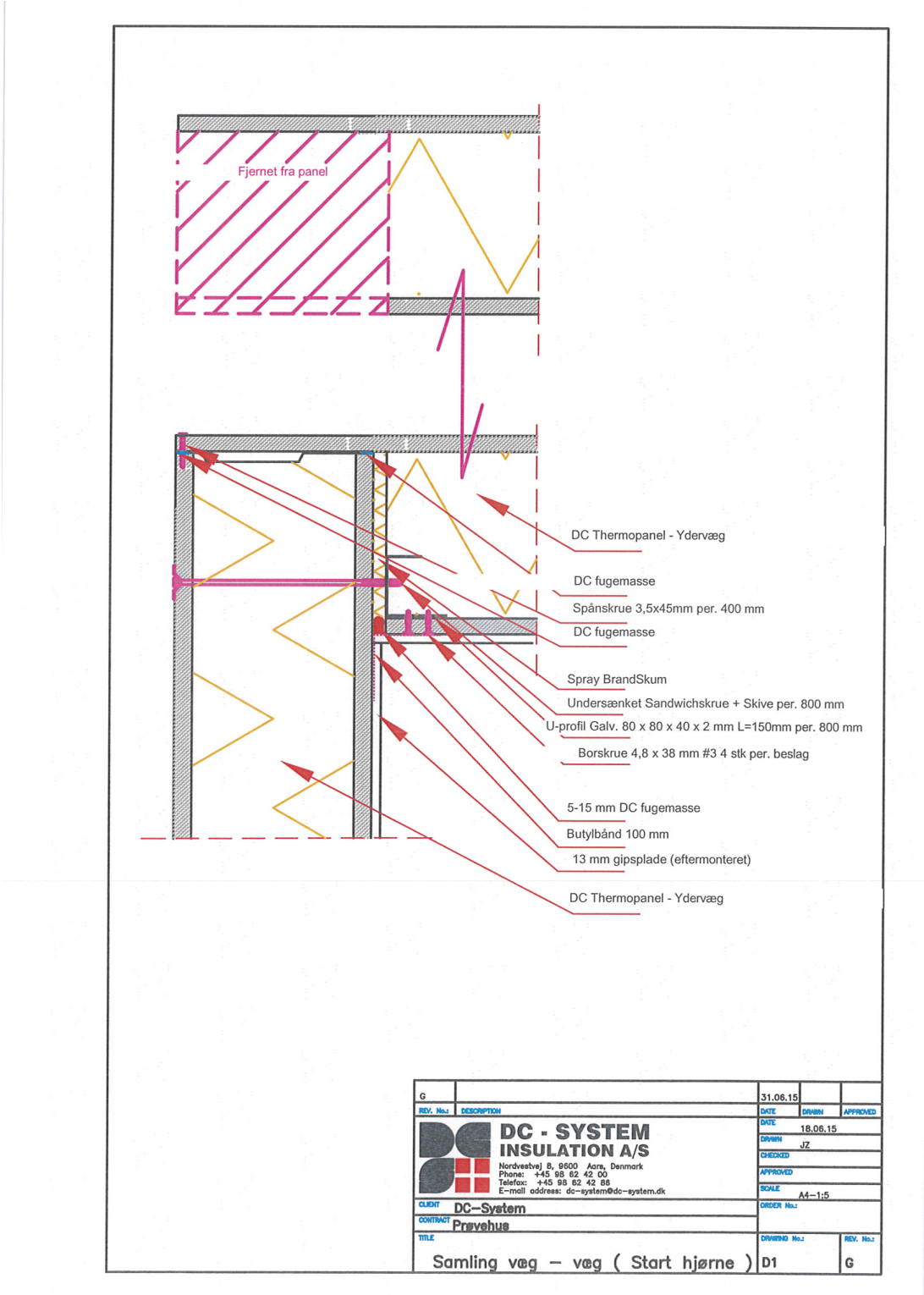

Figure A.5: Detail: Wall-wall (corner). This joint was constructed with removed part of the cement board from the panel inside. **[DC-System, Test House (2015)]**

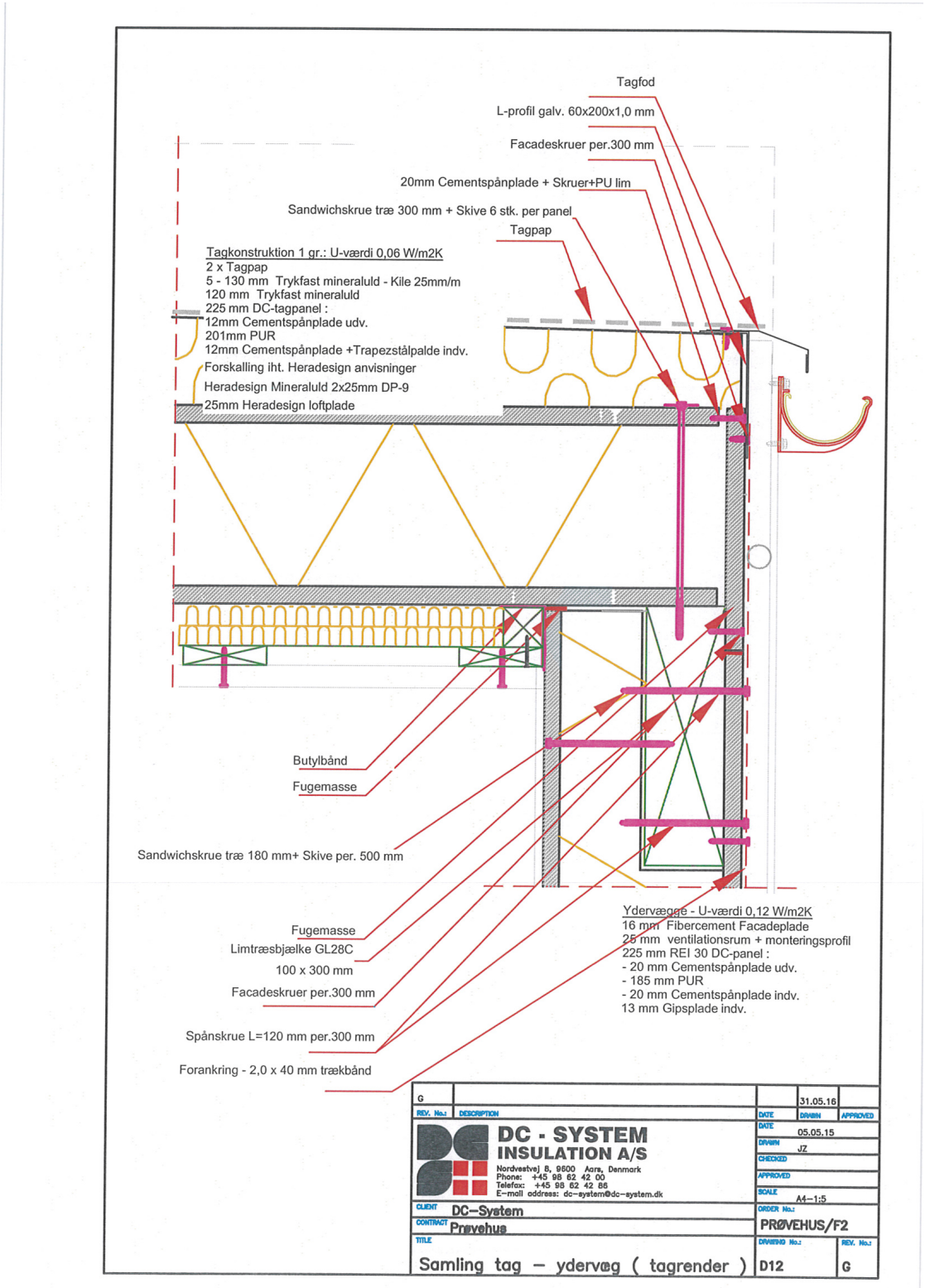

Figure A.6: Detail: Wall-roof (beam). **[DC-System, Test House (2015)]**

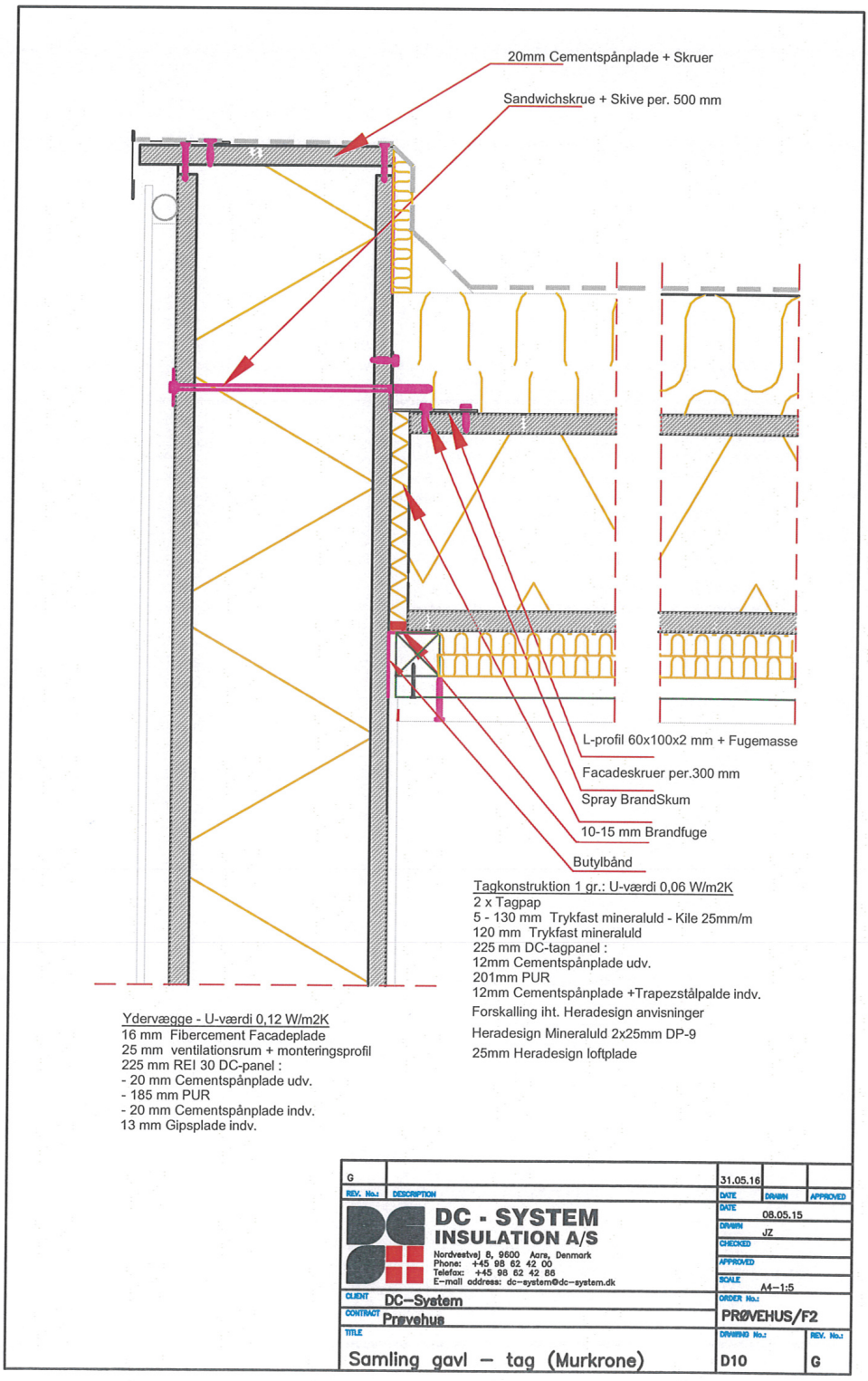

Figure A.7: Detail: Wall-roof (gable).[**DC-System, Test House (2015)**]

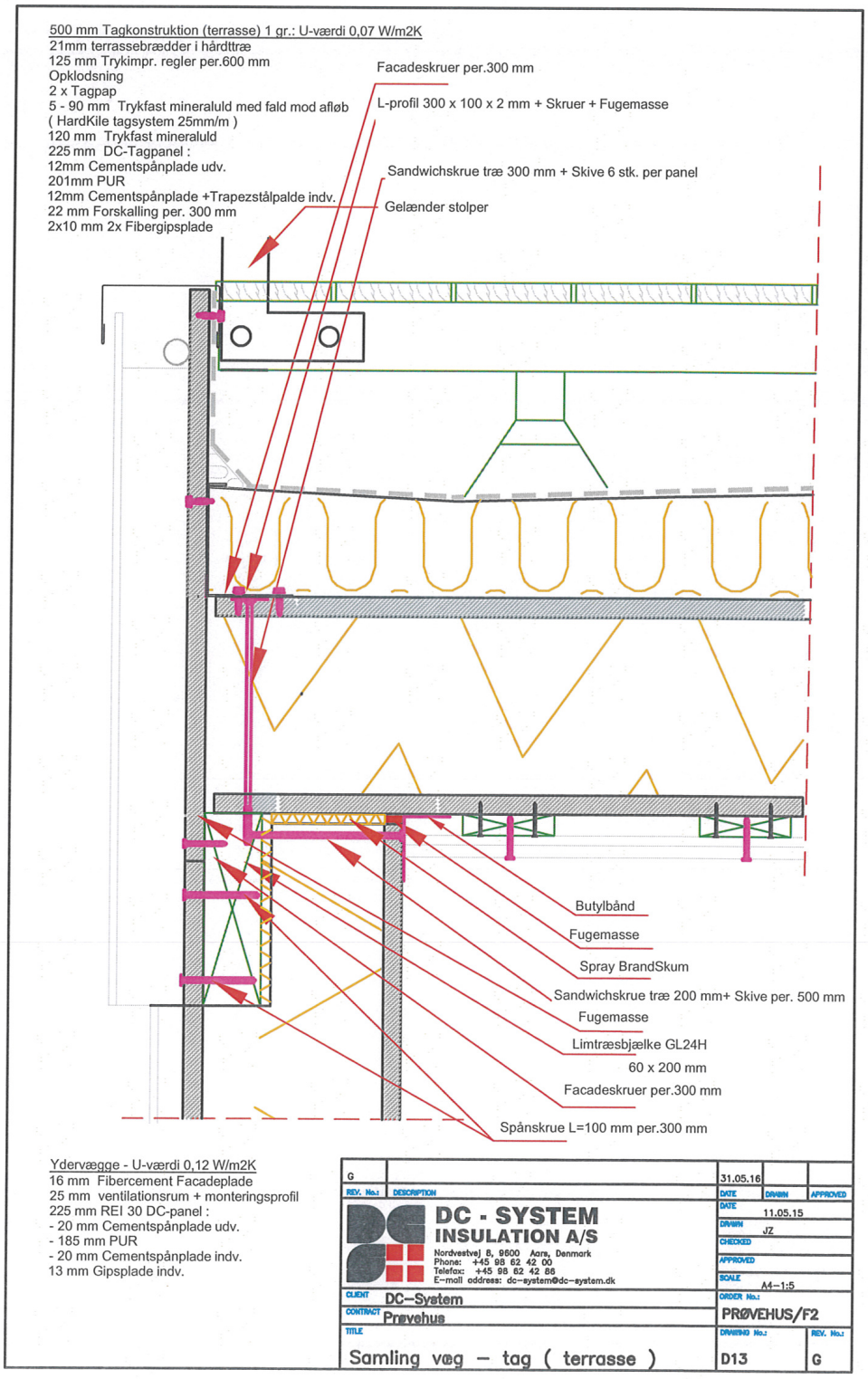

Figure A.8: Detail: Wall-roof (Room 1).[**DC-System, Test House (2015)**]

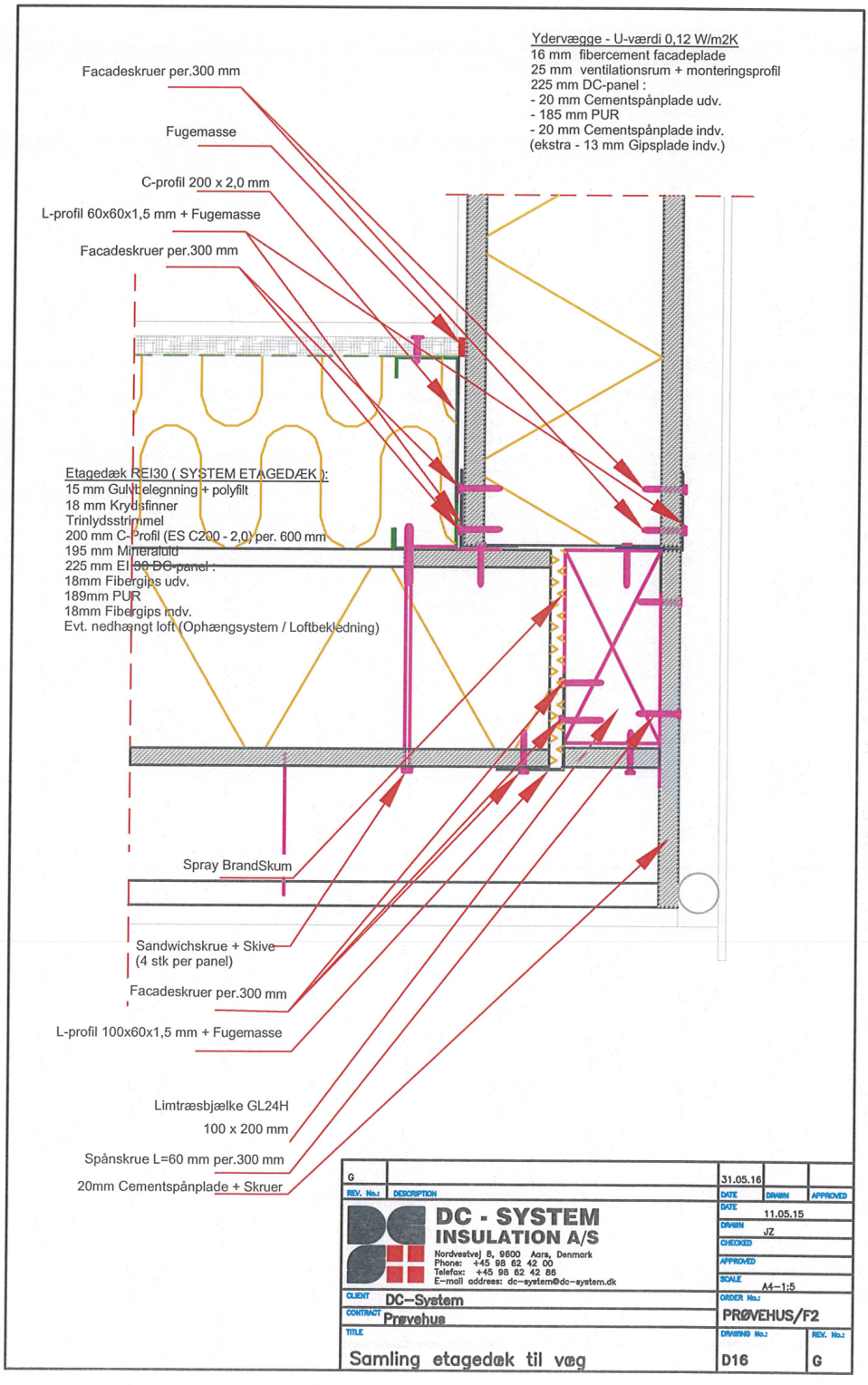

Figure A.9: Detail: Wall-slab (Conference room). [**DC-System**, **Test House (2015)**]

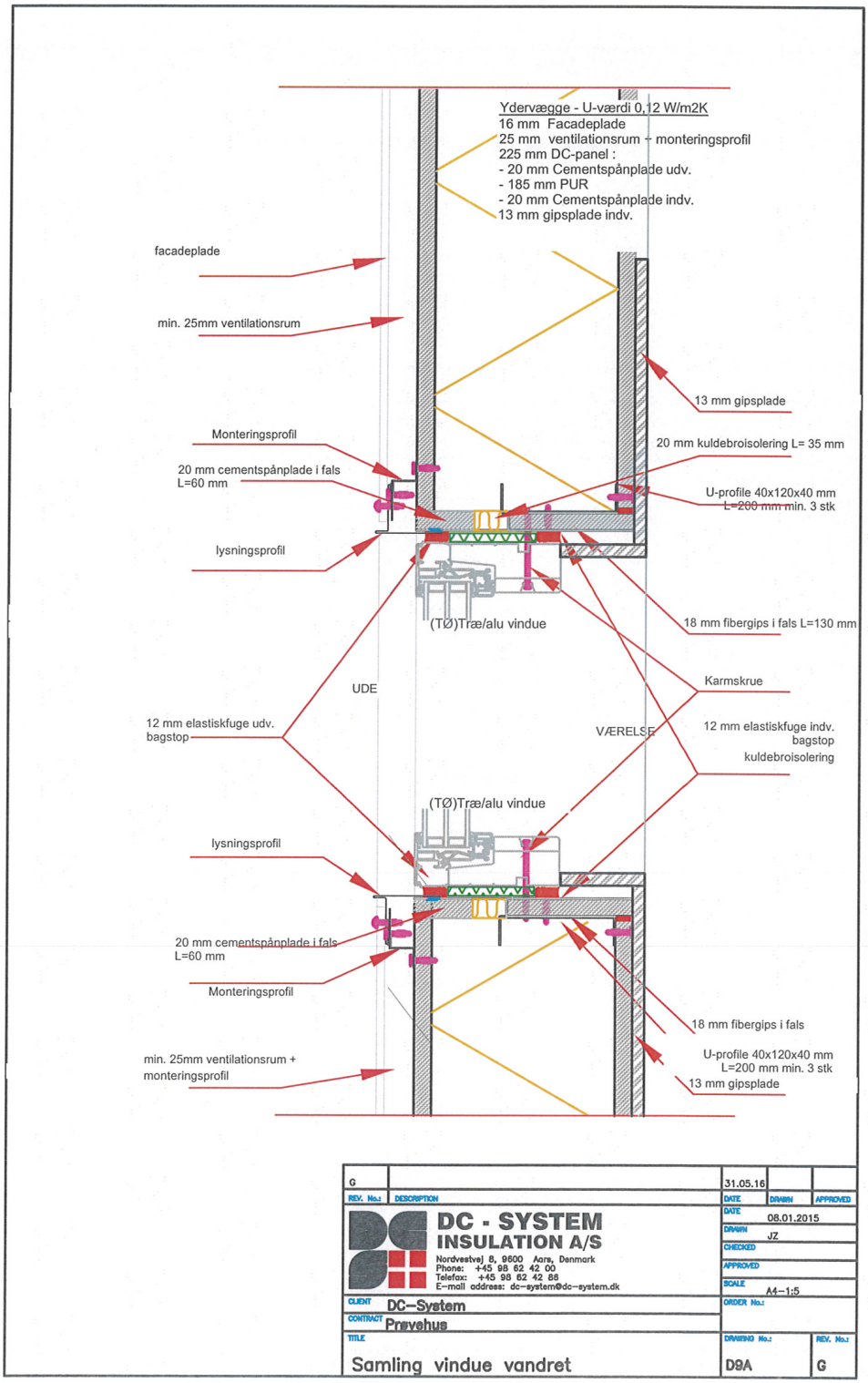

Figure A.10: Detail: Wall-window. **[DC-System, Test House (2015)]**

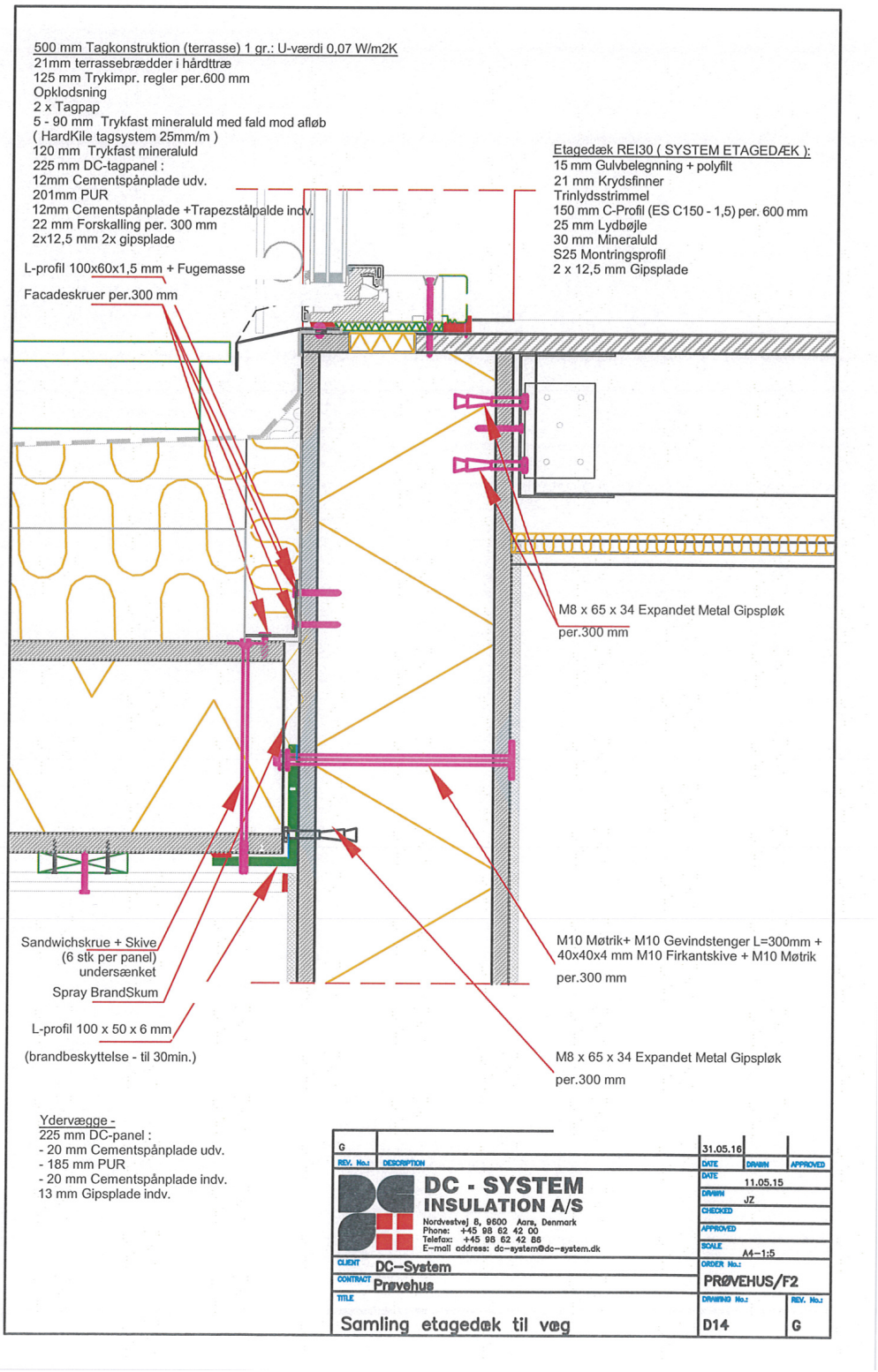

Figure A.11: Detail: Room 1 roof - building. [**DC-System, Test House (2015)**]

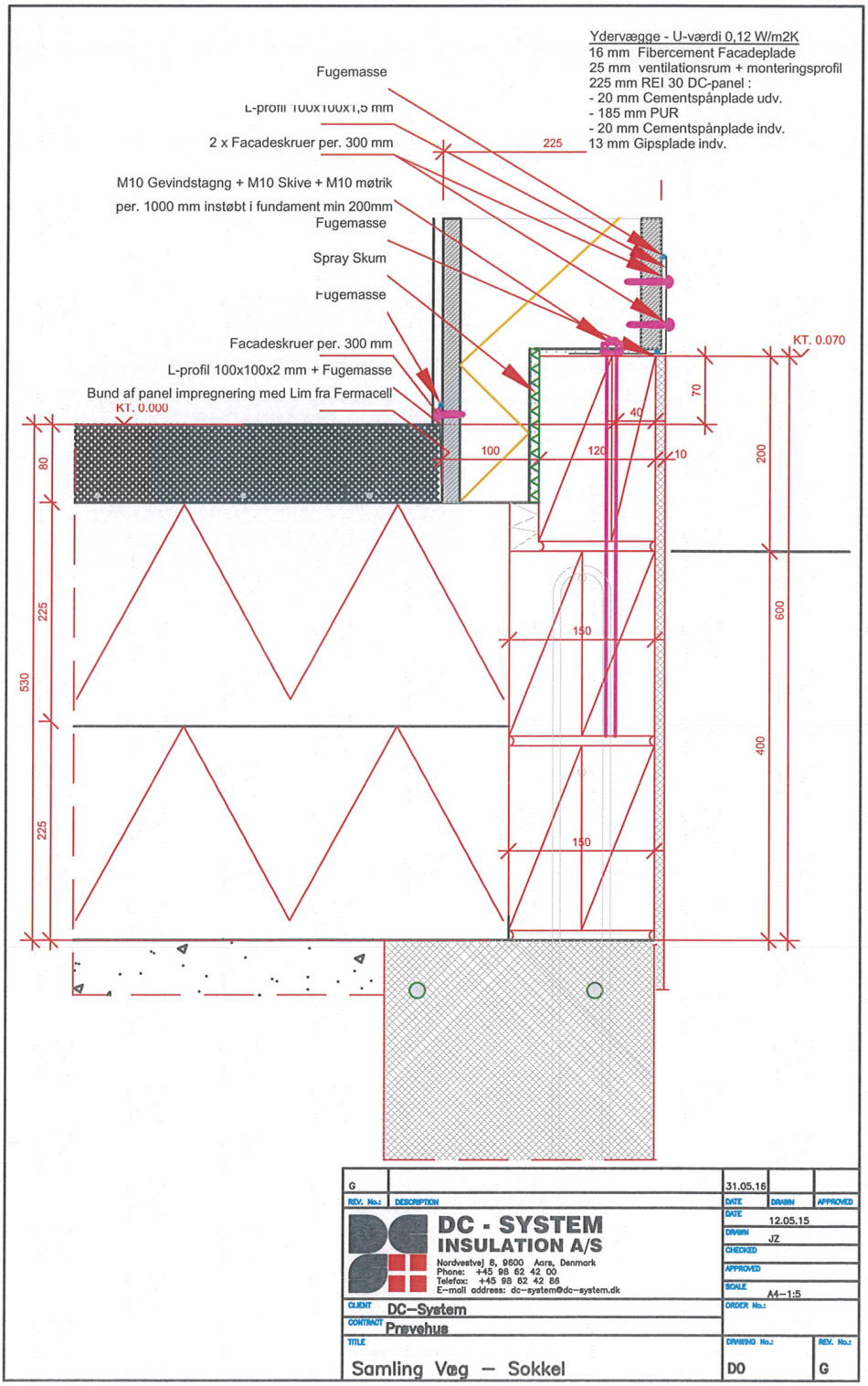

Figure A.12: Detail: Wall-foundation. [**DC-System, Test House (2015)**]

A.3 Doors and windows

DATABLAD - ENERGIFORHOLD

VELFAC®

Projektnr.	Projektnavn	Vor ref.	Side	Dato
160551-0101	Prøvehus	CJ	1	03.07.15

			Mængde			Vindue				
Pos.	Alt	Type	Antal	Aw	A	Uw*	Ff*	gg*	LT*	Ew***
3		V1.H	2	1.85	3.70	0.93	0.78	0.51	0.71	-5.9
6		V1.V	1	1.85	1.85	0.93	0.78	0.51	0.71	-5.9
9		V2	1	0.91	0.91	0.94	0.78	0.51	0.71	-6.8
12		V3	1	0.68	0.68	1.02	0.73	0.51	0.71	-19.0
15		V4.V	1	2.32	2.32	0.90	0.79	0.51	0.71	-2.2
18		V4.H	1	2.32	2.32	0.90	0.79	0.51	0.71	-2.2
21		TD1	1	5.05	5.05	0.84	0.82	0.51	0.71	6.2
24		V5.1	1	5.05	5.05	0.86	0.81	0.51	0.71	3.4
27		V5.2	1	2.53	2.53	0.87	0.81	0.51	0.71	2.5
30		D2	1	4.20	4.20	0.81	0.74	0.53	0.74	3.8
36		D3	1	2.07	2.07	0.95	0.28	0.53	0.35	-56.7

Figure A.13: Doors and windows in the test house - data sheet. **[VELFAC, Test House (2015)]**

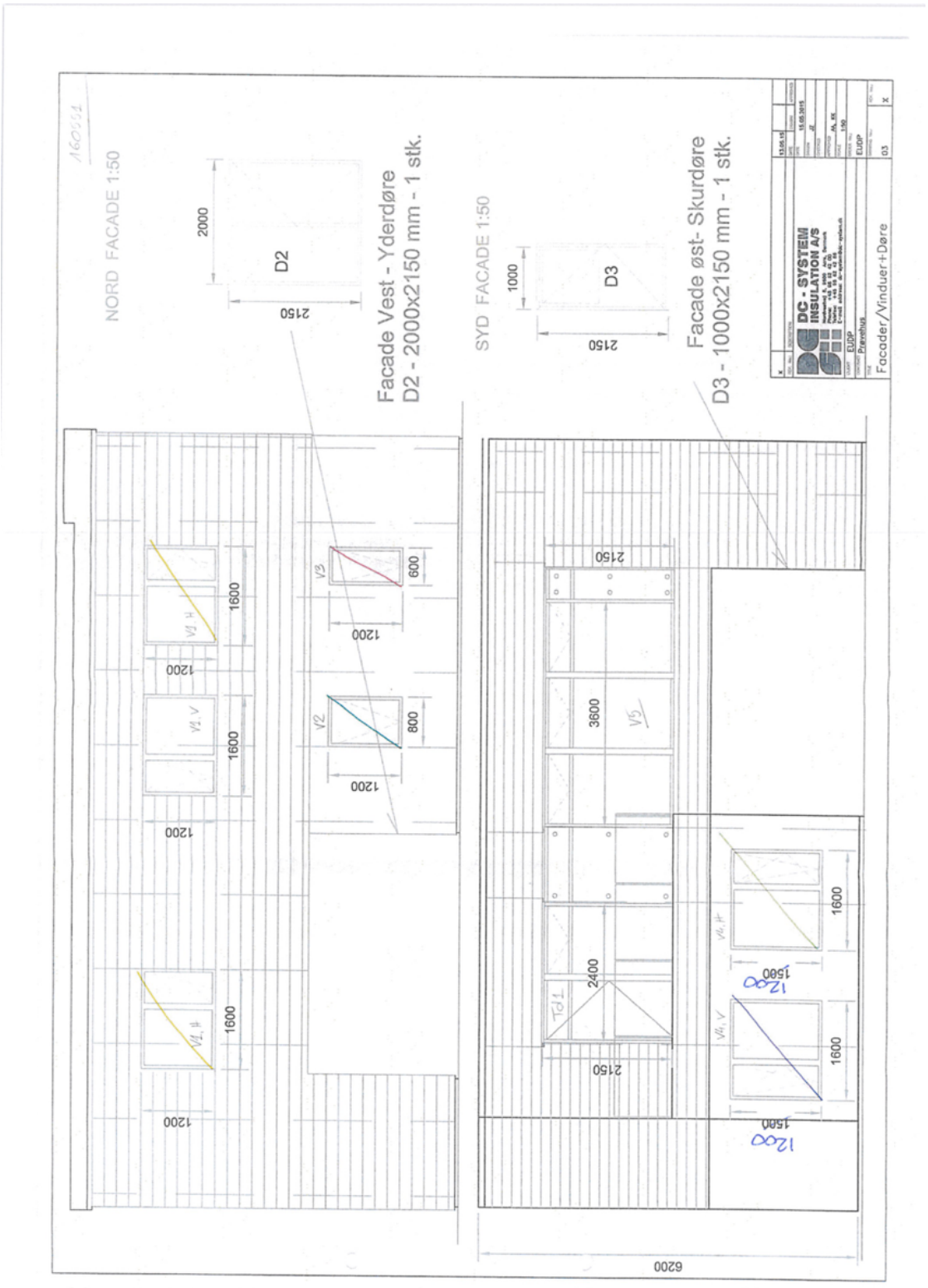

Figure A.14: Doors and windows in the test house - drawings. [**DC-System**, **Test House (2015)**]

Appendix B

Weather station

B.1 2D Ultrasonic Anemometer calibration

The 2D ultrasonic anemometer has been calibrated, in order to obtain an equation, describing the wind speed as a function of the voltage output. In order to calibrate the 2D ultrasonic anemometers, the following instruments are needed:

- FT702 ultrasonic anemometer number 361
- Wind tunnel
- Laptop with LabView
- NI-USB 6009 Datalogger
- 7-28 V power supply
- Micro manometer number 128
- Mensor barometer number 324
- F200 precision thermometer number 325
- Honeywell HIH-4000 humidity sensors

Procedure

The 2D ultrasonic anemometer has been located in front of the wind tunnel. Furthermore, the anemometer has been connected to the NI-USB 6009 datalogger and a 24V power supply. By use of the orifice plates and the micro manometer, the wind tunnel produces a controlled wind speed, where after the corresponding output voltage from the anemometer is read off.

The pressure drop across the orifice plate is used to calculate the velocity, as shown in equation B.1 and B.2.

$$v_{23mm} = 0,744 \cdot \Delta p^{0,4516} \tag{B.1}$$

$$v_{46mm} = 2,886 \cdot \Delta p^{0,49} \tag{B.2}$$

However, the true wind speed depends in the density of the air. Thus, the true velocity is calculated with equation B.3.

$$v_{true} = v_n \cdot \sqrt{\frac{1,2}{\rho_{air}}} \tag{B.3}$$

In order to calculate the density of the air, the pressure, temperature and relative humidity must be known. These values are determined with the Mensor barometer, the F200 precision thermometer and the HIH-4000 humidity sensors, respectively.

This procedure is repeated for five different points, in order to produce a conversion formula.

Results

Due to limited experiment range (just two orifice plates which give low air velocity up to approx. 5 m/s), the obtained conversion formula B.4 is deemed to be inaccurate since the measurement range of the sensor is 0-70 m/s.

$$v_n = 20,198 \cdot Voltage_n + 0,6699 \tag{B.4}$$

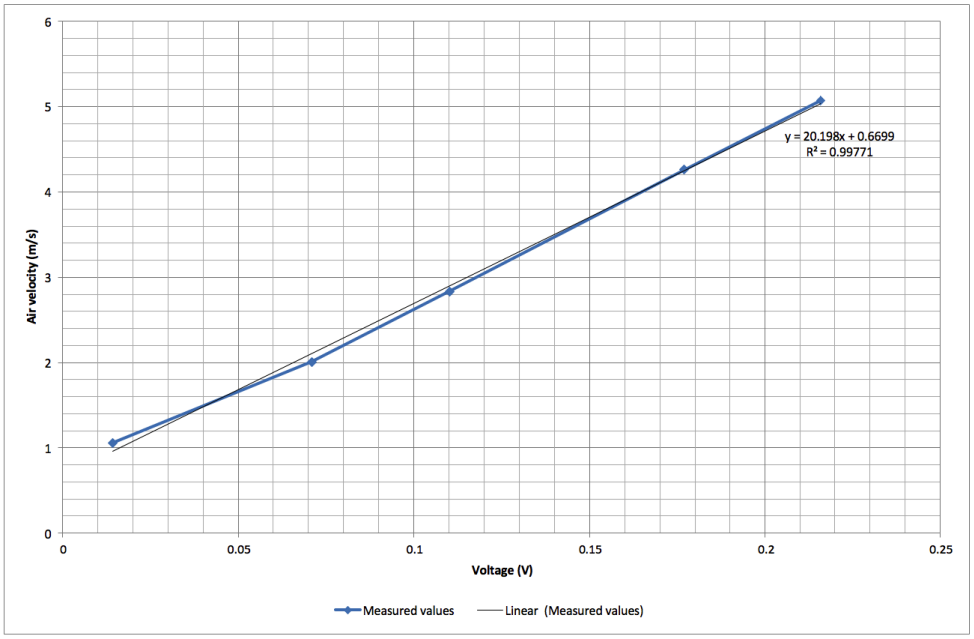

Figure B.1: Unreliable anemometer calibration.

It has been decided that conversion formula from another calibration procedure should be used. The following calibration has been performed by research assistant of the IEEE lab, Kim Trangbæk Jønsson. Moreover, the wind direction recalculation formula B.5 has been taken from the sensor's manual, tested and approved.

$$dir_n = 100 \cdot Voltage_n \tag{B.5}$$

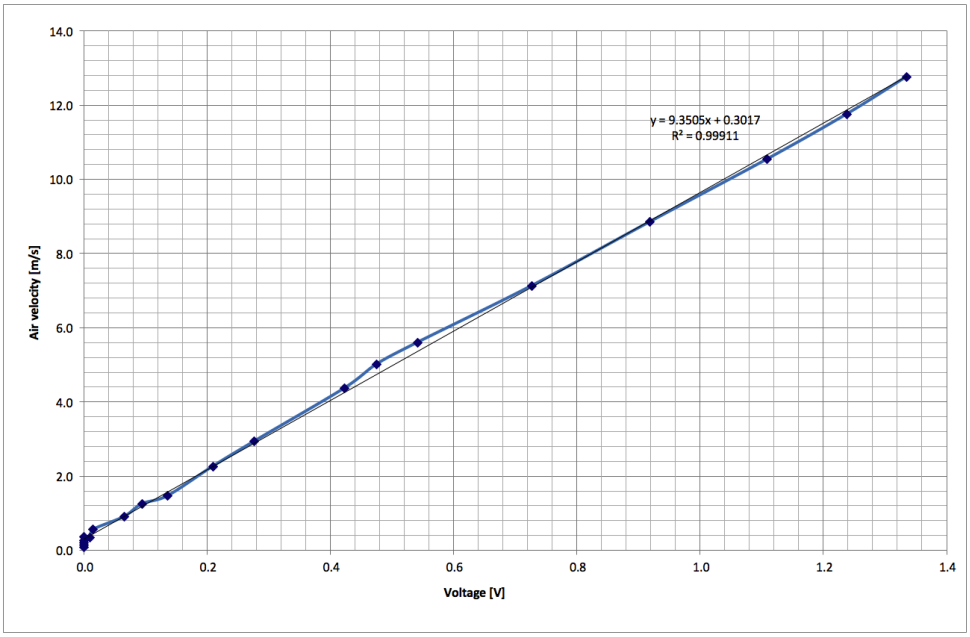

Figure B.2: Reliable anemometer calibration plot with recalculation formula.

B.2 Pyranometers calibration

Two different pyranometers have been used: CPM22 and SPN1. CMP22 is considered more accurate and has been thus used to determine the total solar irradiance, while the SPN1 has been used to determine the sky diffuse proportion of the solar irradiance. When both total and diffusive solar irradiance are known, the direct solar irradiance can be calculated as $\phi_{Direct} = \phi_{Total} - \phi_{Diffuse}$.

Procedure

Due to lack of laboratory equipment for pyranometers calibration, rough estimations of their reliability have been performed. Recalculation formulas have been taken from the technical manuals of the sensors. The pyranometers have been located outside on a cloudy day in February; 19/02/18 at 11.30. According to the DRY2013 weather data file, the total solar irradiance in February varies approximately from 25 W/m^2 to 30 W/m^2, while CMP22 indicates 26 W/m^2. Moreover, figure B.4 can be used as quasi-calibration method. Thus, the accuracy of the pyranometers is deemed acceptable.

B.3 Temperature sensor

The Pt100-sensor is used for precise temperature monitoring applications, where errors in measurement have to be excluded. The linear relationship of the resistor to temperature, simplifies its use in many electronic applications. The Pt100-sensor is a temperature dependent component. The resistance of the Pt100-sensor rises linearly with the temperature. The accuracy of the sensor is ± 0.5°C. Pt100 sensor conforms to DIN EN 60751.[**Reissmann (2018)**]

LabView script with inserted recalculation formulas from the technical manual of the sensor was used in the experiment.

B.4 Weather station setup

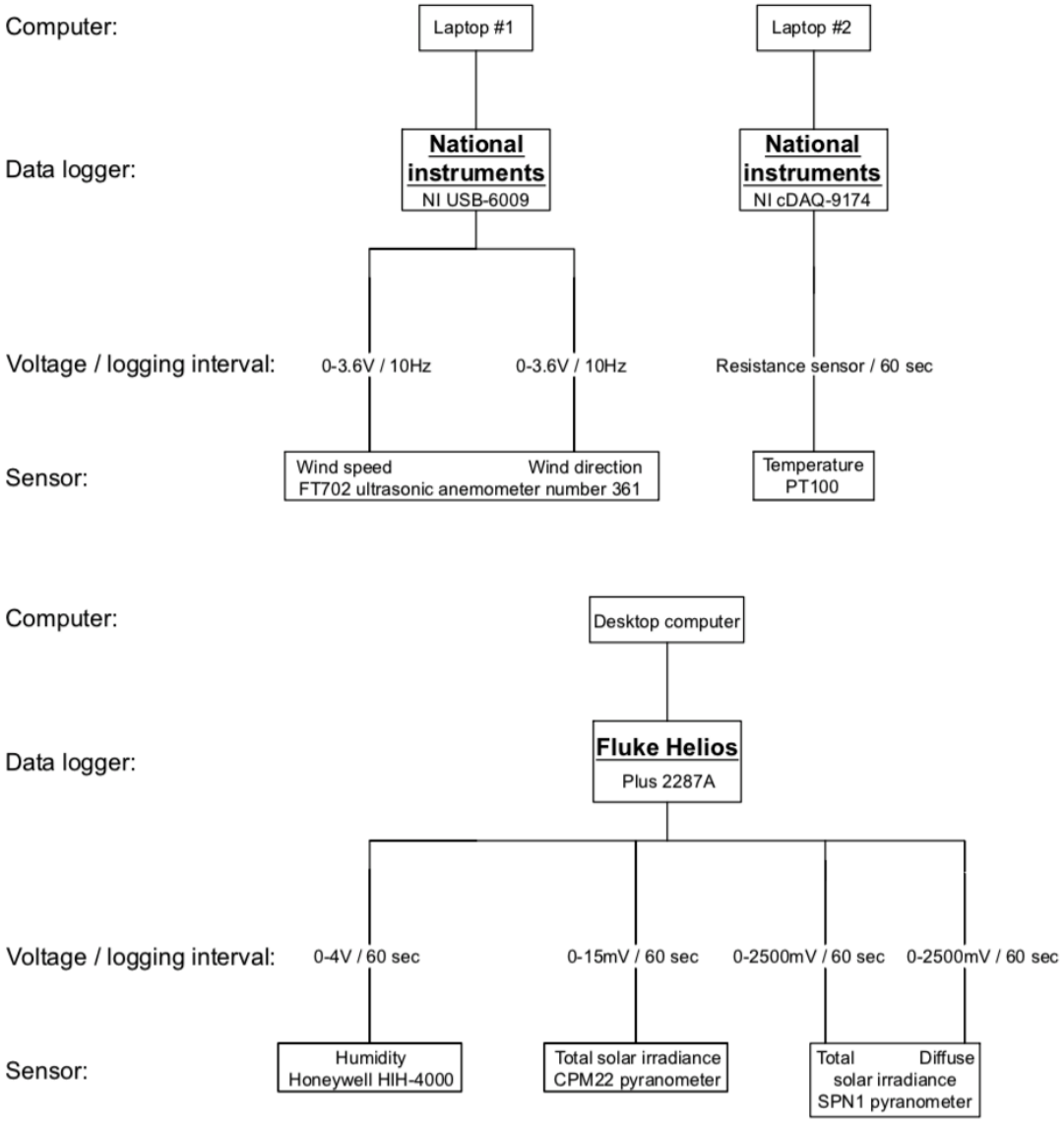

Figure B.3: The weather station scheme.

B.5 Meteoblue.com validation

The following figures present weather condition for Aars, Nothern Jutland, Denmark. The aim of this section is to demonstrate convergence of the results obtained from the weather station sensors and Meteoblue.com website. Although only the relative humidity and solar radiation values from the online database were used, the validation has been illustrated taking into consideration all of the investigated parameters to provide high quality input for the simulations. Adjustment factors have been implemented for the solar radiation data from the website to fit them closer to the measured values by the pyranometers which are deemed to be more precise. Coefficients were found by solving for lowest average standard deviation between two given values of the Meteoblue.com and measured data.

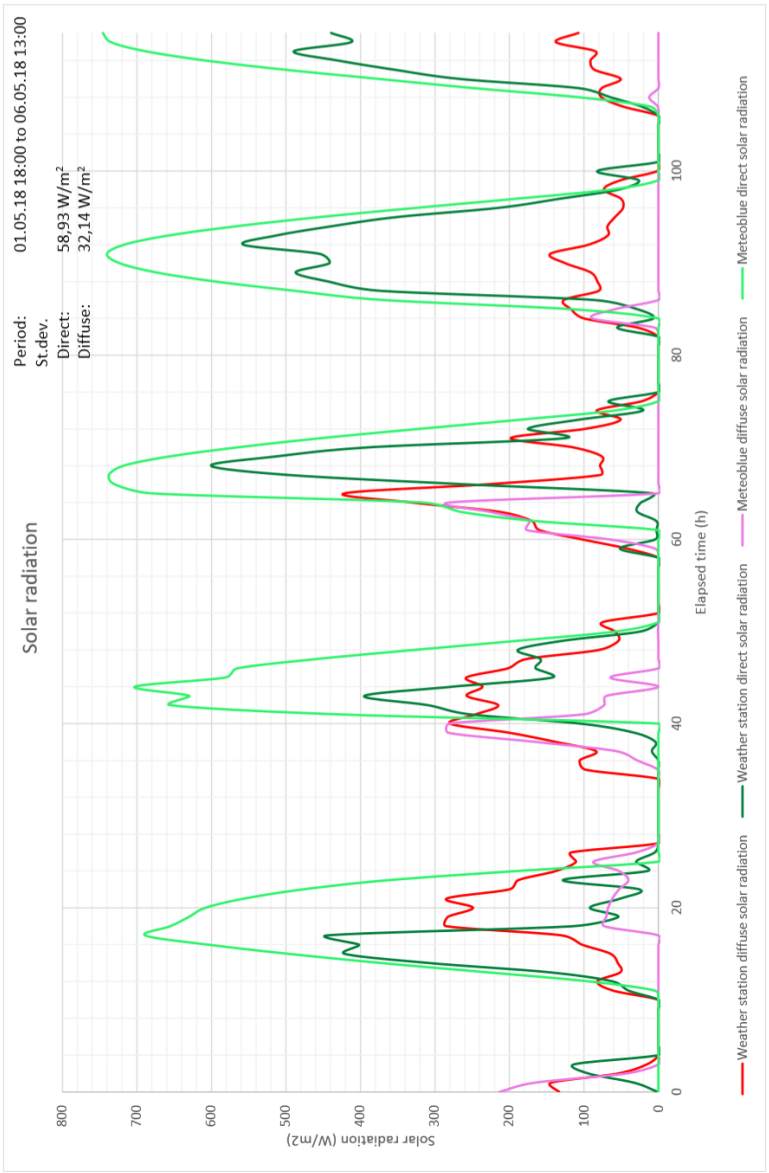

Figure B.4: Solar radiation comparison - no adjustments

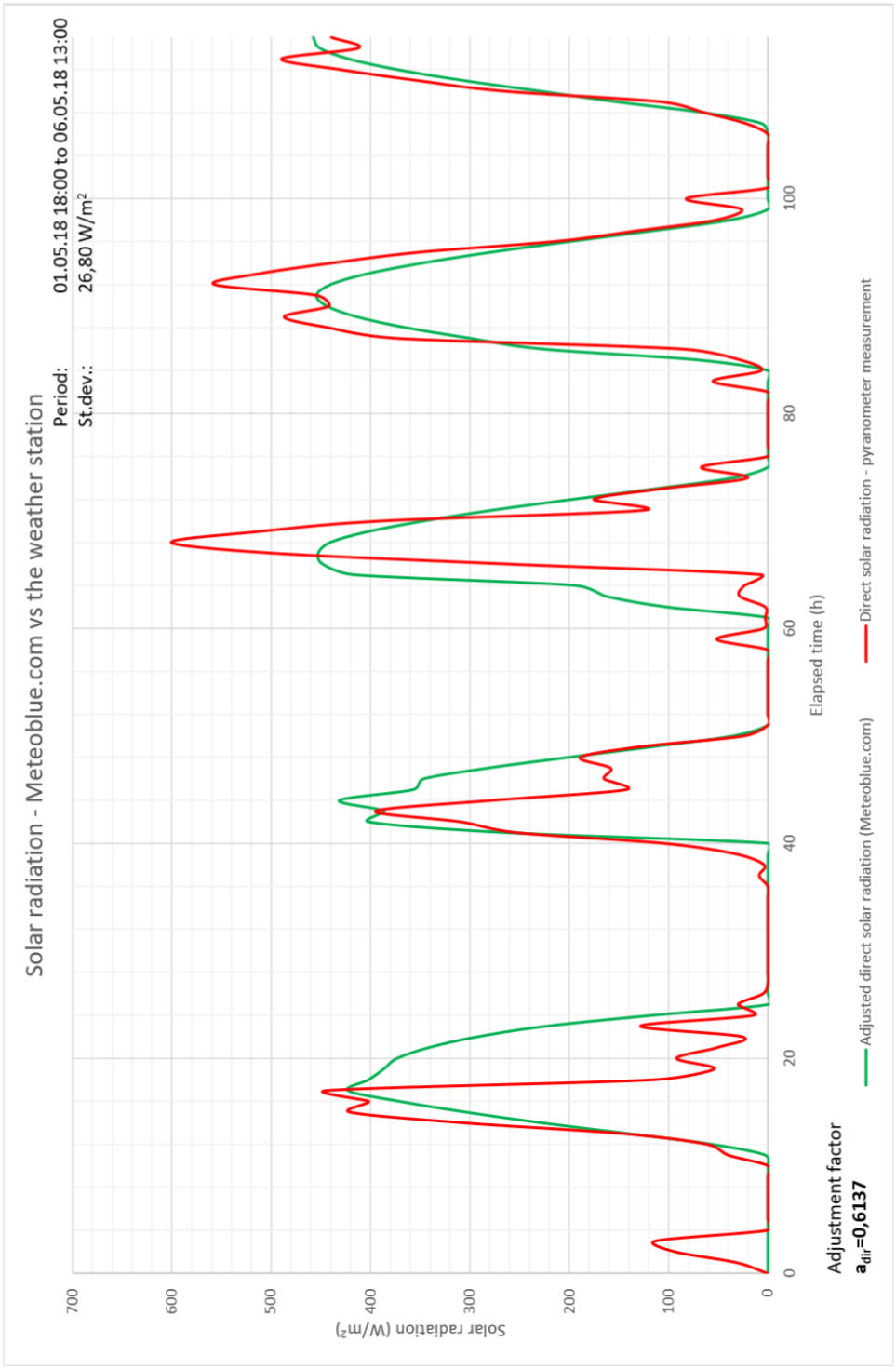

Figure B.5: Solar radiation validation - direct solar radiation adjustment.

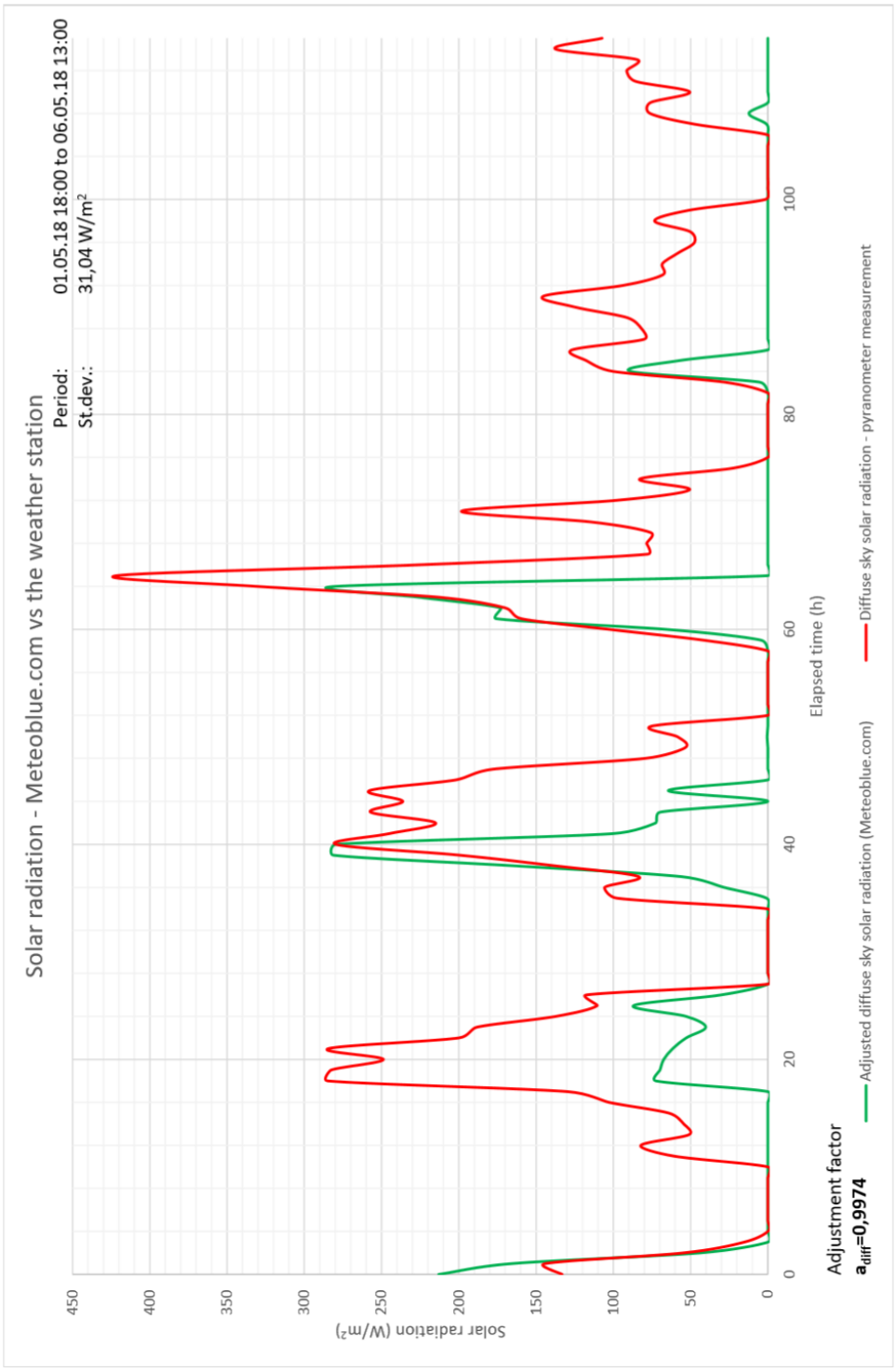

Figure B.6: Solar radiation validation - diffuse sky solar radiation adjustment.

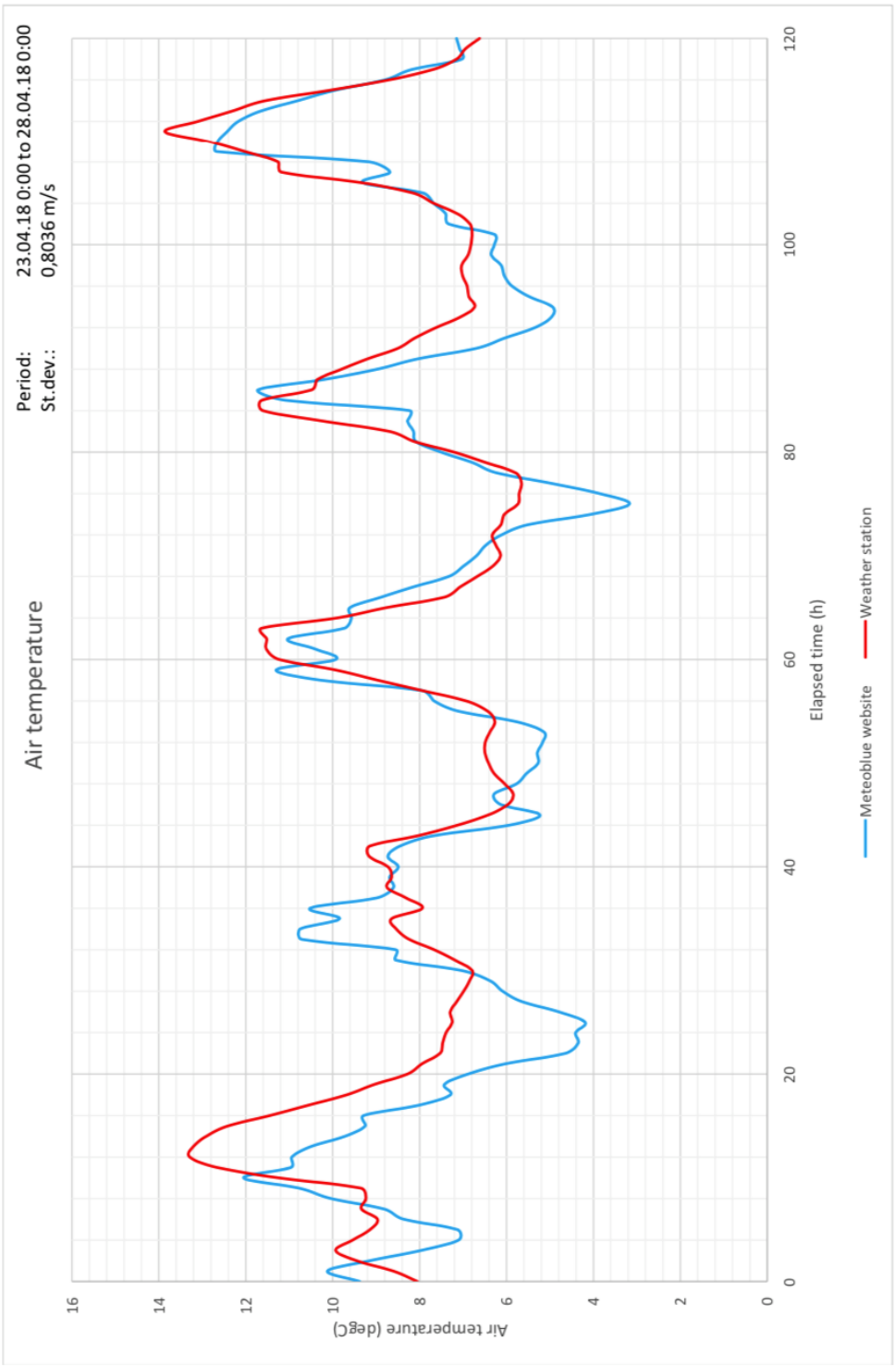

Figure B.7: Air temperature validation

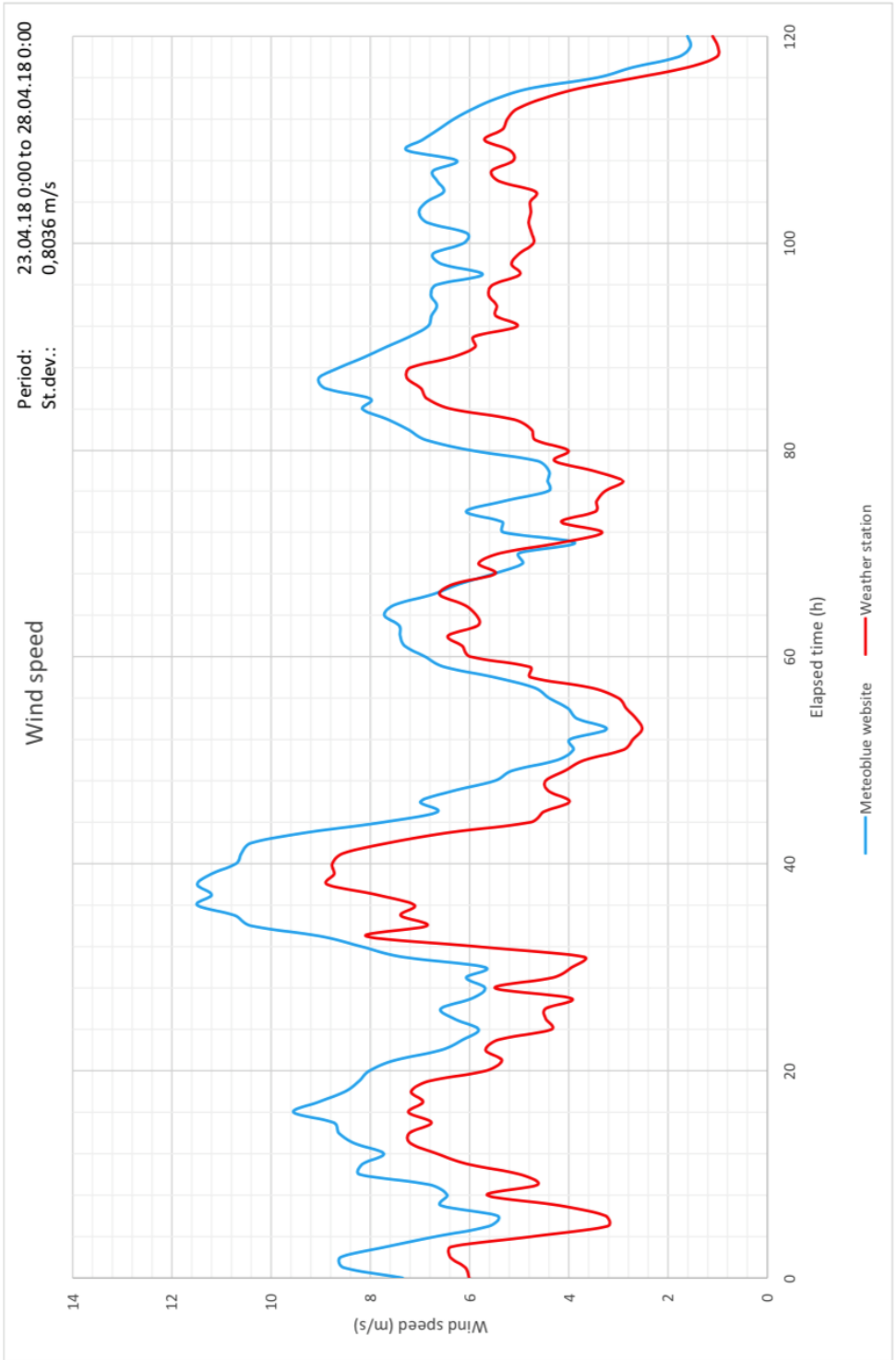

Figure B.8: Wind speed validation

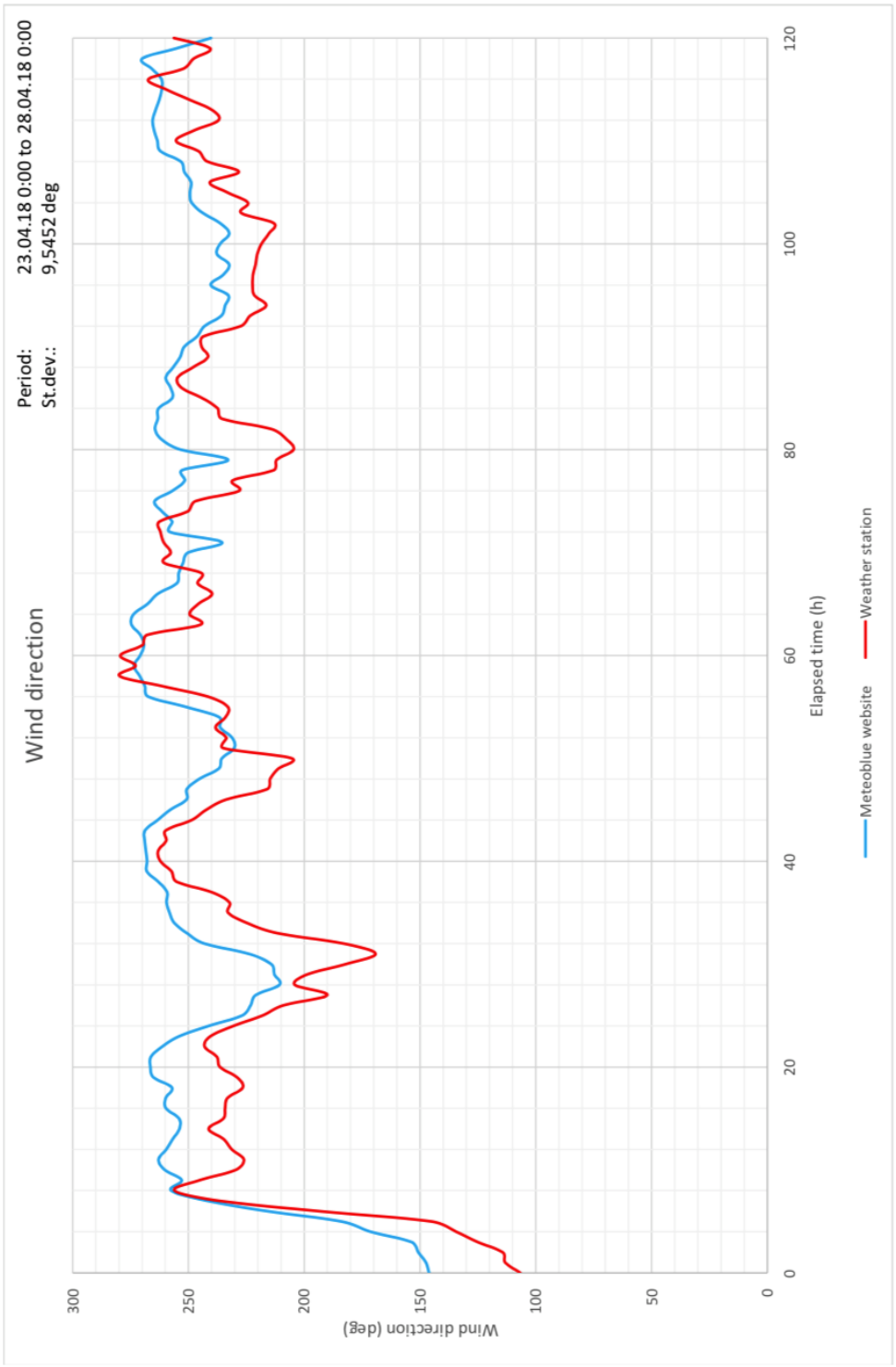

Figure B.9: Wind direction validation

B.6 Thermal imaging weather conditions

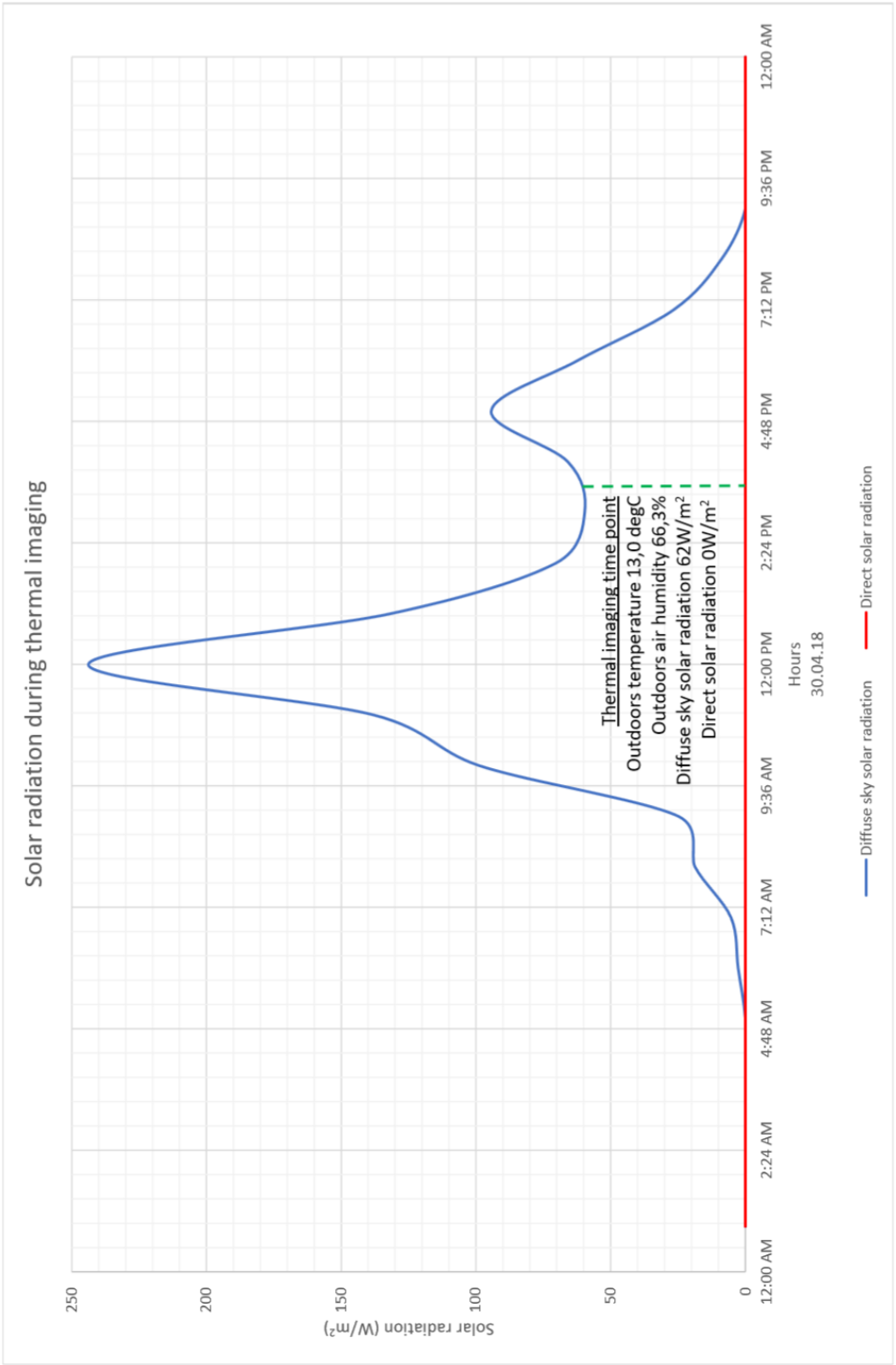

Figure B.10: Outdoors conditions during thermal imaging.

Appendix C

Comsol input

C.1 Mesh quality

Table C.1: Comsol - mesh quality.

2D models			**Quality measure (avg.)**	
Model	**Mesh area m^2**	**No. elements**	**Skewness**	**Growth rate**
A.1 Wall-wall corner	0,4095	12752	0,9034	0,9443
A.2 Wall-wall corner (util. room)	0,4864	14737	0,8973	0,9498
A.3 Wall-roof (beam)	0,5555	17415	0,8940	0,9216
A.4 Wall-roof (gable)	0,5940	17696	0,8875	0,8985
A.5 Wall-roof (Room 1)	0,4822	16040	0,9077	0,9357
A.6 Wall-roof (Room 1 - gable)	0,5406	14498	0,8975	0,9107
A.7 Room 1 roof - building	0,6122	16851	0,9164	0,9587
A.8 Wall-slab (Conf. room)	0,5772	23567	0,8898	0,9094
A.9 Wall-window	0,2562	26430	0,8982	0,8670
A.10 Wall-foundation	485,1	51923	0,9040	0,8890
3D models			**Quality measure (avg.)**	
Model	**Mesh volume m^3**	**No. elements**	**Skewness**	**Growth rate**
B+C Room 1 - wall -roof (gable)	2,072	3396291	0,6374	0,6438

C.2 Mesh independence test

Table C.2: Mesh independence test for 2D wall-wall (corner) model.

Element size	Number of elements	Normal total heat flux (W/m)	Relative error
User-defined	1066390	4,2832	Benchmark
Extremely fine	12595	4,2800	0,07%
Extra fine	4193	4,2785	0,11%
Finer	2060	4,2752	0,19%
Fine	2198	4,2775	0,13%
Normal	2198	4,2775	0,13%
Coarse	1829	4,2754	0,18%
Coarser	1683	4,2754	0,18%
Extra coarse	1277	4,2710	0,28%
Extremely coarse	1134	4,2711	0,28%

Appendix D

BSim baseline model input

D.1 Materials

Table D.1: Baseline model materials. Part 1 of 2.

Building element	Partition	Material	Thickness (m)
External walls	TH_wall1	TH_AMROC	0,020
		TH_PUR	0,185
		TH_AMROC	0,020
	TH_wall2	TH_Gypsum board	0,013
		TH_AMROC	0,020
		TH_PUR	0,185
		TH_AMROC	0,020
	TH_wall6	TH_Gypsum board	0,013
		TH_Stone wool 36	0,045
		TH_AMROC	0,020
		TH_PUR	0,185
		TH_AMROC	0,020
Internal walls	TH_wall3	TH_Gypsum board	0,013
		TH_FERMACELL	0,018
		TH_PUR	0,114
		TH_FERMACELL	0,018
		TH_Gypsum board	0,013
	TH_wall4	TH_FERMACELL	0,018
		TH_PUR	0,114
		TH_FERMACELL	0,018
	TH_wall5	TH_Gypsum board	0,013
		TH_AMROC	0,020
		TH_PUR	0,185
		TH_AMROC	0,020
		TH_Gypsum board	0,013
	TH_wall2a	TH_AMROC	0,020
		TH_PUR	0,185
		TH_AMROC	0,020
		TH_Gypsum board	0,013

Table D.2: Baseline model materials. Part 2 of 2.

Building element	Partition	Material	Thickness (m)
Floors	TH_floor1	Concrete reinforced v/c 0.4 C420	0,080
		TH_AMROC	0,020
		TH_PUR	0,185
		TH_AMROC	0,020
	TH_floor2	TH_Floor laminate	0,010
		Concrete reinforced v/c 0.4 C420	0,080
		TH_AMROC	0,020
		TH_PUR	0,185
		TH_AMROC	0,020
	TH_slab2	TH_Floor laminate	0,010
		TH_Plywood 22 mm WBP P-30	0,018
		TH_Stone wool 36	0,200
		TH_FERMACELL	0,018
		TH_PUR	0,189
		TH_FERMACELL	0,018
Internal floors	TH_slab1	TH_Floor laminate	0,010
		TH_Plywood 22 mm WBP P-30	0,018
		TH_Stone wool 36	0,150
		(No type) - air layer: Resist. 0,16	0,145
		TH_SoundDampeningBoard	0,025
	TH_slab2a	TH_Floor laminate	0,010
		TH_Plywood 22 mm WBP P-30	0,018
		TH_Stone wool 36	0,200
		TH_FERMACELL	0,018
		TH_PUR	0,189
		TH_FERMACELL	0,018
Roofs	TH_roof1	TH_AMROC	0,012
		TH_PUR	0,201
		TH_AMROC	0,012
		TH_Stone wool 36	0,045
	TH_roof2	TH_SoundDampeningBoard	0,025
		(No type) - air layer: Resist. 0,16	0,070
		TH_AMROC	0,012
		TH_PUR	0,201
		TH_AMROC	0,012
		TH_Stone wool 36	0,188

D.2 Geomtery

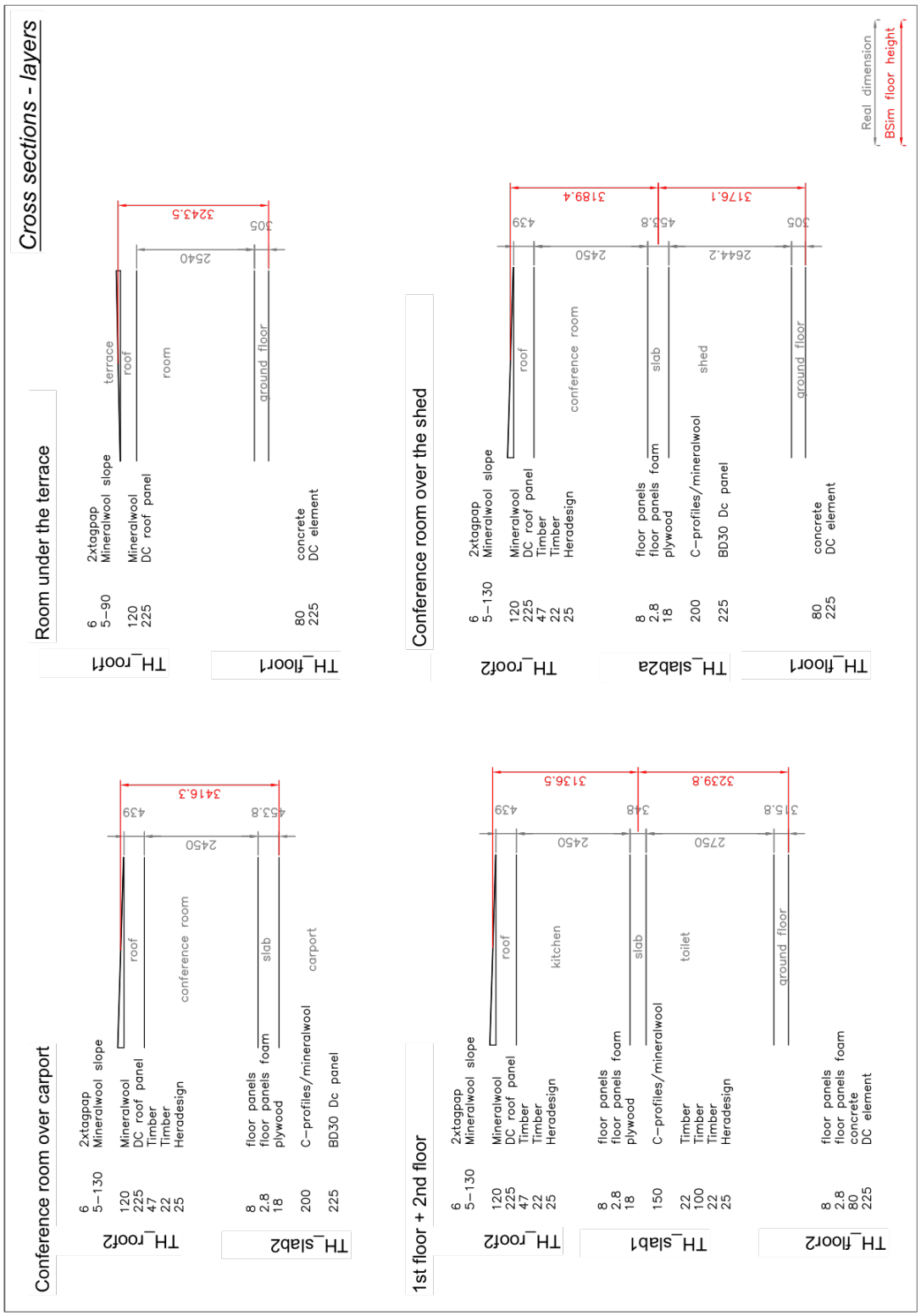

Figure D.1: Baseline model - floors layout.

D.3 Systems

Table D.3: Baseline model systems.

Thermal zone	System	Parameter	Value	Control	Time
0-Shed	Infiltration	Basic AirChange (/h)	0,0057	24/7	24/7
0-Foyer	Infiltration	Basic AirChange (/h)	0,0052	24/7	24/7
	Heating	MaxPow (kW)	0,4	Set point	24/7
		Part to air (-)	0,7		
		Set point (degC)	20		
0-Room1	Infiltration	Basic AirChange (/h)	0,0056	24/7	24/7
	Heating	MaxPow (kW)	0,4	Set point	24/7
		Part to air (-)	0,7		
		Set point (degC)	20		
0-Room2	Infiltration	Basic AirChange (/h)	0,0056	24/7	24/7
	Heating	MaxPow (kW)	0,4	Set point	24/7
		Part to air (-)	0,7		
		Set point (degC)	20		
0-Toilet	Infiltration	Basic AirChange (/h)	0,0052	24/7	24/7
	Heating	MaxPow (kW)	0,4	Set point	24/7
		Part to air (-)	0,7		
		Set point (degC)	20		
	Equipment	Heat Load (kW)	0,2	24/7	24/7
	(hot water tank)	Part to air (-)	0,4		
0-Utility room	Infiltration	Basic AirChange (/h)	0,0052	24/7	24/7
	Heating	MaxPow (kW)	0,4	Set point	24/7
		Part to air (-)	0,7		
		Set point (degC)	20		
	Equipment	Heat Load (kW)	0,11	24/7	24/7
	(Computers + data loggers)	Part to air (-)	0,8		
0-Staircase	Infiltration	Basic AirChange (/h)	0,0052	24/7	24/7
1-Staircase	Infiltration	Basic AirChange (/h)	0,0058	24/7	24/7
1-Kitchen	Infiltration	Basic AirChange (/h)	0,0058	24/7	24/7
	Heating	MaxPow (kW)	0,4	Set point	24/7
		Part to air (-)	0,7		
		Set point (degC)	20		
	Equipment	Heat Load (kW)	0,05	24/7	24/7
	(Fridge)	Part to air (-)	0,8		
1-Conference room	Infiltration	Basic AirChange (/h)	0,0058	24/7	24/7
	Heating	MaxPow (kW)	0,8	Set point	24/7
		Part to air (-)	0,7		
		Set point (degC)	20		

Appendix E

Weather data

This appendix includes raw weather data collected with use of the weather station presented in section 2.2.

- Figure E.1 - Measured solar radiation
- Figure E.2 - Measured air temperature
- Figure E.3 - Measured air relative humidity
- Figure E.4 - Measured wind speed
- Figure E.5 - Measured wind direction

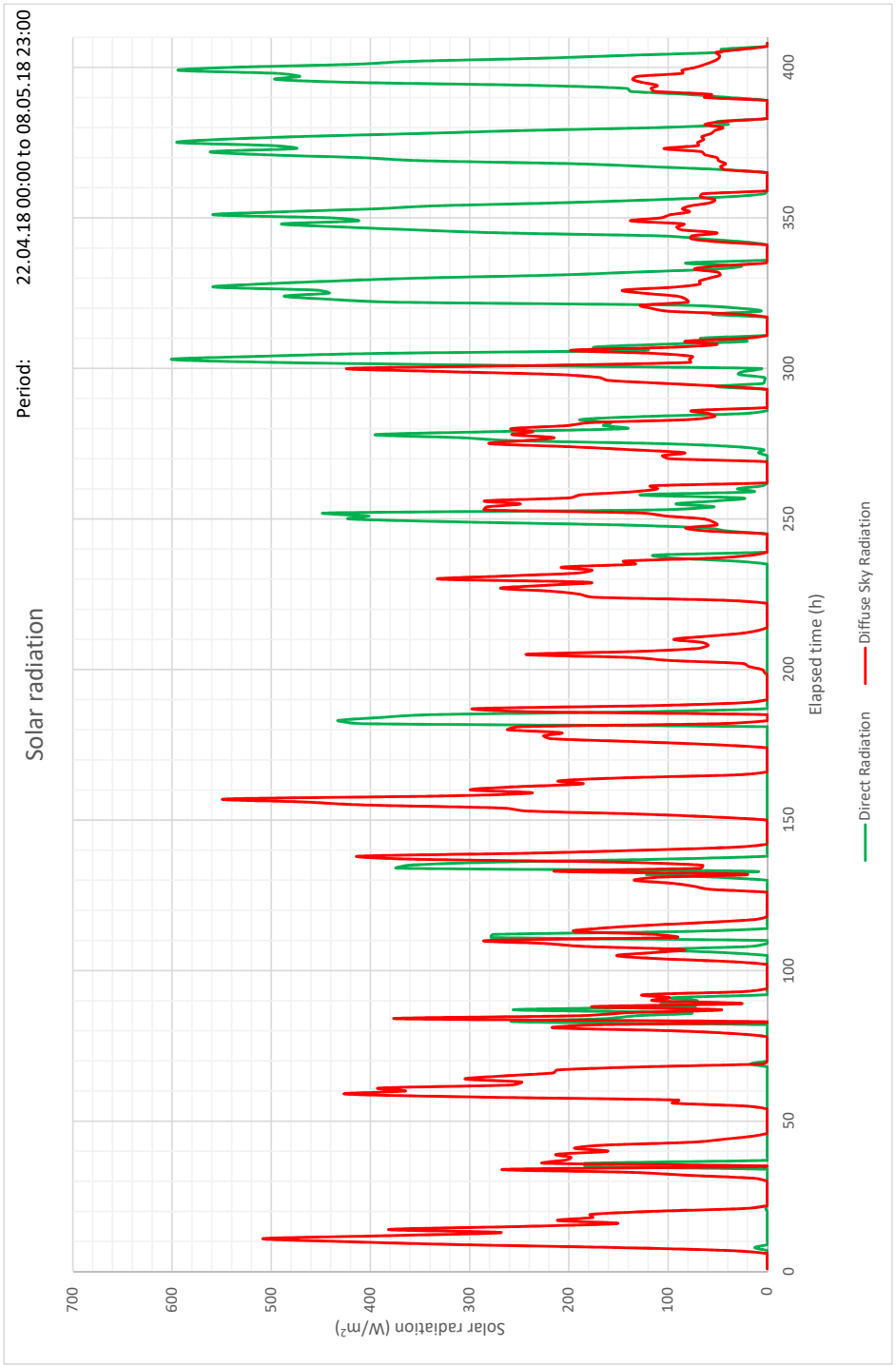

Figure E.1: Measured solar radiation.

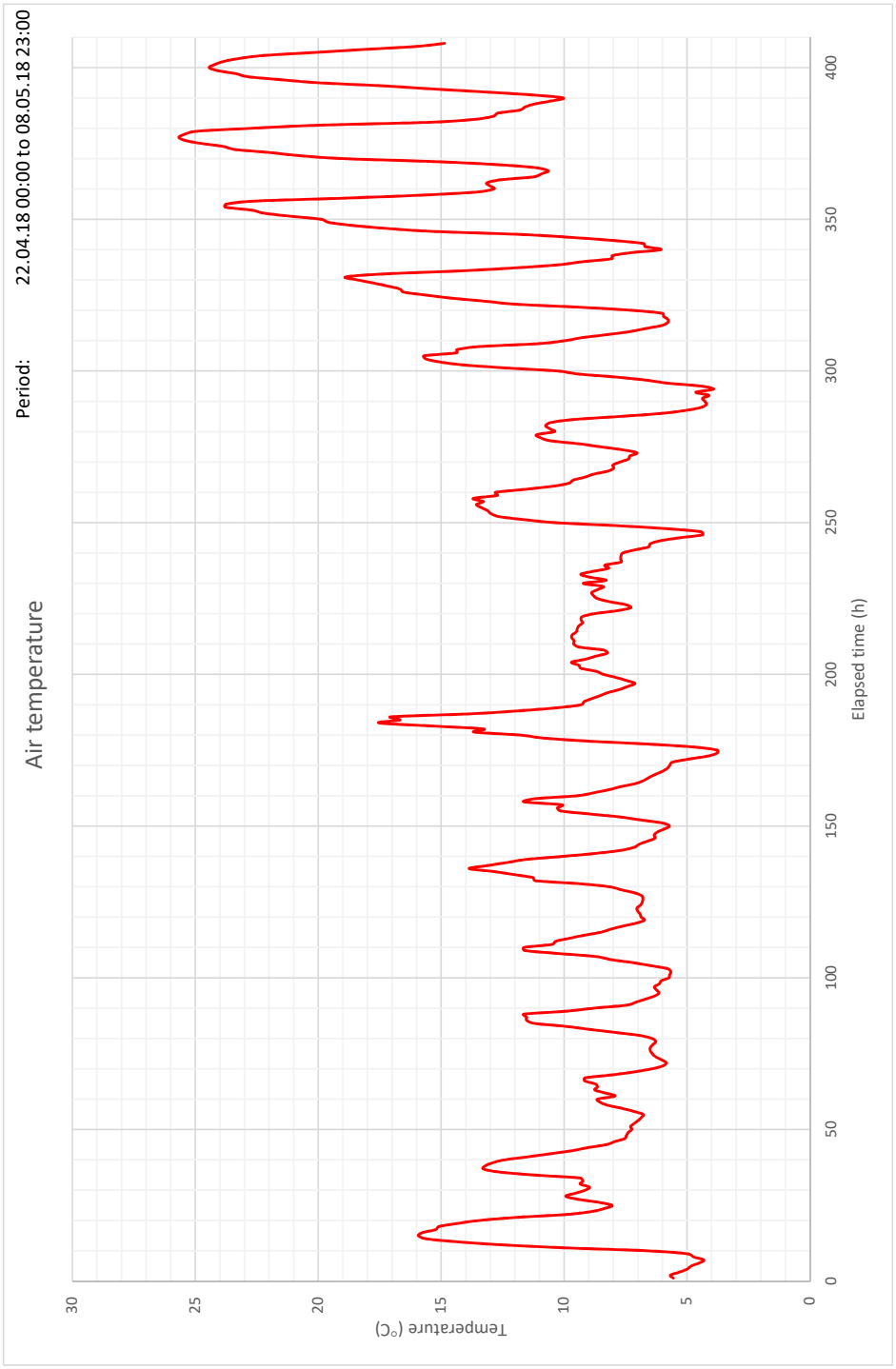

Figure E.2: Measured air temperature.

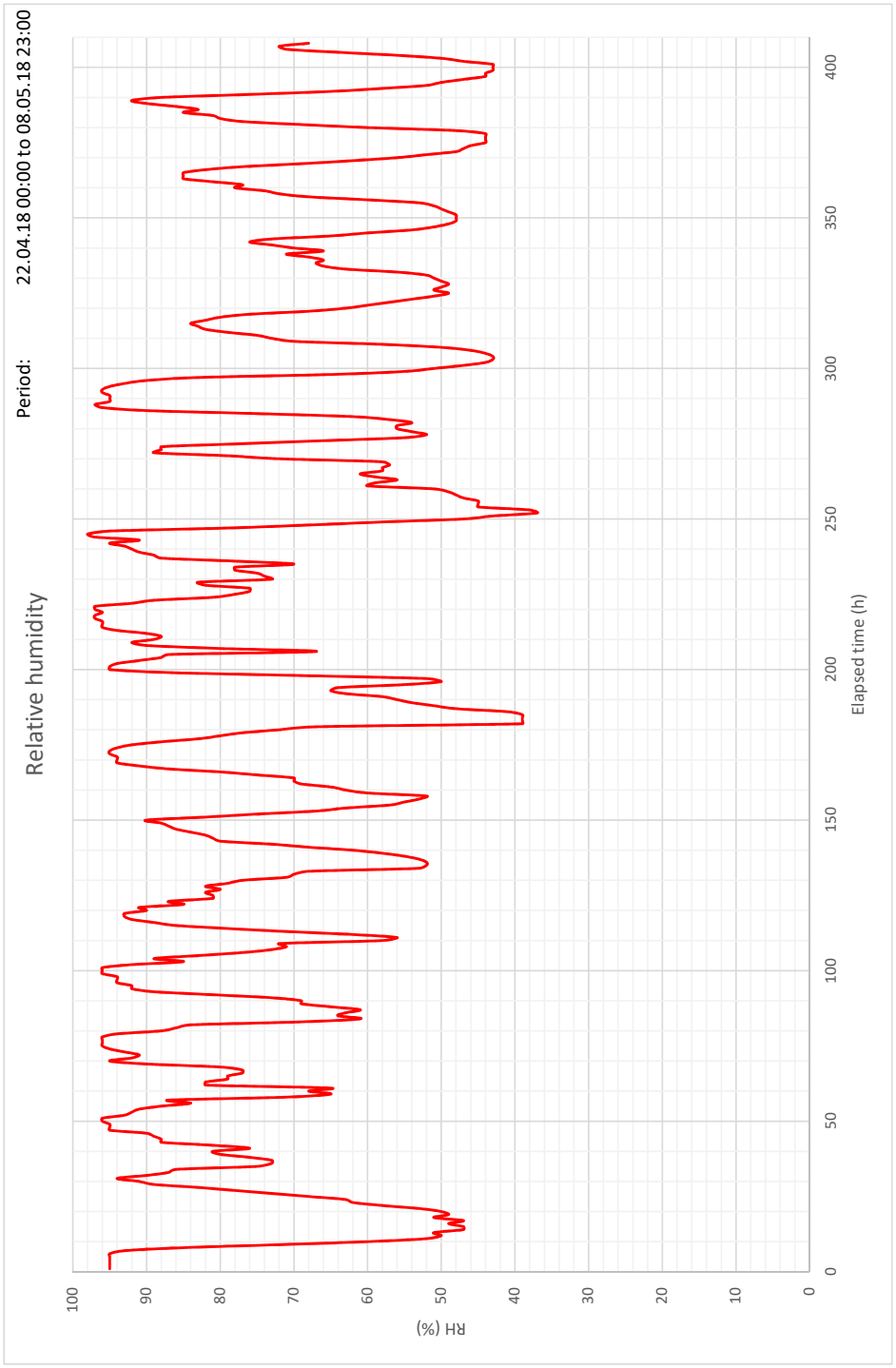

Figure E.3: Measured air relative humidity.

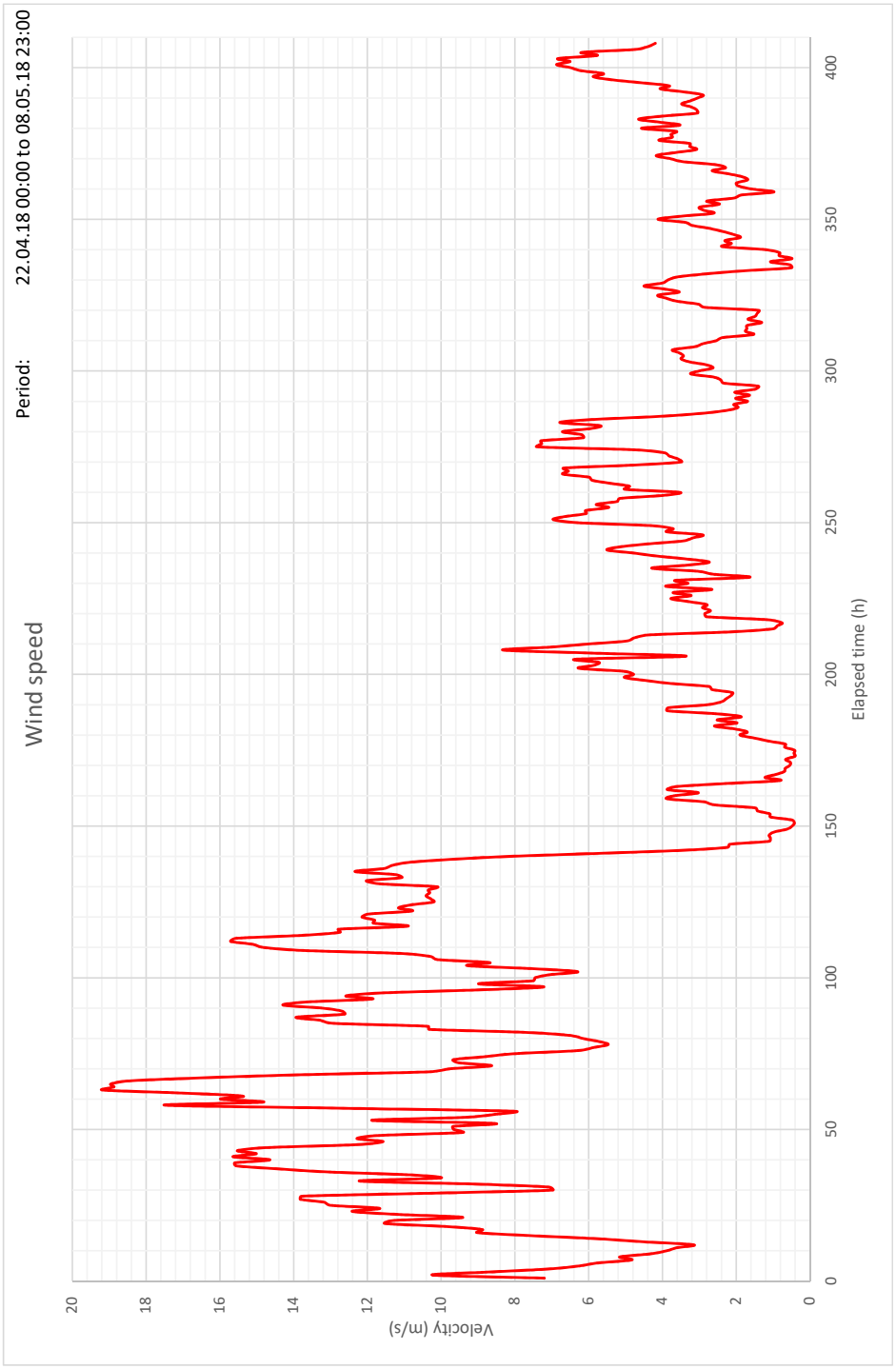

Figure E.4: Measured wind speed.

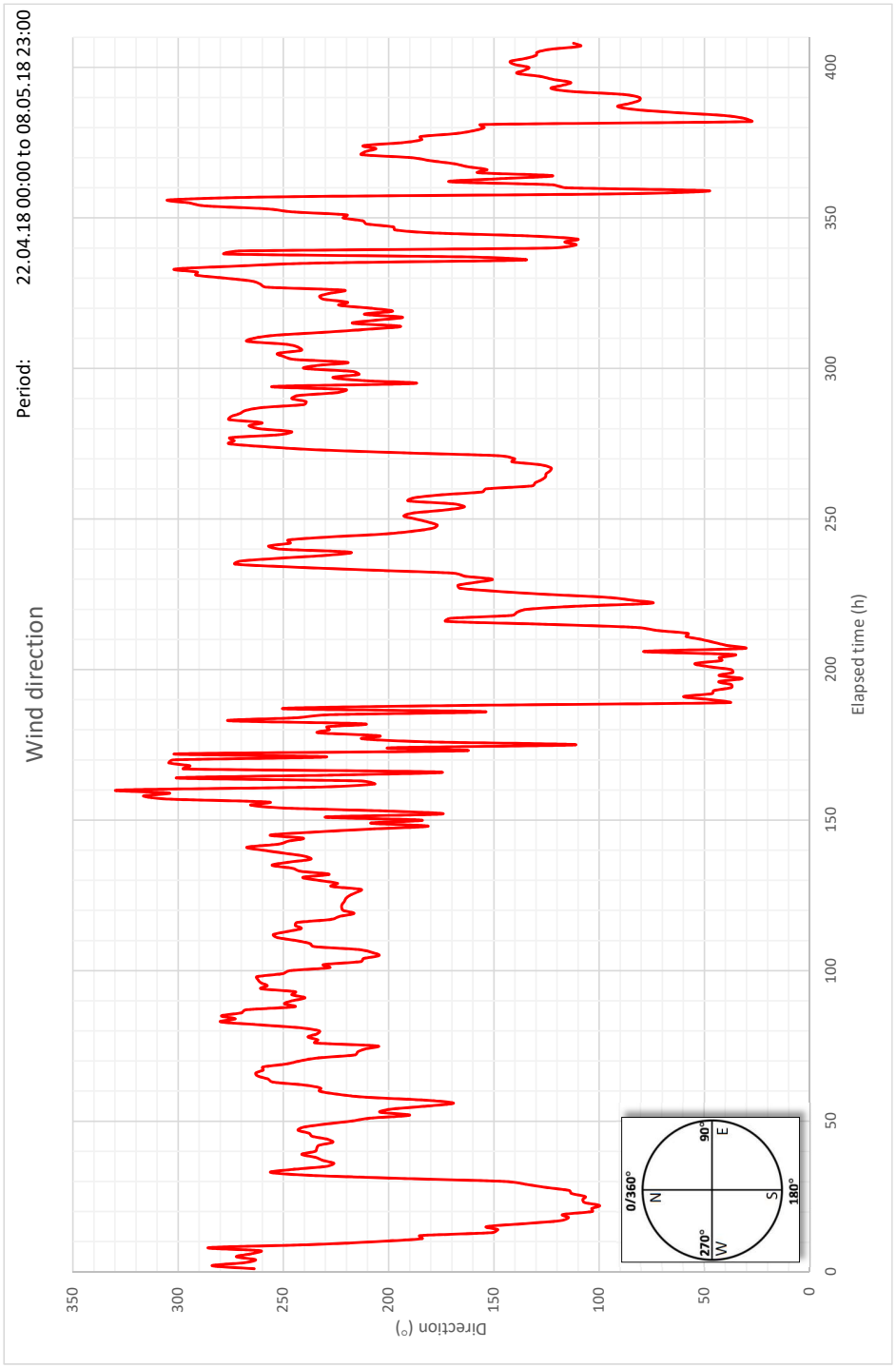

Figure E.5: Measured wind direction.

Appendix F

Materials properties

F.1 Thermal conductivity

This appendix includes thermal conductivity measurement reports:

- F.1 - Thermal conductivity - PUR foam.
- F.2 - Thermal conductivity - Amroc fibre-cement board.
- F.3 - Thermal conductivity - Fermacell fibre-gypsum board.
- F.4 - Thermal conductivity - Rockwool A-Batts.
- F.5 - Thermal conductivity - Gypsum plasterboard.
- F.6 - Thermal conductivity - Glued timber.
- F.7 - Thermal conductivity - Plywood.

AALBORG UNIVERSITET

Test report

Test report acc. EN 12667 and EN12664 paragraph 9

Date	06-04-2018
Report no.	Master thesis
Test owner	Aalborg university
Test tool	Thermal Conductivity Meter 'lambda-Meter EP500e' acc. to EN 1946-2 by Lambda-Messtechnik GmbH Dresden
Test arrangement	Sensor plates horizontal, hot plate on top
Standards	Thickness measurement acc. to EN 823 Thermal conductivity measurement acc. to ISO 8302 and EN 12667
Tester	Adam Emil Swiniarski

Specimen designation	Insulation	Specimen dimension	
Origin of specimen	DC-System Insulation A/S	Area	150 mm x 150 mm
Date of manufact.		Thickness	49,8 mm
Material name	DC PU/PIR foam	Nominal thickness	50 mm
Material description		Specimen mass	51,28 g
		Raw density	45,80 kg/m³

Spec. pre-conditioning

Change in mass during:		
drying	50,13	g
test	51,28	g
Humidity before test	2,24	%
Pressure	1800	Pa

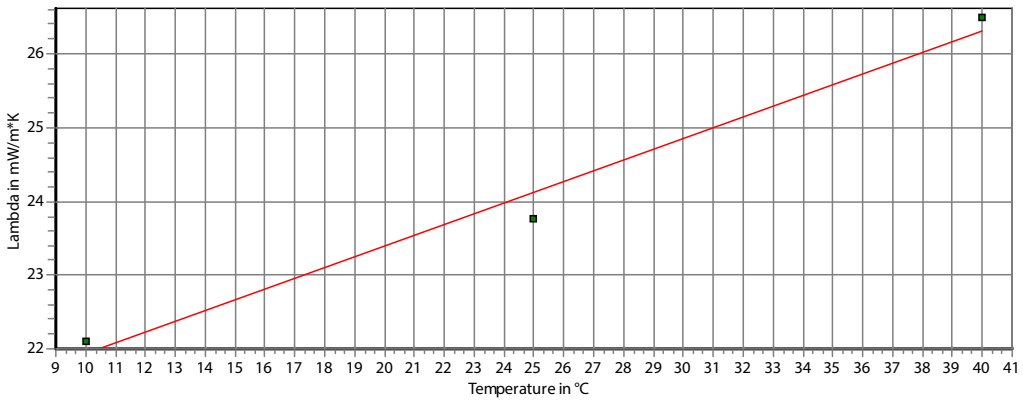

	1. Test	2. Test	3. Test
Test no.	G119_2018-04-	G119_2018-	G119_2018-
Meas.temp. in °C	40	25	10
Diff.temp. in K	15	15	15
Lambda in mW/m*K	26,49	23,77	22,11
R in m²K/W	1,88	2,0951	2,2524

Polynomial
$y = f(T) = 0{,}1460 * T + 20{,}47$

Lambda-10	21,93	mW/(m*K)
R-10	2,2709	m²*K/W
TC	0,1460	mW/(m*K²)

29-04-2018

signature

Figure F.1: Thermal conductivity - PUR foam.

AALBORG UNIVERSITET

Test report

Test report acc. EN 12667 and EN12664 paragraph 9

Date	10-04-2018
Report no.	Master thesis
Test owner	Aalborg university
Test tool	Thermal Conductivity Meter 'lambda-Meter EP500e' acc. to EN 1946-2 by Lambda-Messtechnik GmbH Dresden
Test arrangement	Sensor plates horizontal, hot plate on top
Standards	Thickness measurement acc. to EN 823 Thermal conductivity measurement acc. to ISO 8302 and EN 12667
Tester	Adam Emil Swiniarski

Specimen designation	DC AMROC	**Specimen dimension**	
Origin of specimen		**Area**	150 mm x 150 mm
Date of manufact.		**Thickness**	19,3 mm
Material name	Amroc fiber cement board	**Nominal thickness**	20 mm
Material description		**Specimen mass**	630,49 g
		Raw density	1452,00 kg/m³

Spec. pre-conditioning

Change in mass during:
drying
test

Humidity before test

Pressure 600 Pa

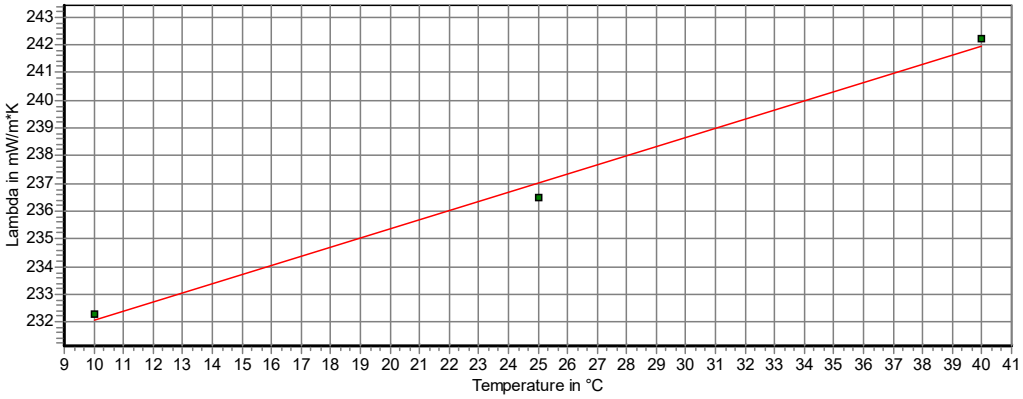

	1. Test	2. Test	3. Test
Test no.	G119_2018-04-	G119_2018-	G119_2018-
Meas.temp. in °C	40	25	10
Diff.temp. in K	15	15	15
Lambda in mW/m*K	242,21	236,52	232,31
R in m²K/W	0,0797	0,0816	0,0831

Polynomial
y = *f*(T) = 0,3300 * T + 228,76

Lambda-10	232,06	mW/(m*K)
R-10	0,0832	m²*K/W
TC	0,3300	mW/(m*K²)

29-04-2018

signature

Figure F.2: Thermal conductivity - Amroc fibre-cement board.

AALBORG UNIVERSITET

Test report

Test report acc. EN 12667 and EN12664 paragraph 9

Date	07-04-2018
Report no.	Master thesis
Test owner	Aalborg university
Test tool	Thermal Conductivity Meter 'lambda-Meter EP500e' acc. to EN 1946-2 by Lambda-Messtechnik GmbH Dresden
Test arrangement	Sensor plates horizontal, hot plate on top
Standards	Thickness measurement acc. to EN 823 Thermal conductivity measurement acc. to ISO 8302 and EN 12667
Tester	Adam Emil Swiniarski

Specimen designation	DC Fermacell	**Specimen dimension**	
Origin of specimen		**Area**	150 mm x 150 mm
Date of manufact.		**Thickness**	17,8 mm
Material name	Fermacell board	**Nominal thickness**	18 mm
Material description		**Specimen mass**	503,37 g
		Raw density	1257,00 kg/m³

Spec. pre-conditioning

Change in mass during:
drying
test

Humidity before test

Pressure 500 Pa

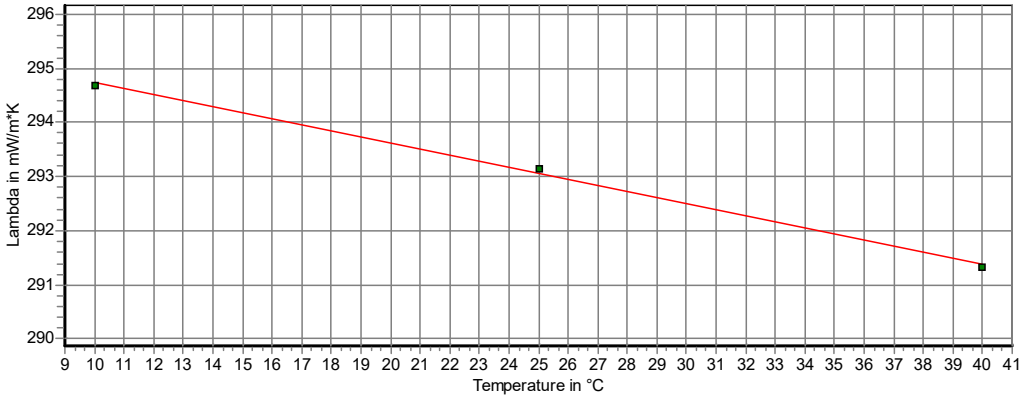

	1. Test	2. Test	3. Test
Test no.	G119_2018-04-	G119_2018-	G119_2018-
Meas.temp. in °C	40	25	10
Diff.temp. in K	15	15	15
Lambda in mW/m*K	291,33	293,14	294,69
R in m²K/W	0,0611	0,0607	0,0604

Polynomial
y = *f*(T) = -0,1120 * T + 295,85

Lambda-10	294,73	mW/(m*K)
R-10	0,0604	m²*K/W
TC	-0,1120	mW/(m*K²)

29-04-2018

signature

Figure F.3: Thermal conductivity - Fermacell fibre-gypsum board.

AALBORG UNIVERSITET

Test report

Test report acc. EN 12667 and EN12664 paragraph 9

Date	27-04-2018
Report no.	Master thesis
Test owner	Aalborg university
Test tool	Thermal Conductivity Meter 'lambda-Meter EP500e' acc. to EN 1946-2 by Lambda-Messtechnik GmbH Dresden
Test arrangement	Sensor plates horizontal, hot plate on top
Standards	Thickness measurement acc. to EN 823 Thermal conductivity measurement acc. to ISO 8302 and EN 12667
Tester	Adam Emil Swiniarski

Specimen designation	Rockwool A-Batts, 45mm	**Specimen dimension**	
Origin of specimen		**Area**	150 mm x 150 mm
Date of manufact.		**Thickness**	47,4 mm
Material name	Rockwool A-Batts, 45mm	**Nominal thickness**	45 mm
Material description		**Specimen mass**	52,17 g
		Raw density	48,90 kg/m³

Spec. pre-conditioning

Change in mass during:
drying
test

Humidity before test

Pressure 2500 Pa

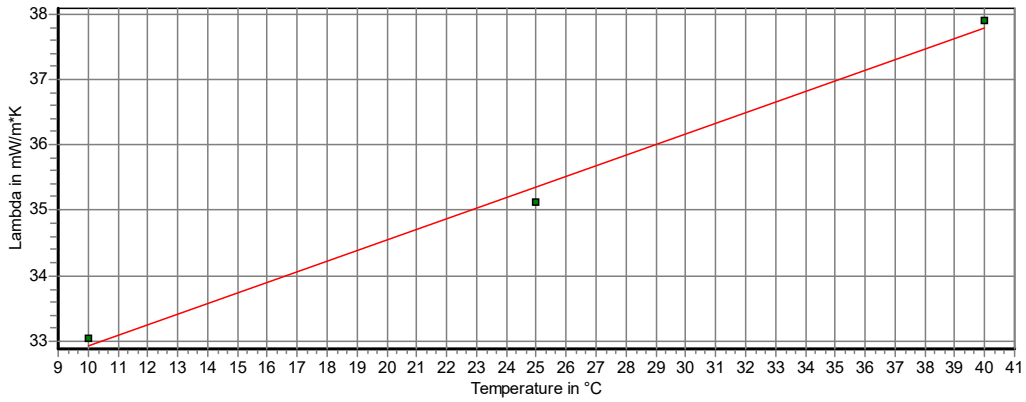

	1. Test	2. Test	3. Test
Test no.	G119_2018-04-	G119_2018-	G119_2018-
Meas.temp. in °C	40	25	10
Diff.temp. in K	15	15	15
Lambda in mW/m*K	37,91	35,12	33,04
R in m²K/W	1,2503	1,3497	1,4346

Polynomial
y = *f*(T) = 0,1623 * T + 31,30

Lambda-10	32,92	mW/(m*K)
R-10	1,4399	m²*K/W
TC	0,1623	mW/(m*K²)

29-04-2018

signature

Figure F.4: Thermal conductivity - Rockwool A-Batts.

AALBORG UNIVERSITET

Test report

Test report acc. EN 12667 and EN12664 paragraph 9

Date	21-04-2018
Report no.	Master thesis
Test owner	Aalborg university
Test tool	Thermal Conductivity Meter 'lambda-Meter EP500e' acc. to EN 1946-2 by Lambda-Messtechnik GmbH Dresden
Test arrangement	Sensor plates horizontal, hot plate on top
Standards	Thickness measurement acc. to EN 823 Thermal conductivity measurement acc. to ISO 8302 and EN 12667
Tester	Adam Emil Swiniarski

Specimen designation	Gypsum board	**Specimen dimension**	
Origin of specimen		**Area**	150 mm x 150 mm
Date of manufact.		**Thickness**	12,2 mm
Material name	Gypsum plasterboard	**Nominal thickness**	10 mm
Material description		**Specimen mass**	190,80 g
		Raw density	695,10 kg/m³

Spec. pre-conditioning

Change in mass during:
drying
test

Humidity before test

Pressure 600 Pa

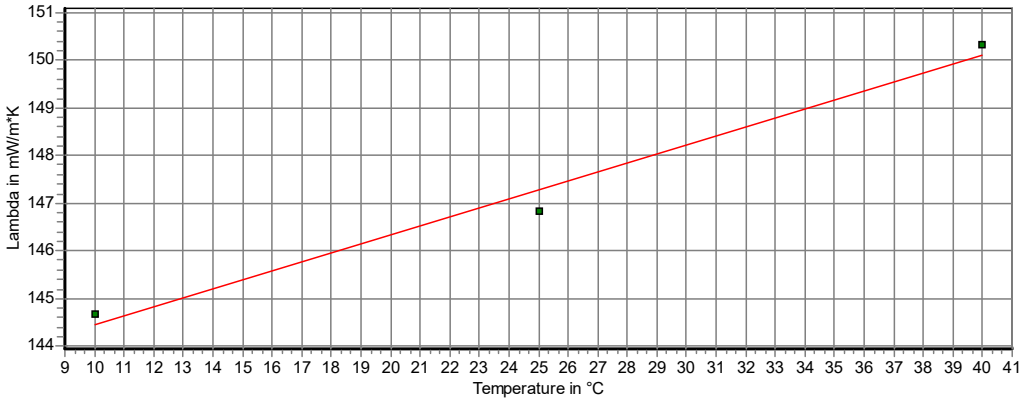

	1. Test	2. Test	3. Test
Test no.	G119_2018-04-	G119_2018-	G119_2018-
Meas.temp. in °C	40	25	10
Diff.temp. in K	15	15	15
Lambda in mW/m*K	150,34	146,84	144,66
R in m²K/W	0,0811	0,0831	0,0843

Polynomial
y = ƒ(T) = 0,1893 * T + 142,55

Lambda-10	144,44	mW/(m*K)
R-10	0,0845	m²*K/W
TC	0,1893	mW/(m*K²)

29-04-2018

signature

Figure F.5: Thermal conductivity - Gypsum plasterboard.

AALBORG UNIVERSITET

Test report

Test report acc. EN 12667 and EN12664 paragraph 9

Date	20-04-2018
Report no.	Master thesis
Test owner	Aalborg university
Test tool	Thermal Conductivity Meter 'lambda-Meter EP500e' acc. to EN 1946-2 by Lambda-Messtechnik GmbH Dresden
Test arrangement	Sensor plates horizontal, hot plate on top
Standards	Thickness measurement acc. to EN 823 Thermal conductivity measurement acc. to ISO 8302 and EN 12667
Tester	Adam Emil Swiniarski

Specimen designation	Limtræ GL30C	**Specimen dimension**	
Origin of specimen		**Area**	150 mm x 150 mm
Date of manufact.		**Thickness**	89,3 mm
Material name	Wooden beam	**Nominal thickness**	90 mm
Material description		**Specimen mass**	907,70 g
		Raw density	451,80 kg/m³

Spec. pre-conditioning

Change in mass during:
drying
test

Humidity before test

Pressure 500 Pa

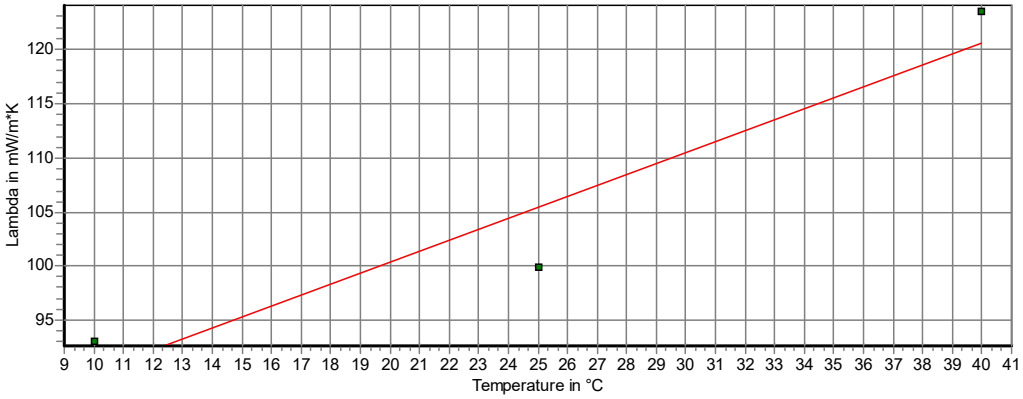

	1. Test	2. Test	3. Test
Test no.	G119_2018-04-	G119_2018-	G119_2018-
Meas.temp. in °C	40	25	10
Diff.temp. in K	15	15	15
Lambda in mW/m*K	123,38	99,86	93,15
R in m²K/W	0,7238	0,8943	0,9587

Polynomial
y = *f*(T) = 1,0077 * T + 80,27

Lambda-10	90,35	mW/(m*K)
R-10	0,9884	m²*K/W
TC	1,0077	mW/(m*K²)

29-04-2018

signature

Figure F.6: Thermal conductivity - Glued timber.

AALBORG UNIVERSITET

Test report

Test report acc. EN 12667 and EN12664 paragraph 9

Date	22-04-2018
Report no.	Master thesis
Test owner	Aalborg university
Test tool	Thermal Conductivity Meter 'lambda-Meter EP500e' acc. to EN 1946-2 by Lambda-Messtechnik GmbH Dresden
Test arrangement	Sensor plates horizontal, hot plate on top
Standards	Thickness measurement acc. to EN 823 Thermal conductivity measurement acc. to ISO 8302 and EN 12667
Tester	Adam Emil Swiniarski

Specimen designation	Plywood	**Specimen dimension**	
Origin of specimen		**Area**	150 mm x 150 mm
Date of manufact.		**Thickness**	16,9 mm
Material name	Plywood	**Nominal thickness**	15 mm
Material description		**Specimen mass**	179,99 g
		Raw density	473,30 kg/m³

Spec. pre-conditioning

Change in mass during:
drying
test

Humidity before test

Pressure 600 Pa

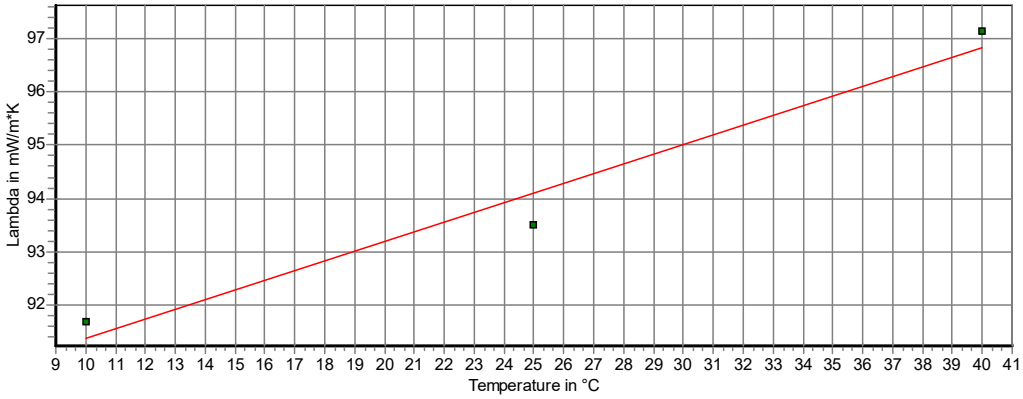

	1. Test	2. Test	3. Test
Test no.	G119_2018-04-	G119_2018-	G119_2018-
Meas.temp. in °C	40	25	10
Diff.temp. in K	15	15	15
Lambda in mW/m*K	97,14	93,5	91,69
R in m²K/W	0,174	0,1807	0,1843

Polynomial
y = ƒ(T) = 0,1817 * T + 89,57

Lambda-10	91,39	mW/(m*K)
R-10	0,1849	m²*K/W
TC	0,1817	mW/(m*K²)

29-04-2018

signature

Figure F.7: Thermal conductivity - plywood.

F.2 Ad-/Desorption isotherms

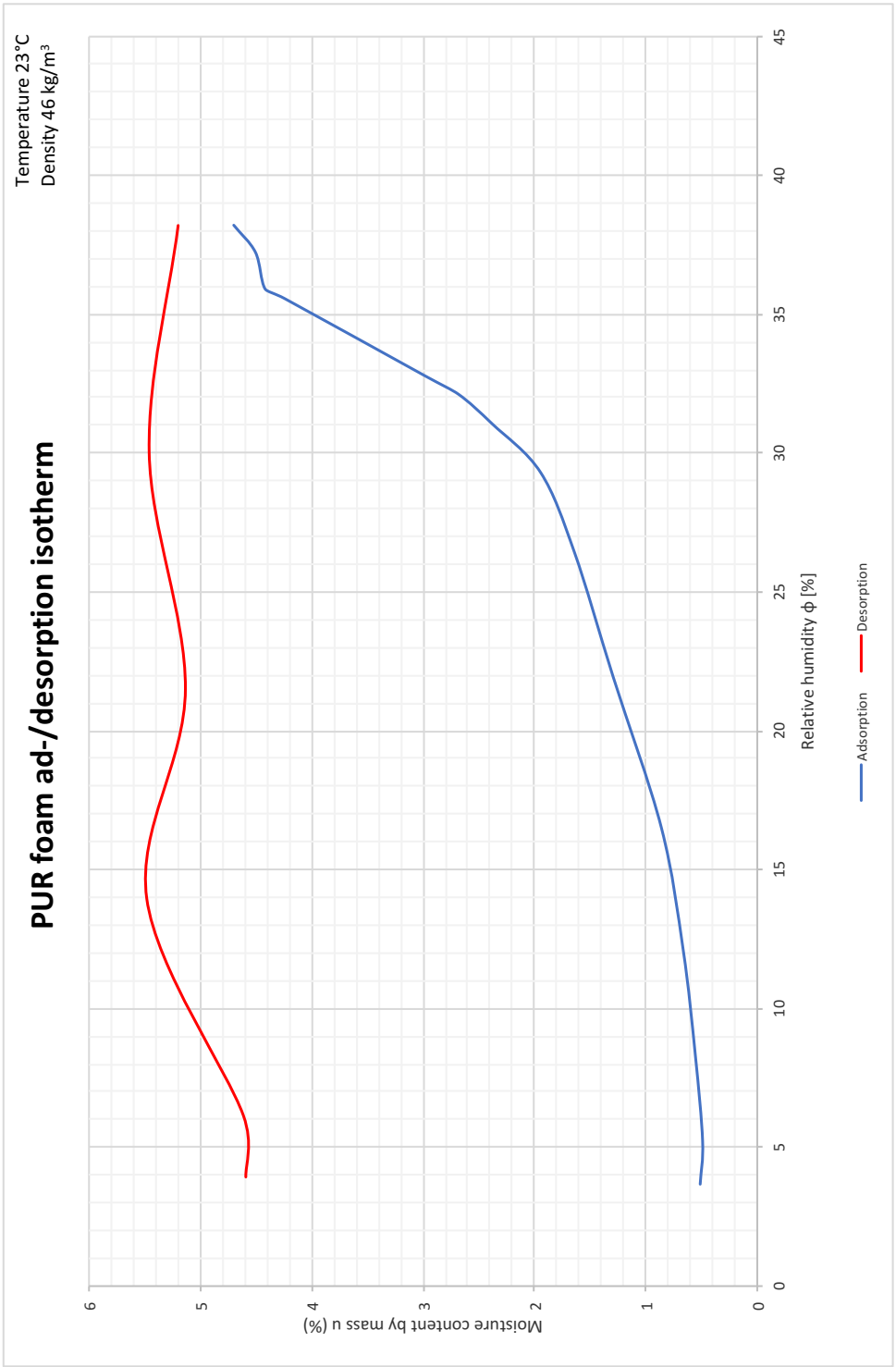

Figure F.8: PUR foam isotherm.

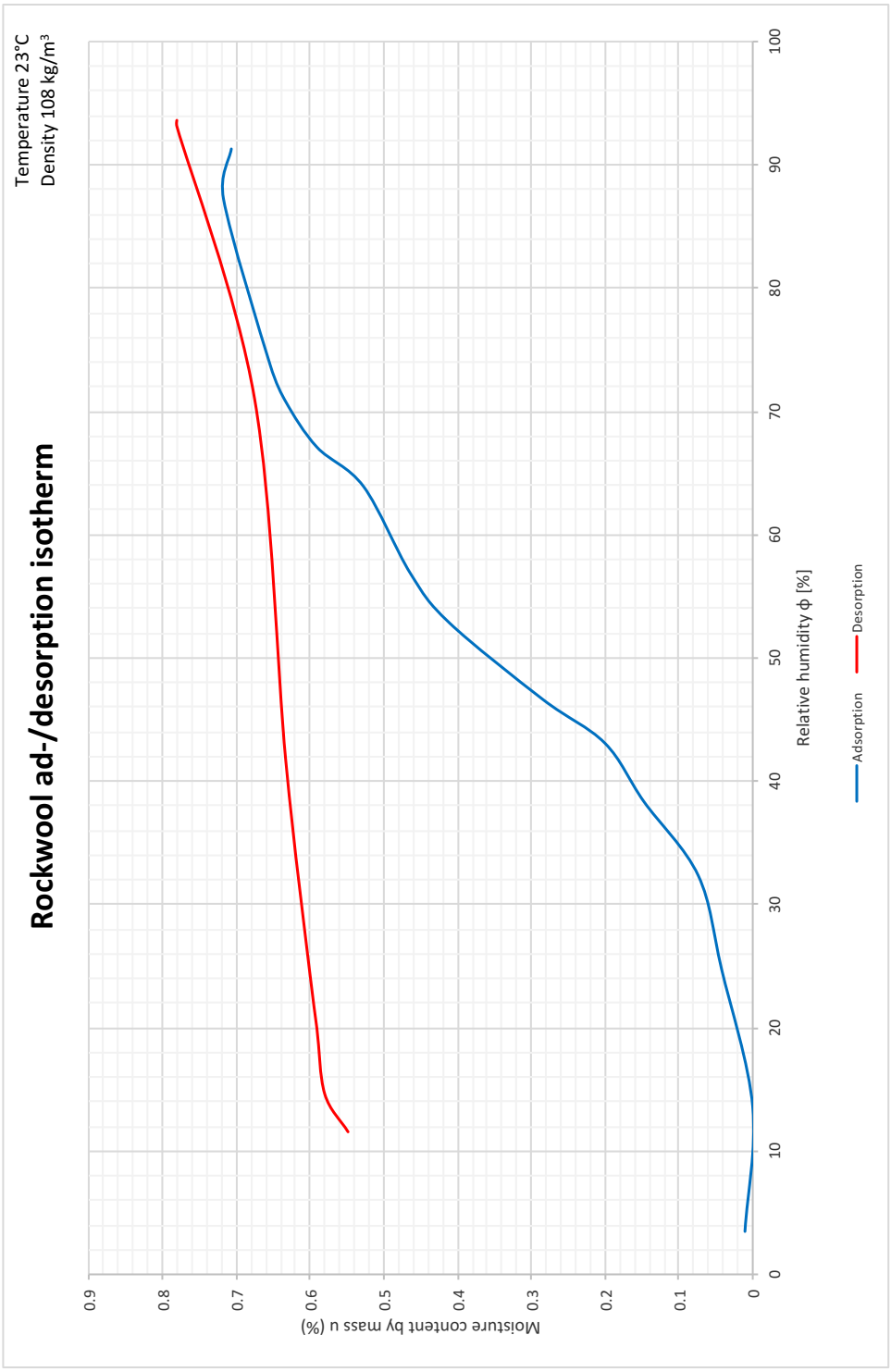

Figure F.9: Rock wool isotherm.

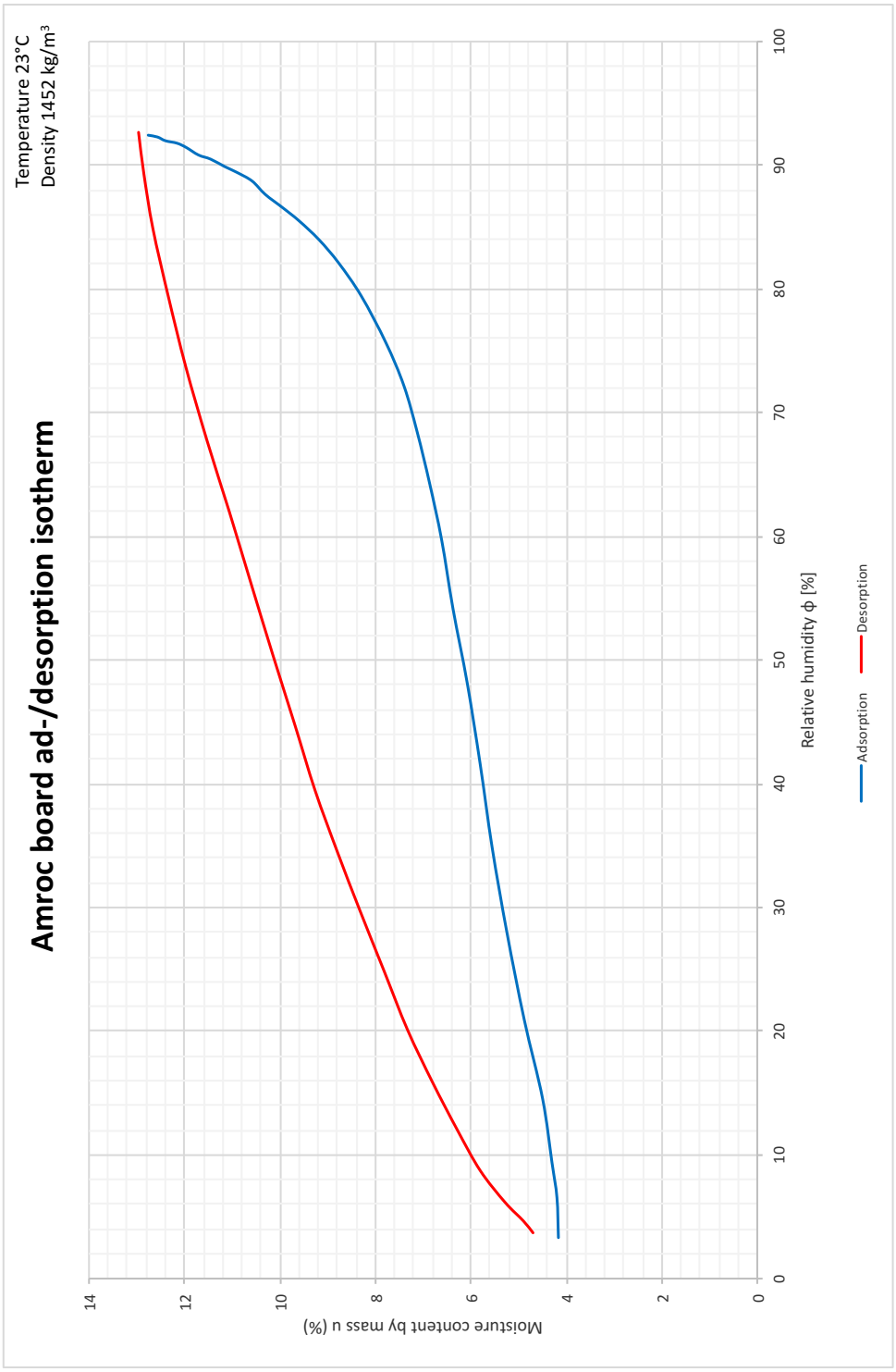

Figure F.10: Amroc board isotherm.

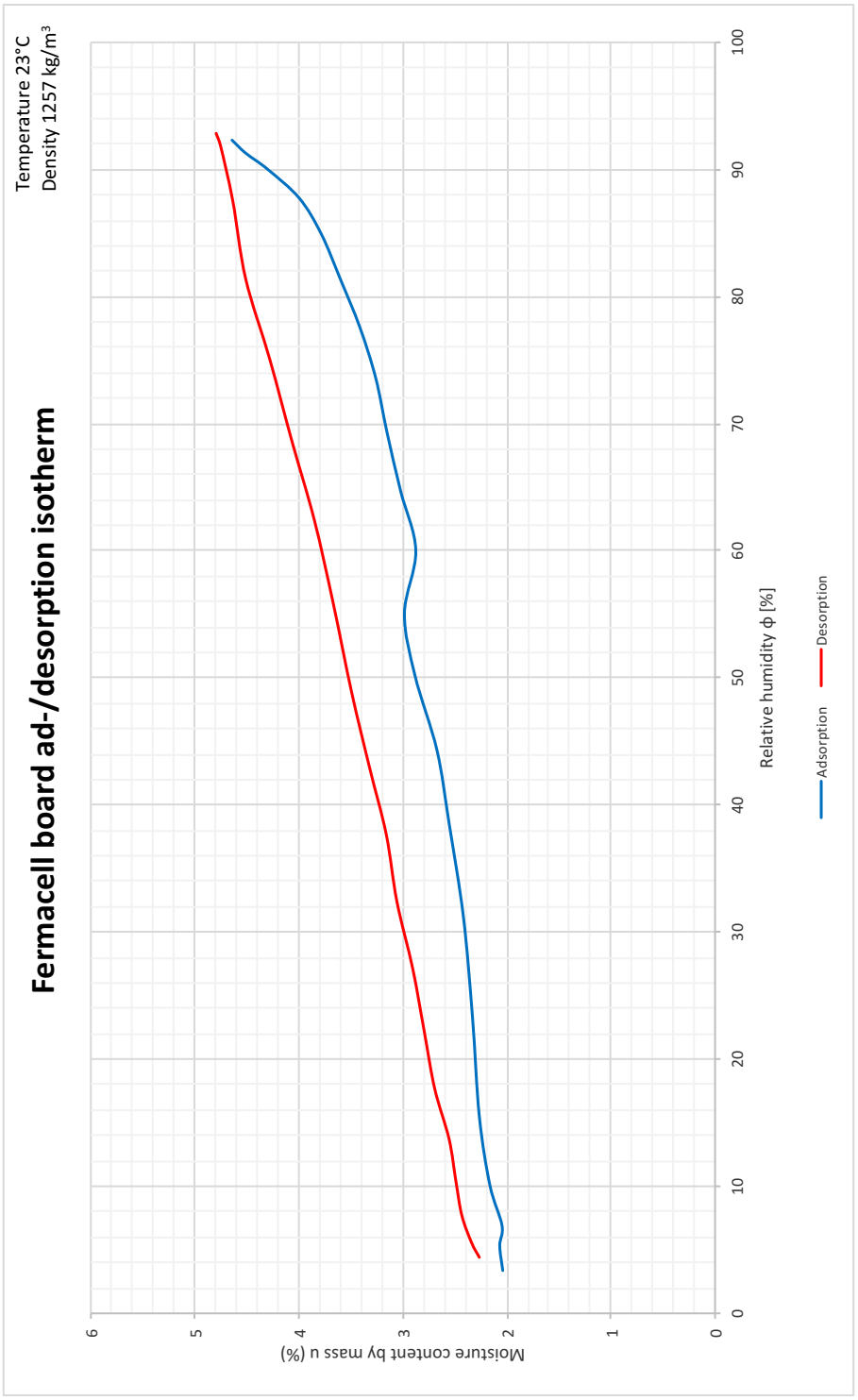

Figure F.11: Fermacell board isotherm.

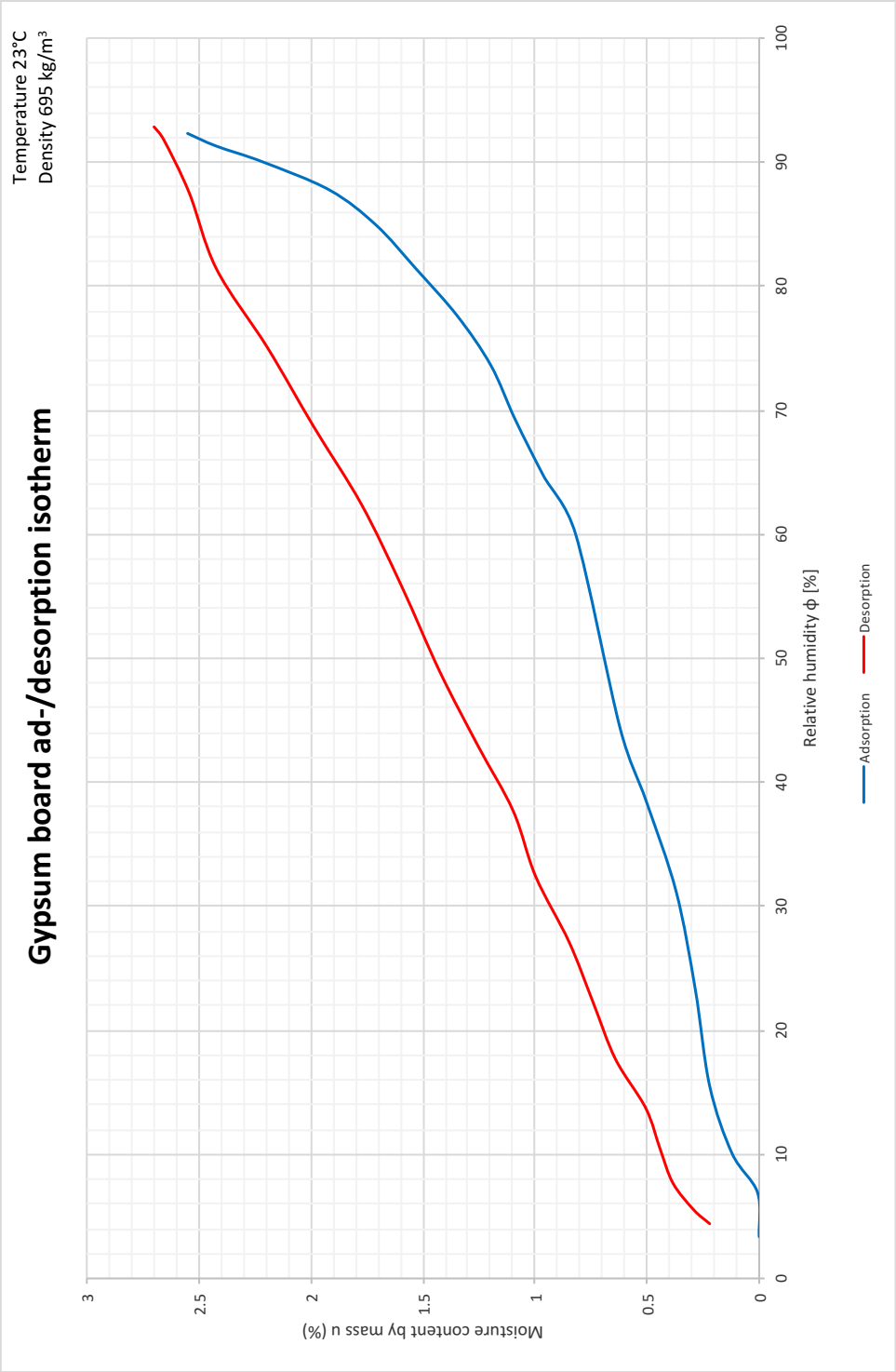

Figure F.12: Gypsum plasterboard isotherm.

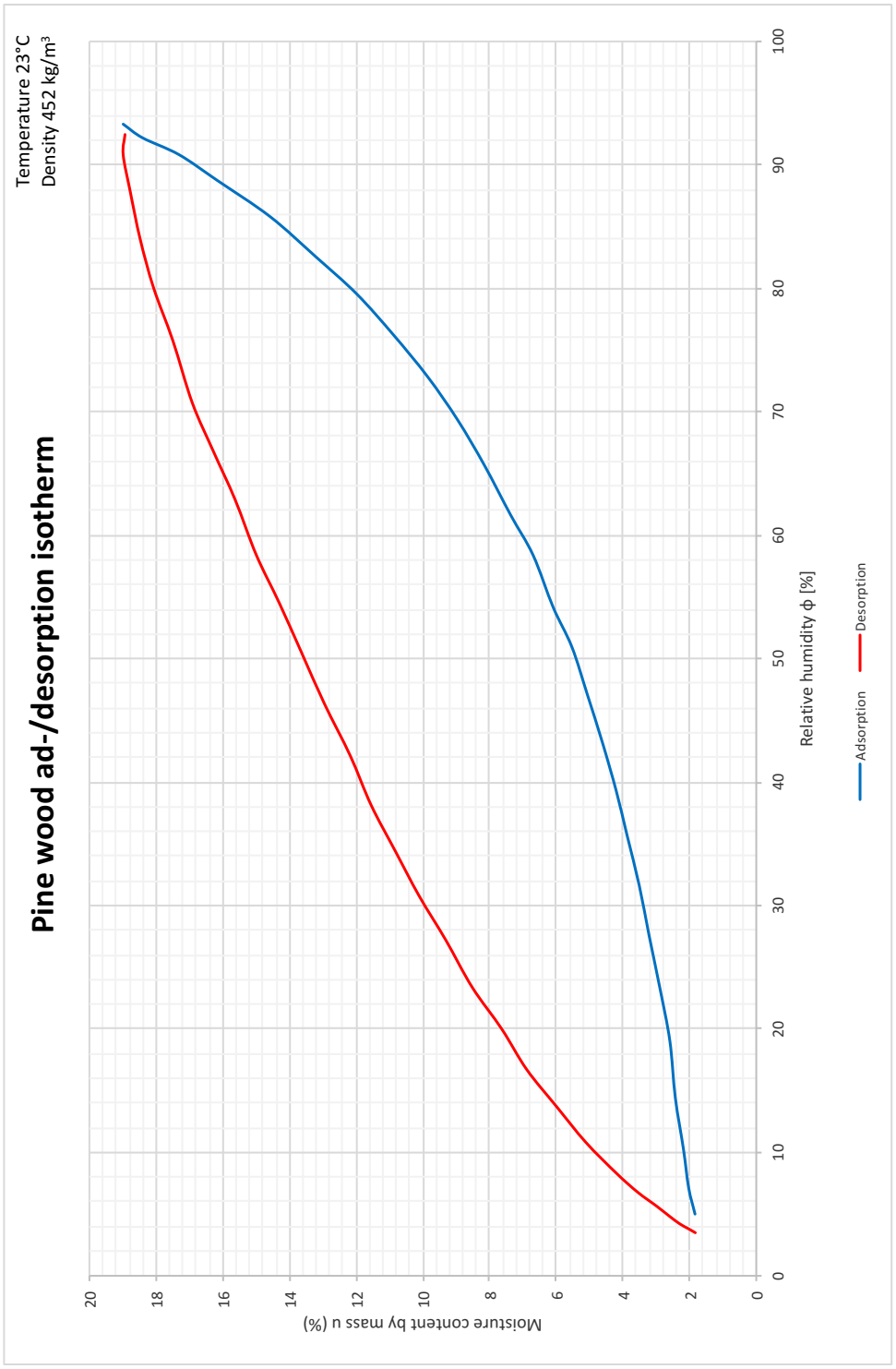

Figure F.13: Pine wood isotherm.

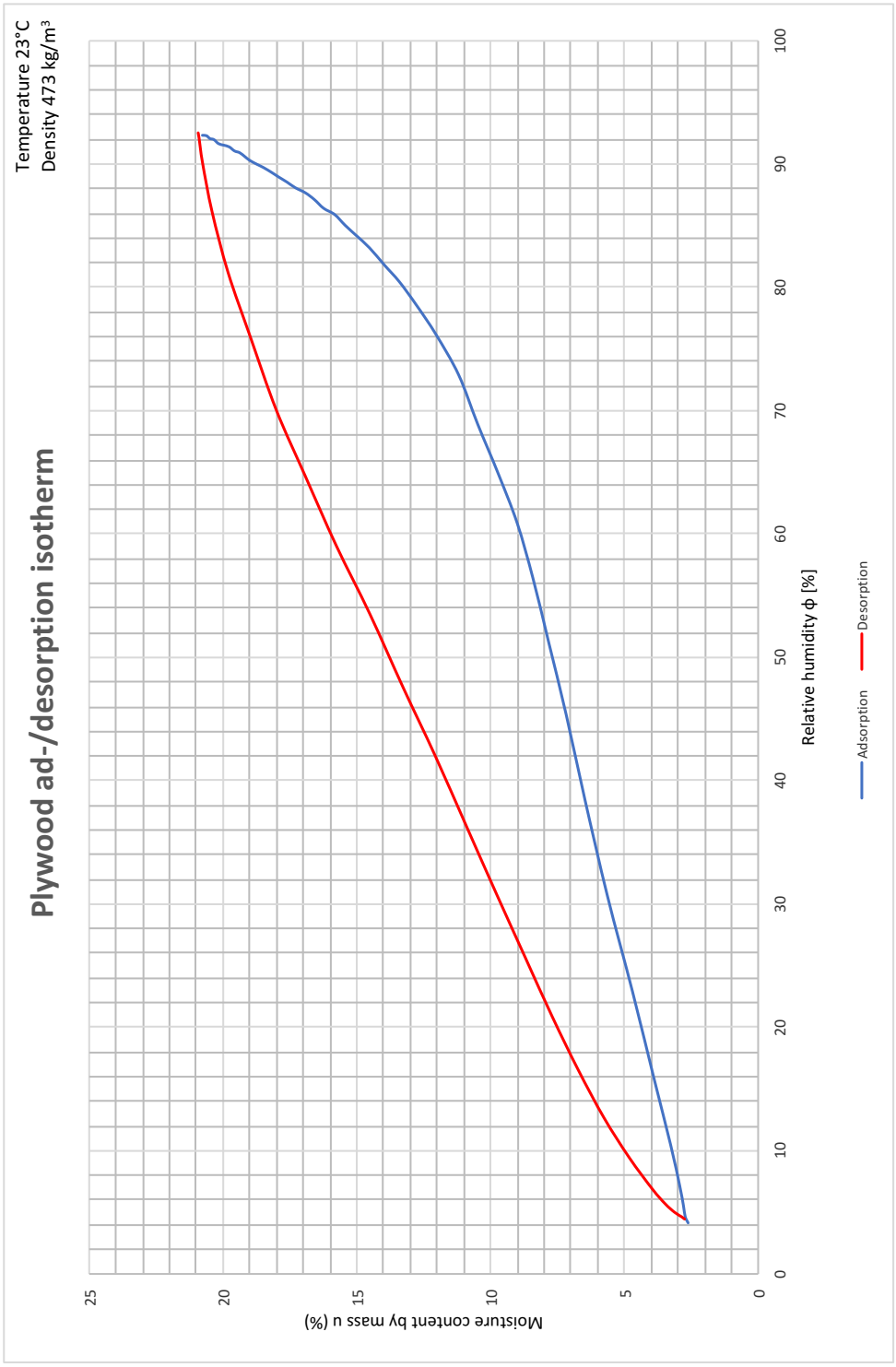

Figure F.14: Plywood isotherm.

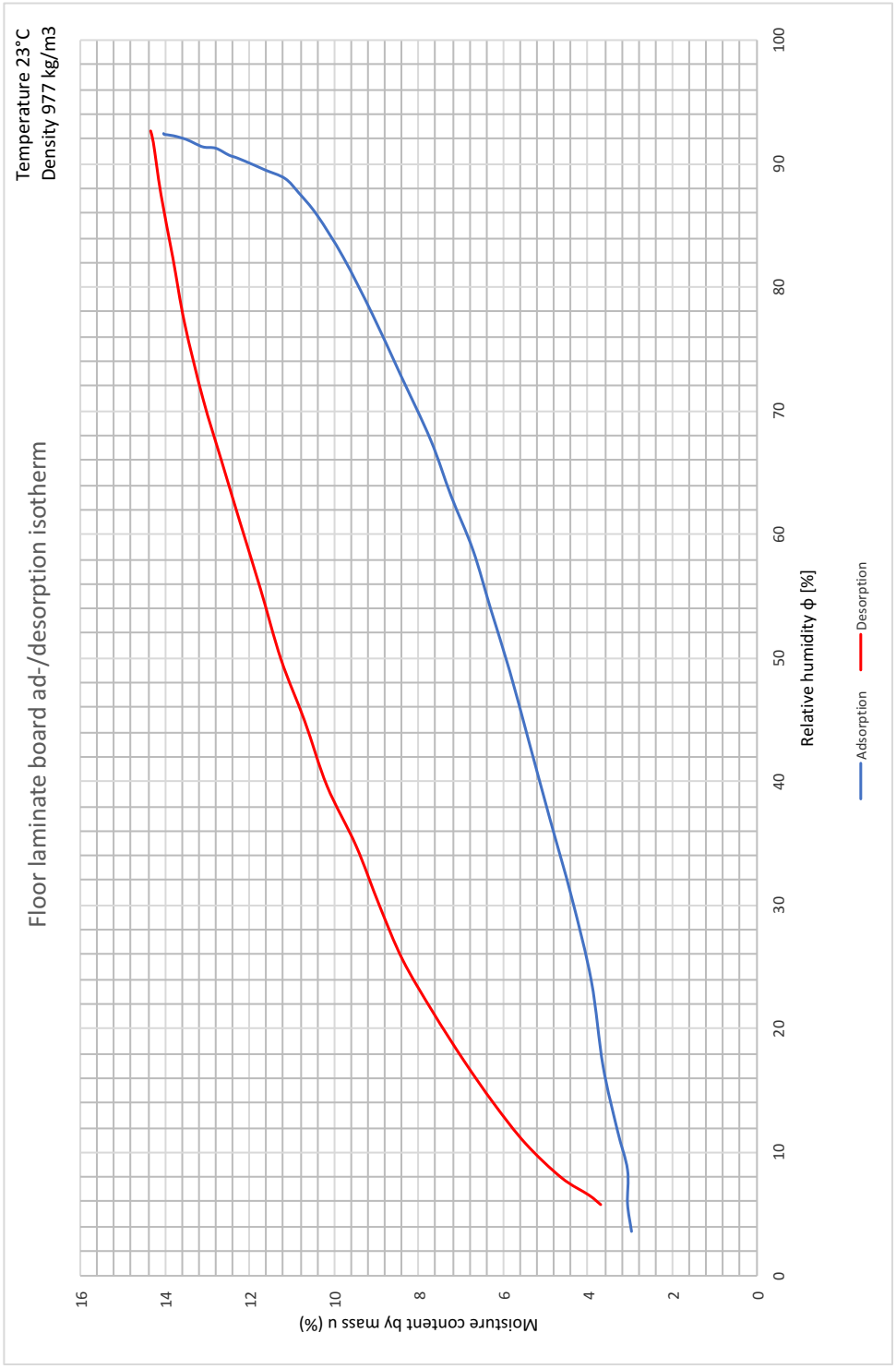

Figure F.15: Floor laminate isotherm.

Appendix G

Comsol Multiphysics results

G.1 Linear heat loss calculation

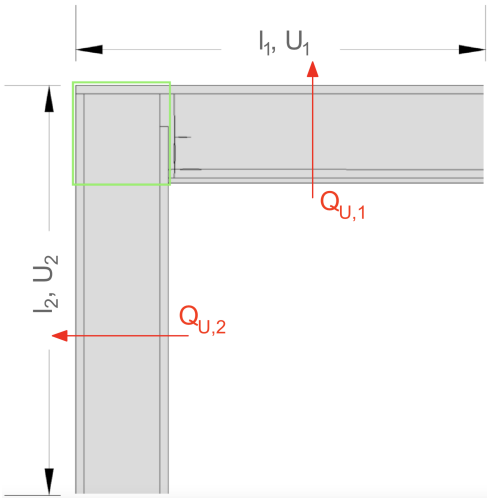

Figure G.1: BSim linear heat loss calculation principle.

Correction factors ψ_{BSim} for BSim cold bridges calculations have been derived from the following equations:

$$Q_u = (U_1 \cdot l_1 + U_2 \cdot l_2) \cdot dT \tag{G.1}$$

$$\psi_{BSim} = \frac{Q_{Comsol} - Q_U}{dT} \tag{G.2}$$

Where:

Q_u	Heat loss derived from elements' U-values [W/m]
U_i	Thermal transmittance of building element i [W/m^2K]
l_i	Distance on which U_i applies [m]
dT	Temperature difference between two sides of the elements [°C]
Q_{Comsol}	Line integration of normal total heat flux from Comsol [W/m]

Table G.1: Linear heat loss calculation for BSim simulations: l_1=l_2=1m; dT=1°C

No.	Joint	U_1	U_2	Q_U	Q_{Comsol}	ψ_{BSim}
		(W/m^2K)	(W/m^2K)	(W/m)	(W/m)	(W/mK)
A.1	Wall-wall (corner)	0.118	0.116	0.235	0.214	-0.021
A.2	Wall-wall corner (utility room)	0.102	0.102	0.204	0.175	-0.029
A.3	Wall-roof (beam)	0.065	0.117	0.182	0.177	-0.005
A.4	Wall-roof (gable)	0.074	0.117	0.191	0.154	-0.037
A.5	Wall-roof (Room 1)	0.118	0.086	0.204	0.182	-0.023
A.6	Wall-roof (Room 1 - gable)	0.117	0.084	0.201	0.168	-0.034
A.7	Room 1 roof-building	0.117	0.055	0.142	0.109	-0.032
A.8	Wall-slab (Conference room)	0.117	0.069	0.186	0.175	-0.011

Linear heat loss in wall-foundation joint has been calculated in accordance with Annex D.1 [**DS 418 (2011)**]. Values used in equations are listed below.

$$U_{wall} = 0.117 W/m^2 K \tag{G.3}$$

$$U_{floor} = 0.054 W/m^2 K \tag{G.4}$$

$$Q_i = 4.578 W/m \tag{G.5}$$

$$T_{ref} = 17.09^{\circ} C \tag{G.6}$$

Where:

U_{wall}	Thermal transmittance of the wall
U_{floor}	Thermal transmittance of the floor
Q_i	Total average heat flow through the internal surfaces (September to May of the 10th year)
T_{ref}	Temperature in the reference point in the same period as Q_i

Linear heat loss in wall-window joint has been calculated in accordance with Annex C.1 [**DS 418 (2011)**]. Values have been obtained in simulations with dT=1°C).

$$Q_{joint} = 0.302 W/m \tag{G.7}$$

$$Q_{wall} = 0.123 W/m \tag{G.8}$$

$$Q_{window} = 0.084 W/m \tag{G.9}$$

Where:

Q_{joint}	Two dimensional heat flow through inner surface for the entire joint
Q_{wall}	Two dimensional heat flow through inner surface only for the wall
Q_{winow}	Two dimensional heat flow through inner surface only for the window

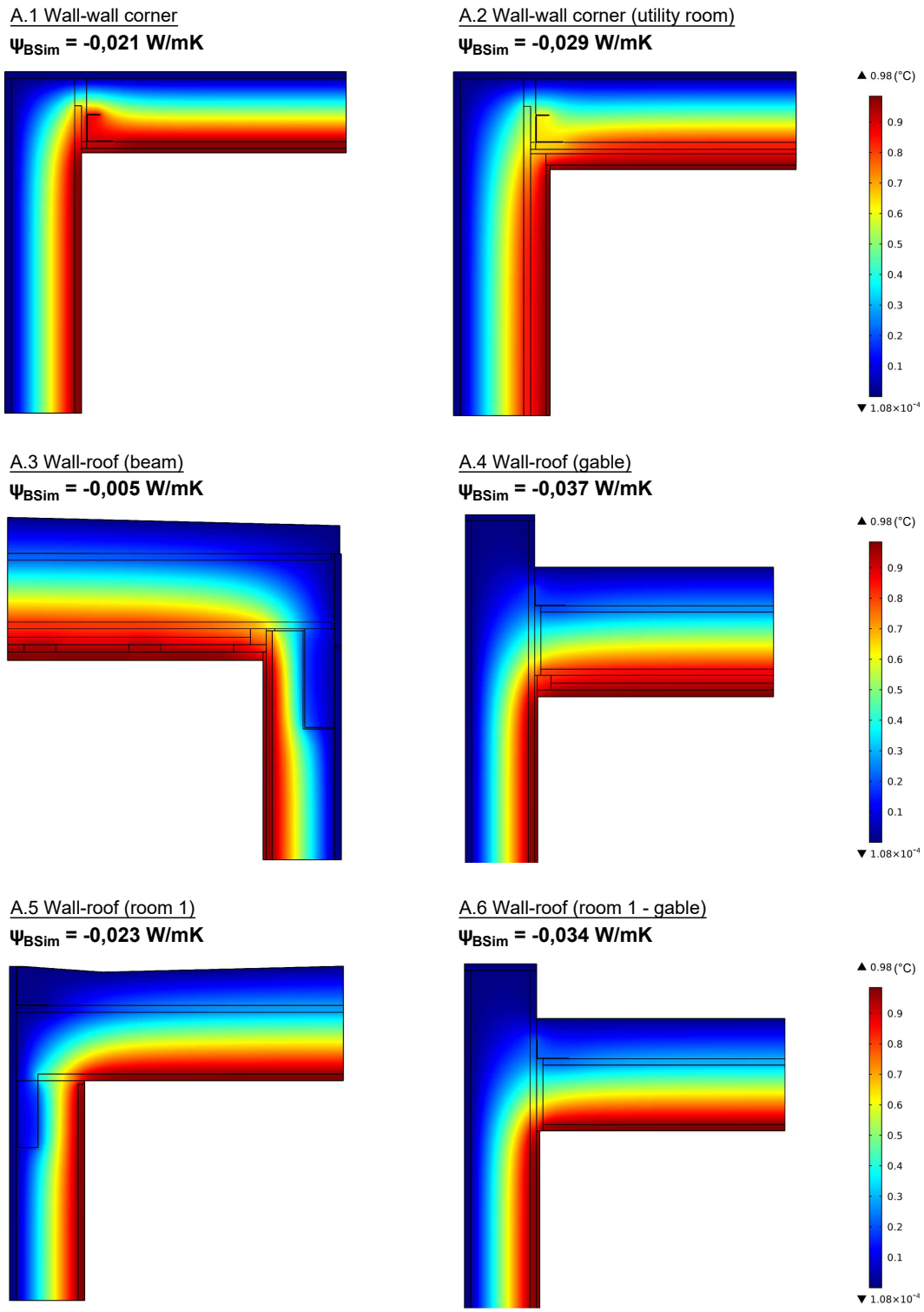

Figure G.2: Linear heat loss plots (part 1 of 2).

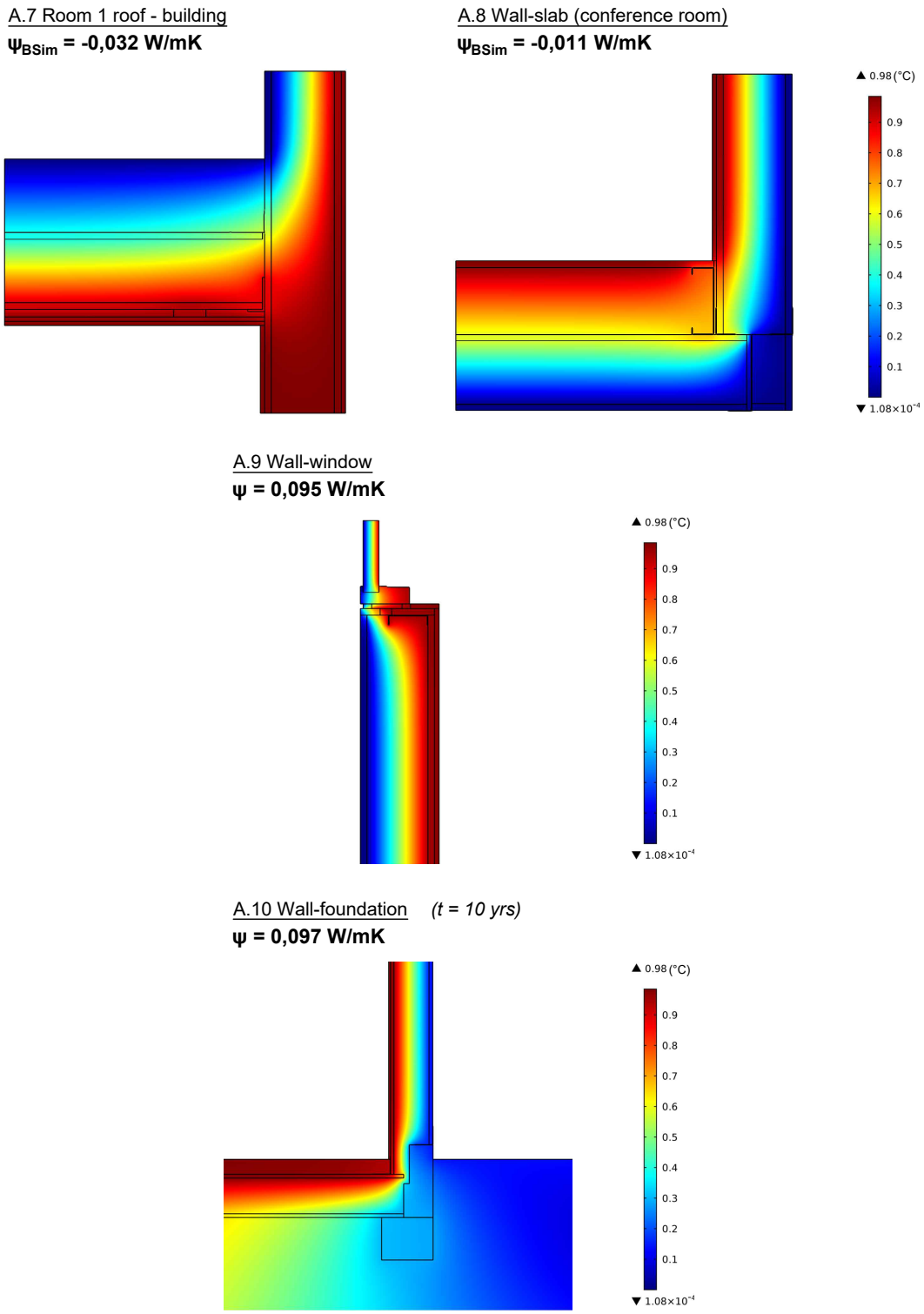

Figure G.3: Linear heat loss plots (part 2 of 2).

Appendix H

BSim results

H.1 Data treatment

The temperature retrieved from BSim simulations is called TopMean which is the value obtained form the simulations is the operative (experienced) indoor temperature mean over the hour. It is derived as average of mean radiant (area weighted surface temperature) and indoor air temperature. **[BSim (2013)]**

This number is compared with the one measured by the sensors present in the Test House. To combine them it in comprehensive, easy to read parameter, two different tools (recalculation schemes) have been applied.

- Deviation D which expresses the difference between simulated $a_{sim,i}$ and measured $a_{meas,i}$ parameter i. It also indicates if the outcome of simulation is overestimated (positive D) or underestimated (negative D). Deviation illustrates the divergence of the distributions together with it tendency towards too low or too high evaluation.

$$D = a_{sim,i} - a_{meas,i} \tag{H.1}$$

- Absolute error E expresses the difference between simulated $a_{sim,i}$ and measured $a_{meas,i}$ parameter i without indicating kind of the divergence. In other words, it captures how much two distributions are apart, ignoring their relation (positive or negative).

$$E = max(a_{sim,i}; a_{meas,i}) - min(a_{sim,i}; a_{meas,i}) \tag{H.2}$$

The absolute water content calculation for the measured temperature and relative humidity inside the wall structure has been evaluated with use of Air Psychrometric Chart. To automatize interpolations, Excel spreadsheet has been used **[PXL HVAC (2016)]**. What is more, to reduce the influence of this approximation inaccuracy between measured and simulated values, the raw data (temperatures and relative humidity) retrieved from BSim has been also subjected to Air Psychrometric Chart treatment to obtain absolute water content values.

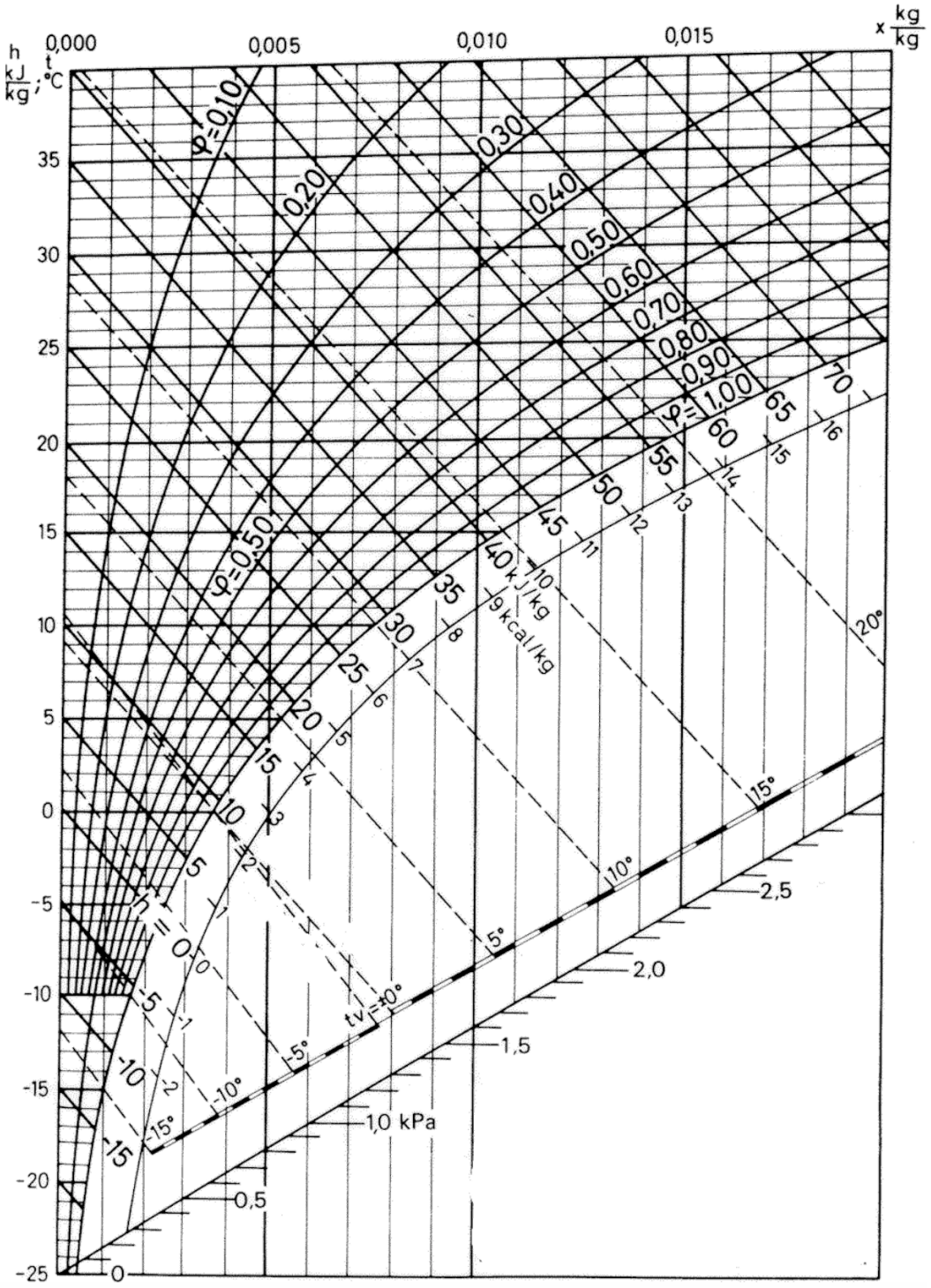

Figure H.1: Air Psychrometric Chart. [**engineeringtoolbox.com (2018)**]

H.2 Thermal zones - temperature plots

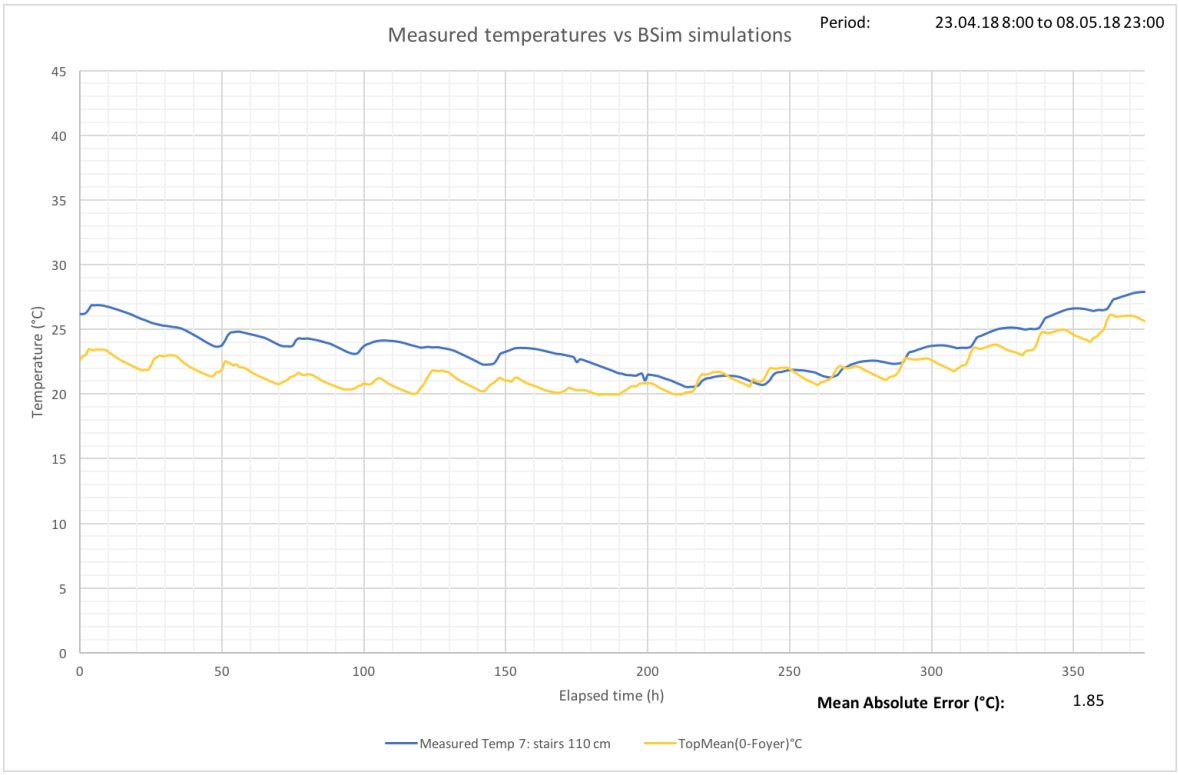

Figure H.2: Simulated vs measured temperature - Foyer.

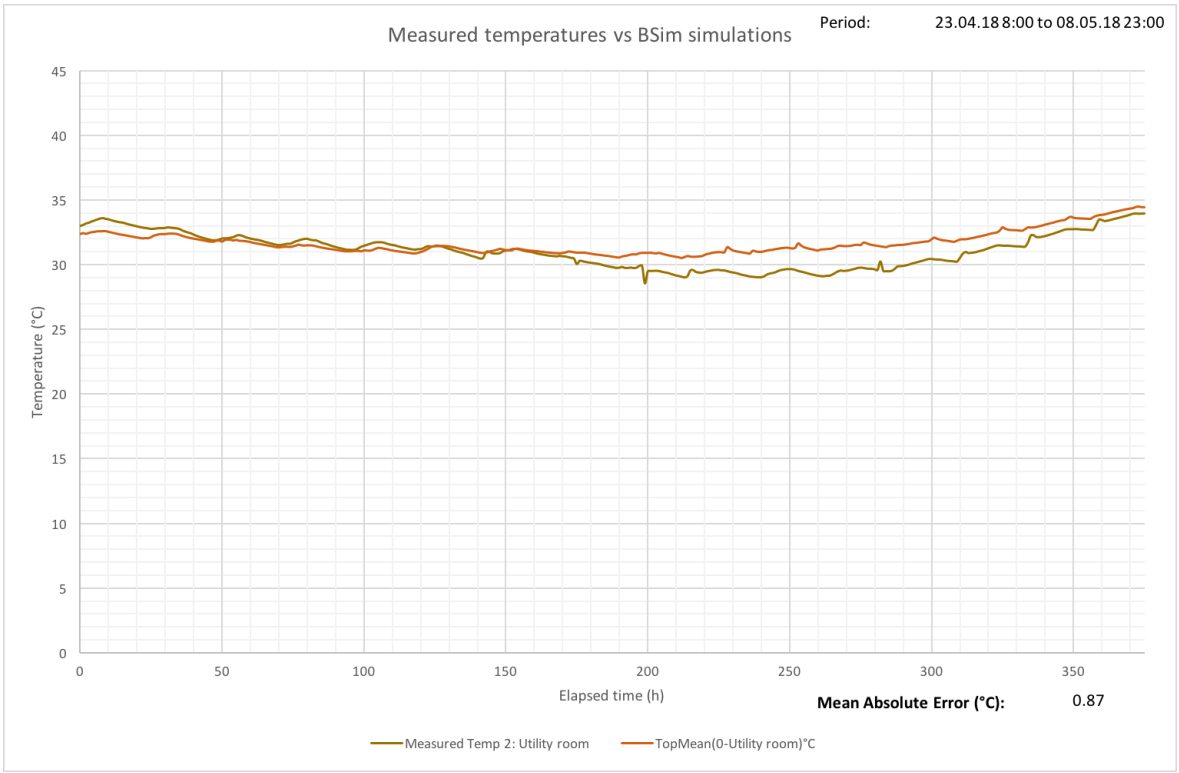

Figure H.3: Simulated vs measured temperature - Utility room.

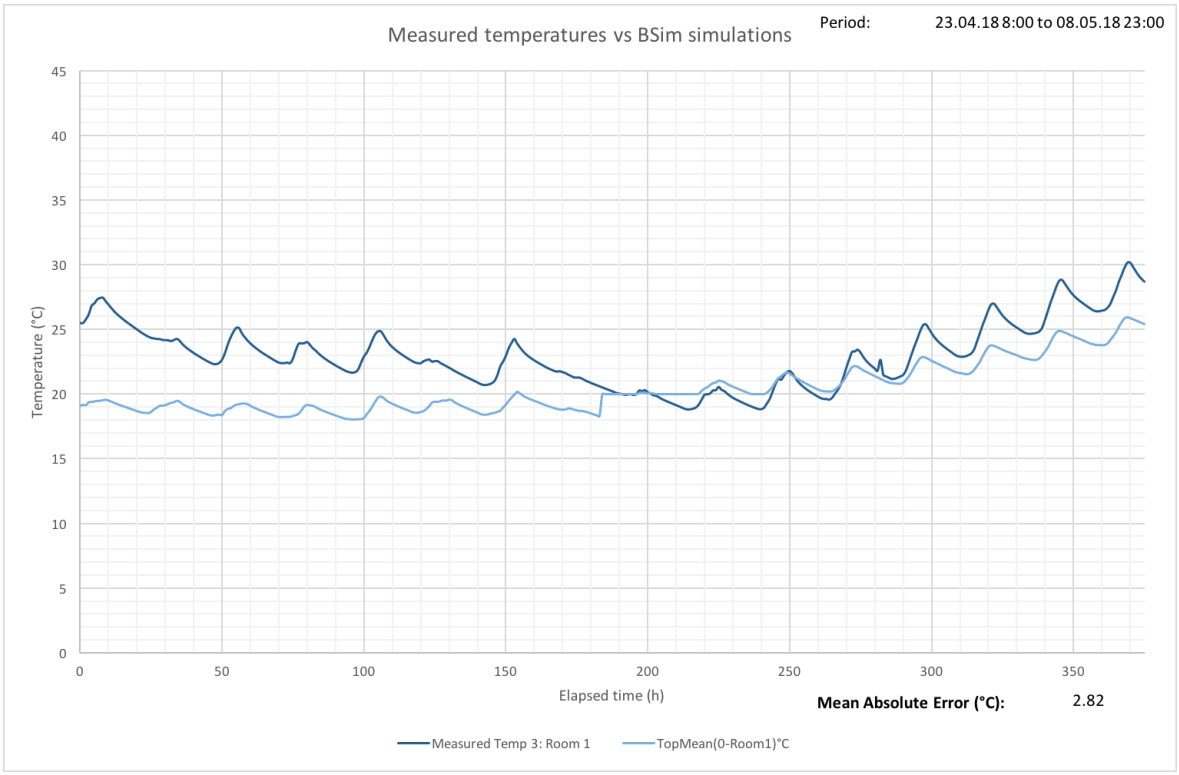

Figure H.4: Simulated vs measured temperature - Room 1.

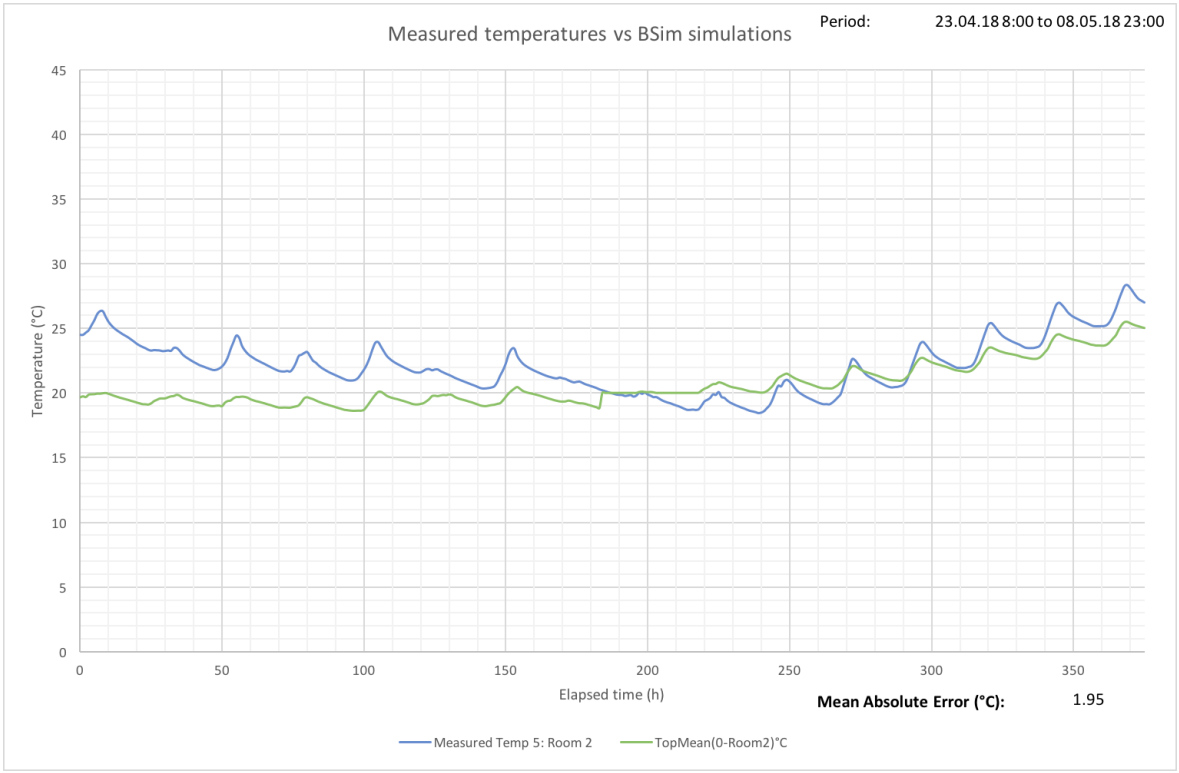

Figure H.5: Simulated vs measured temperature - Room 2.

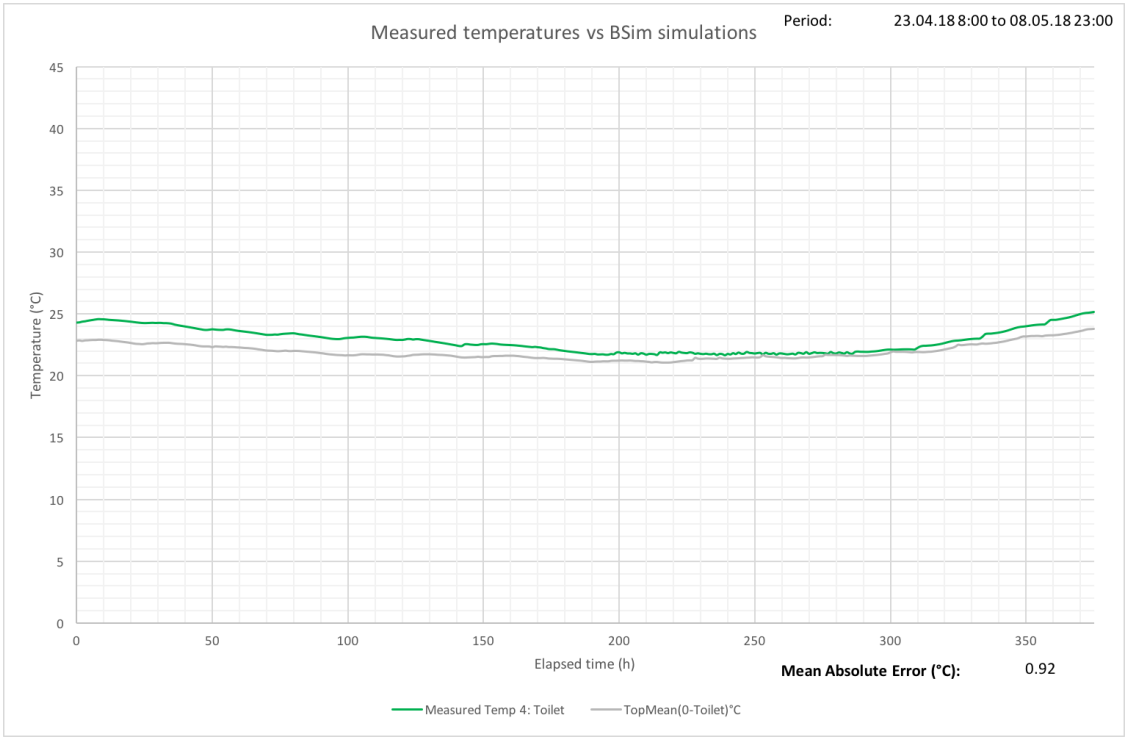

Figure H.6: Simulated vs measured temperature - Toilet.

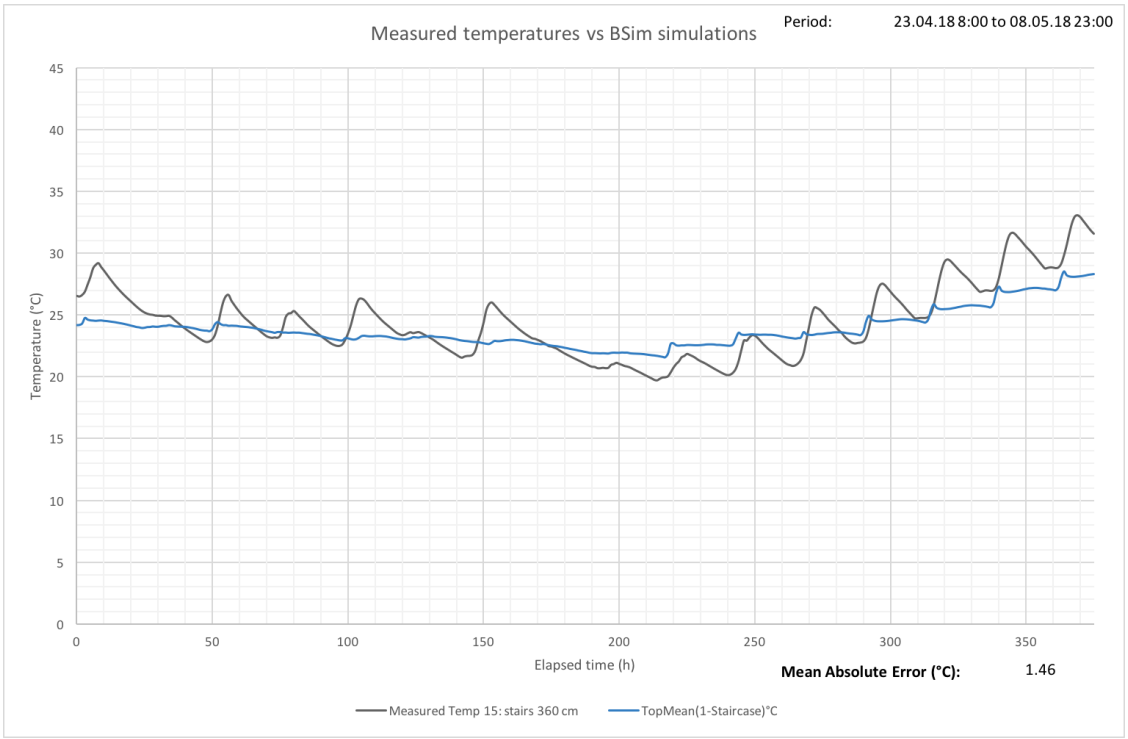

Figure H.7: Simulated vs measured temperature - Staircase 1.

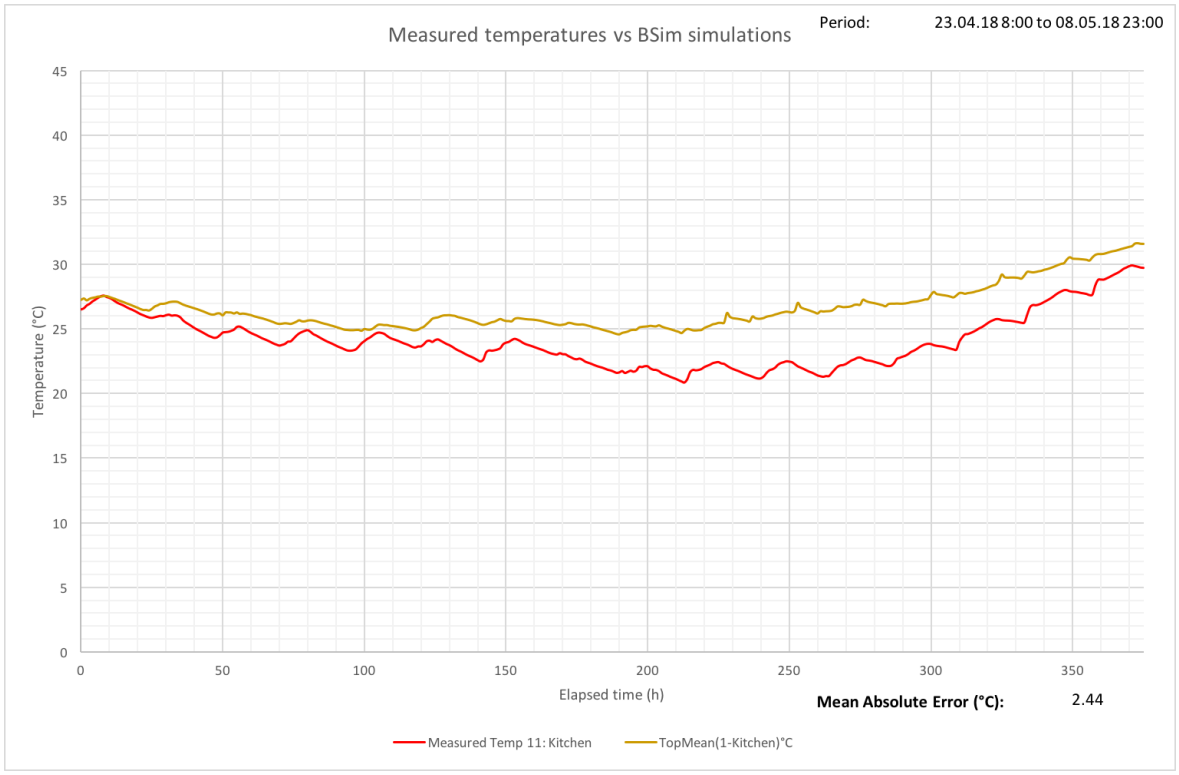

Figure H.8: Simulated vs measured temperature - Kitchen.

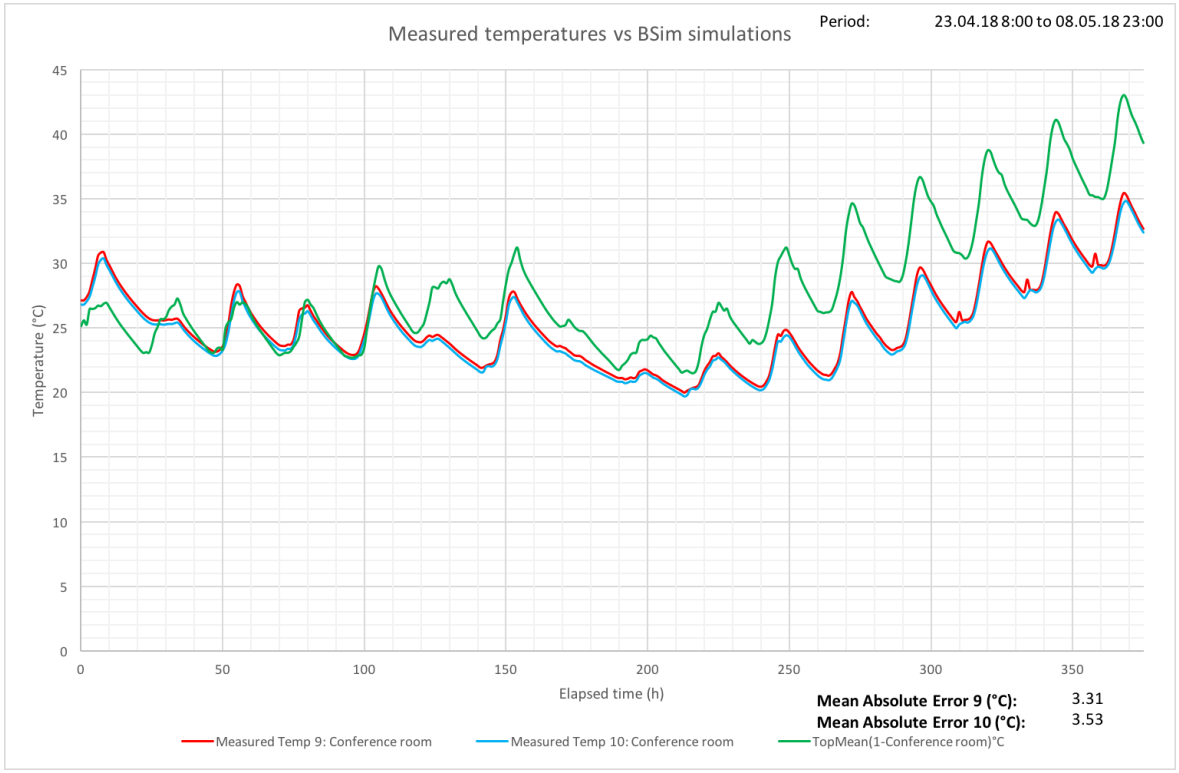

Figure H.9: Simulated vs measured temperature - Conference room.

H.3 Wall structure - temperature plots

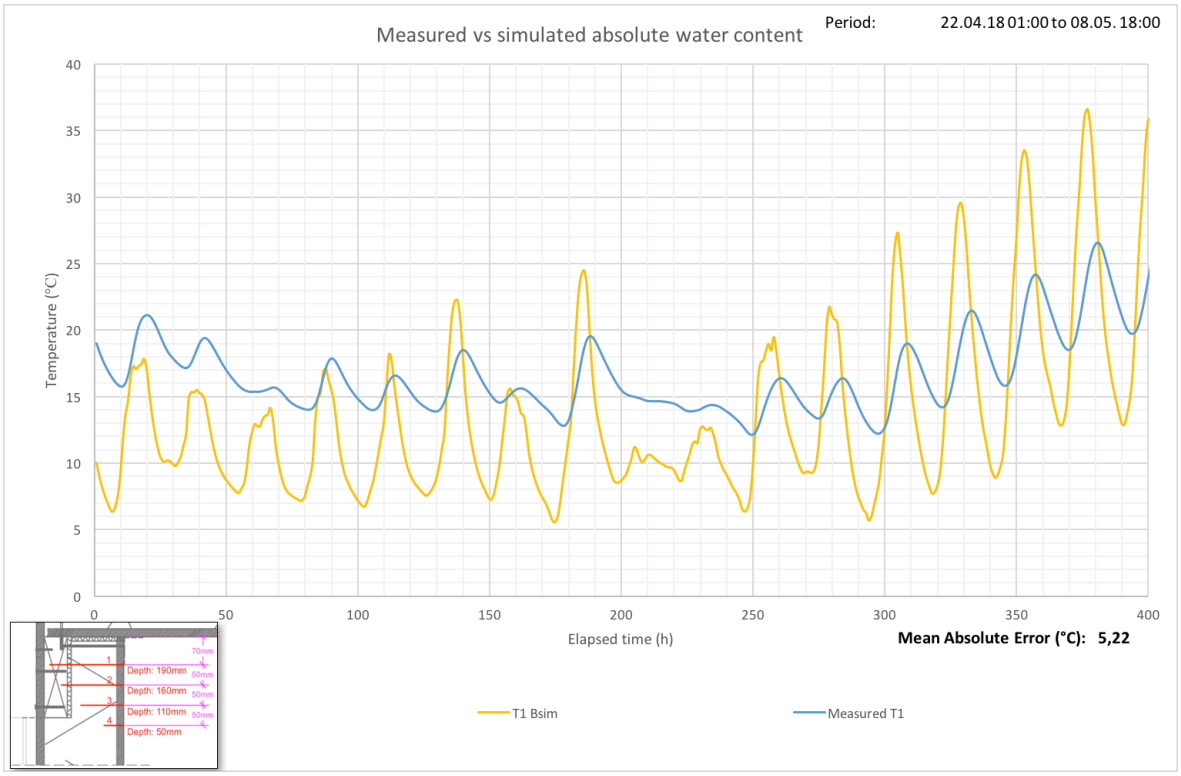

Figure H.10: Simulated vs measured temperature - sensor 1.

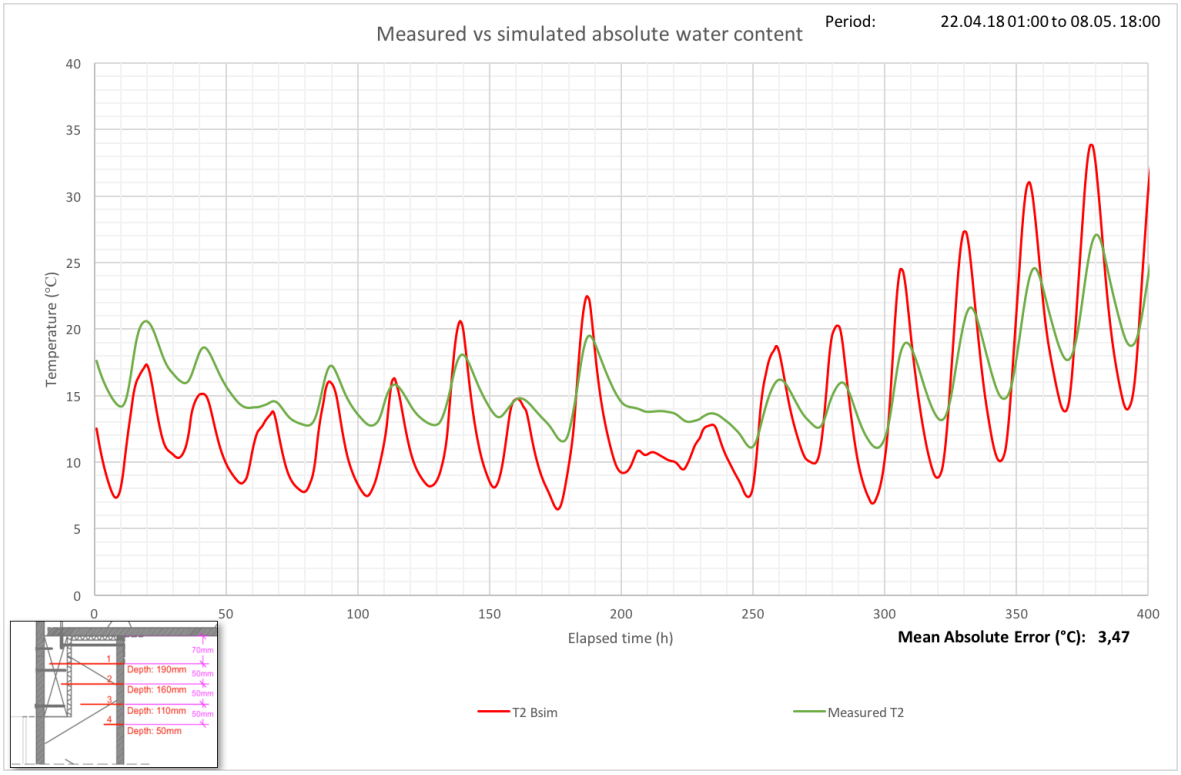

Figure H.11: Simulated vs measured temperature - sensor 2.

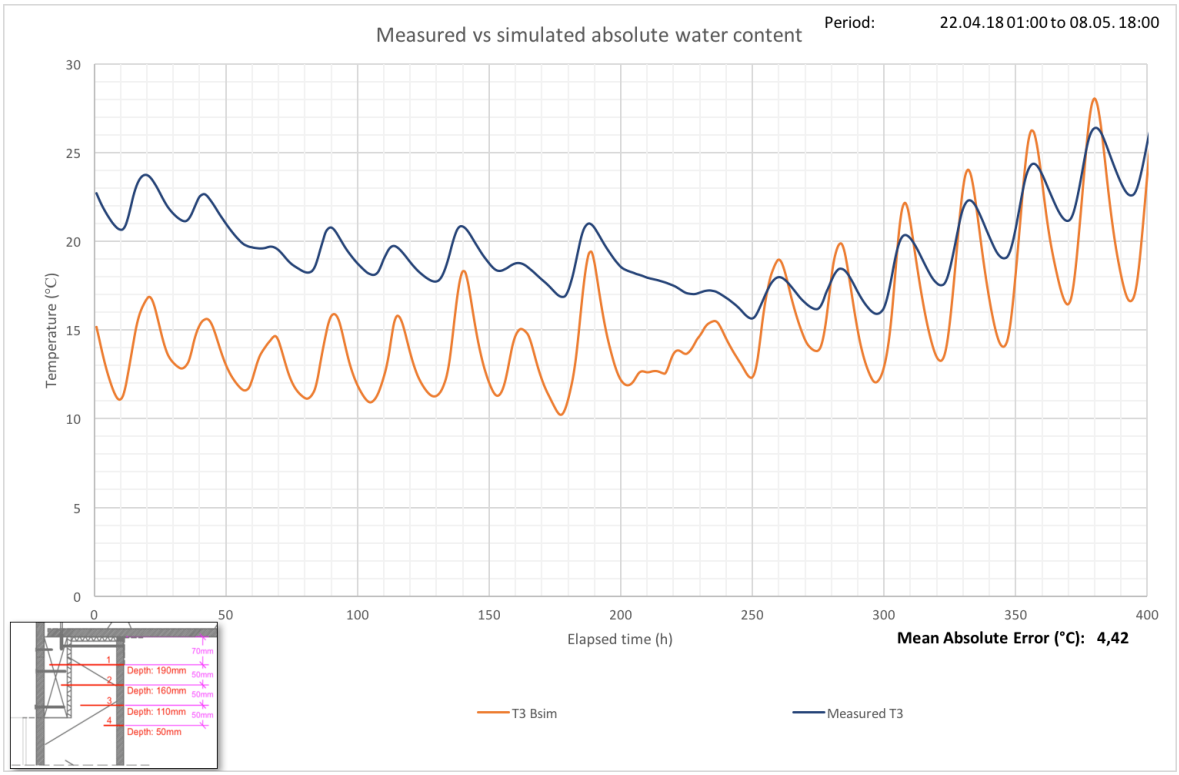

Figure H.12: Simulated vs measured temperature - sensor 3.

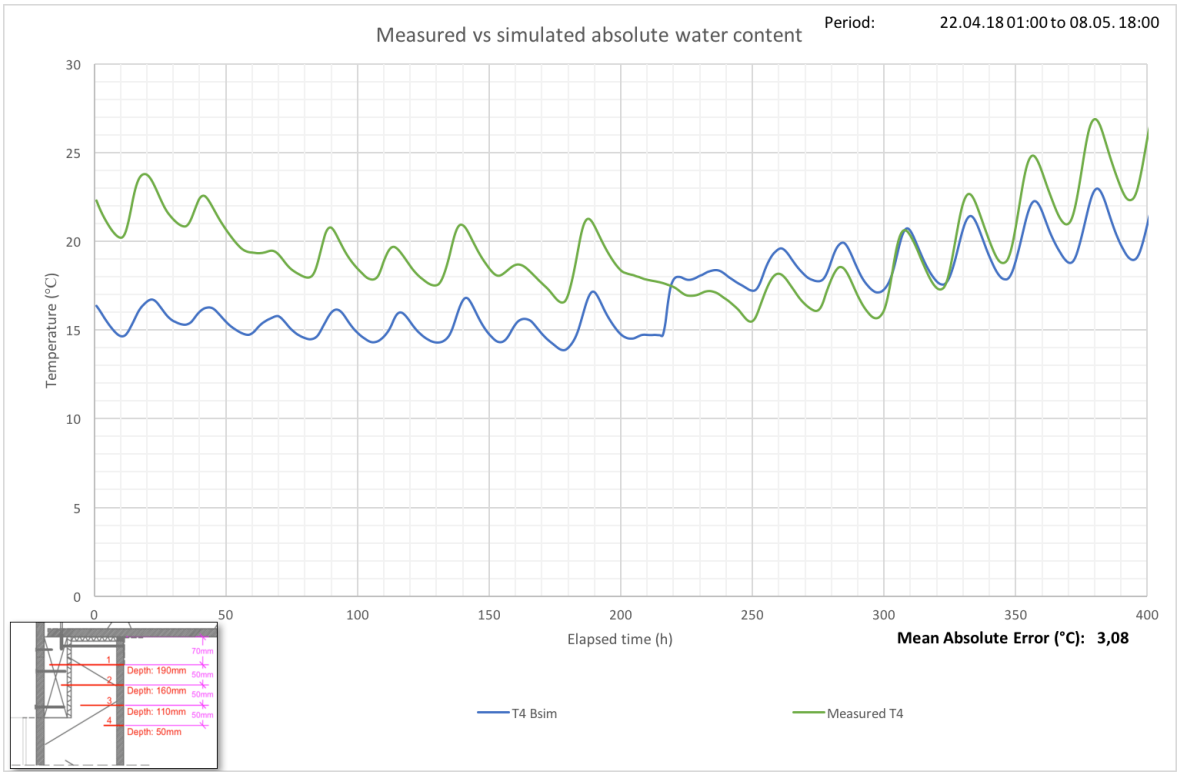

Figure H.13: Simulated vs measured temperature - sensor 4.

H.4 Wall structure - relative humidity plots

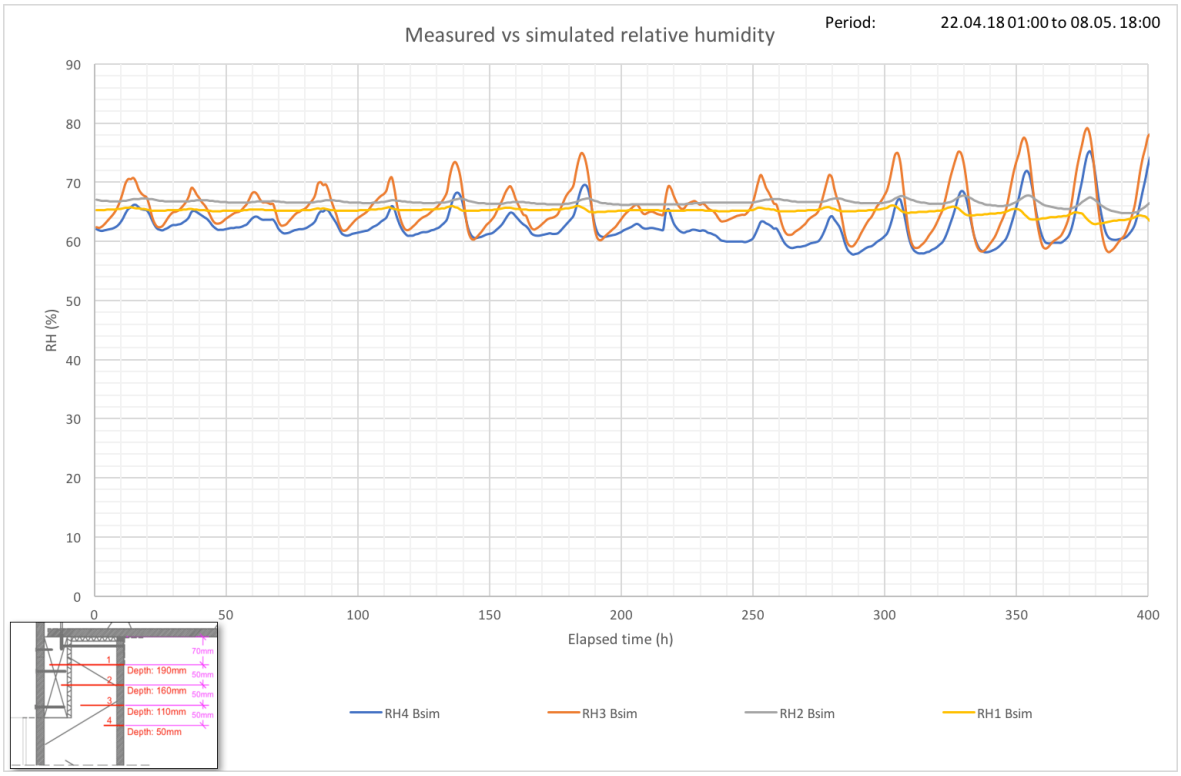

Figure H.14: Simulated relative humidity.

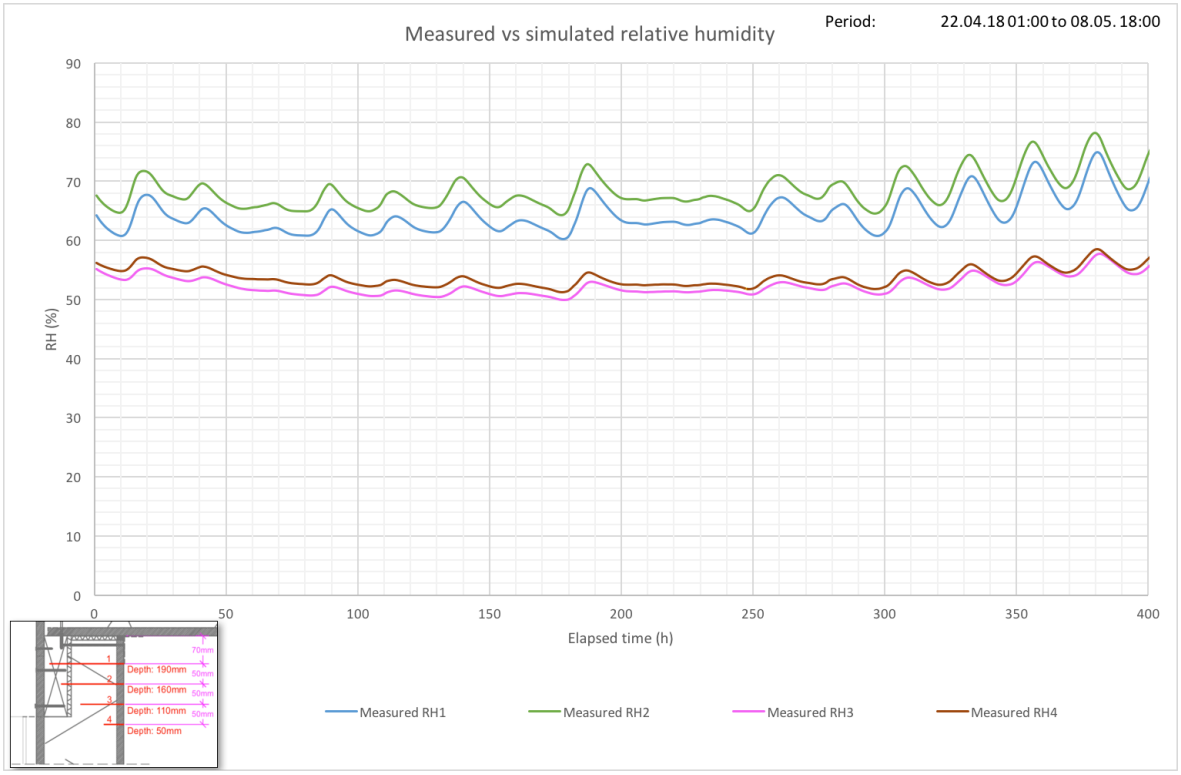

Figure H.15: Measured relative humidity.

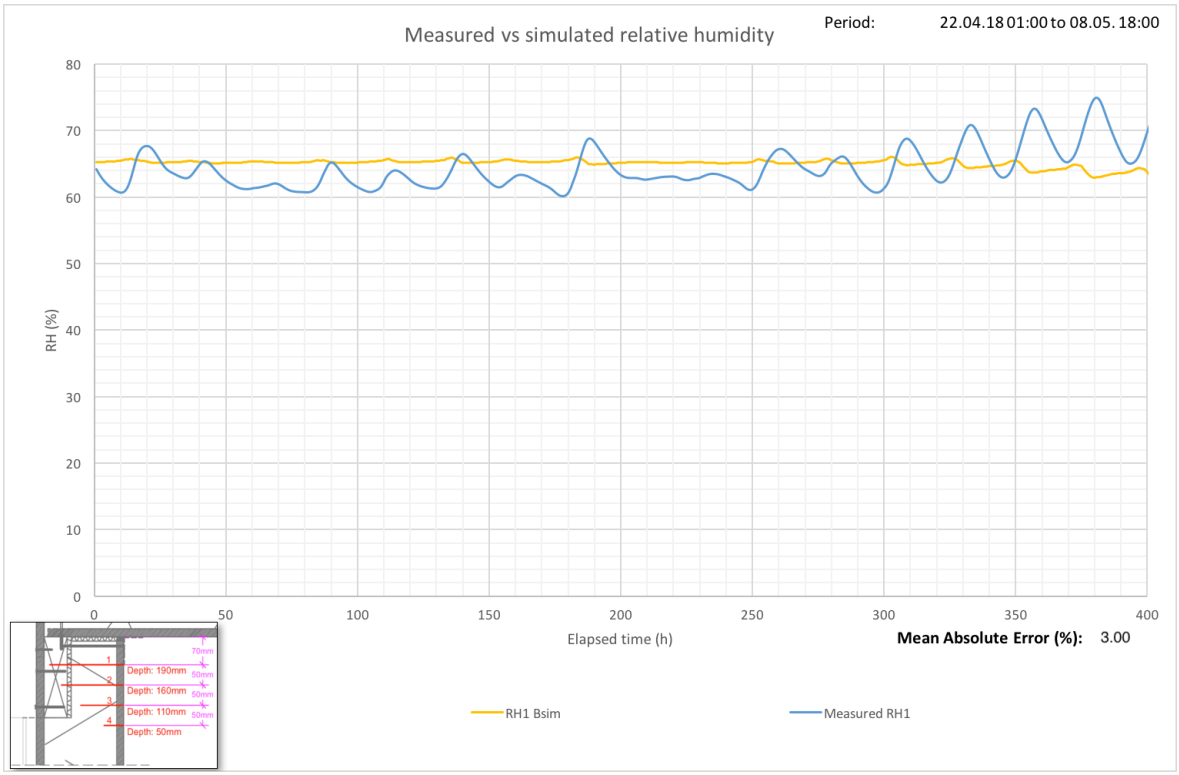

Figure H.16: Simulated vs measured relative humidity - sensor 1.

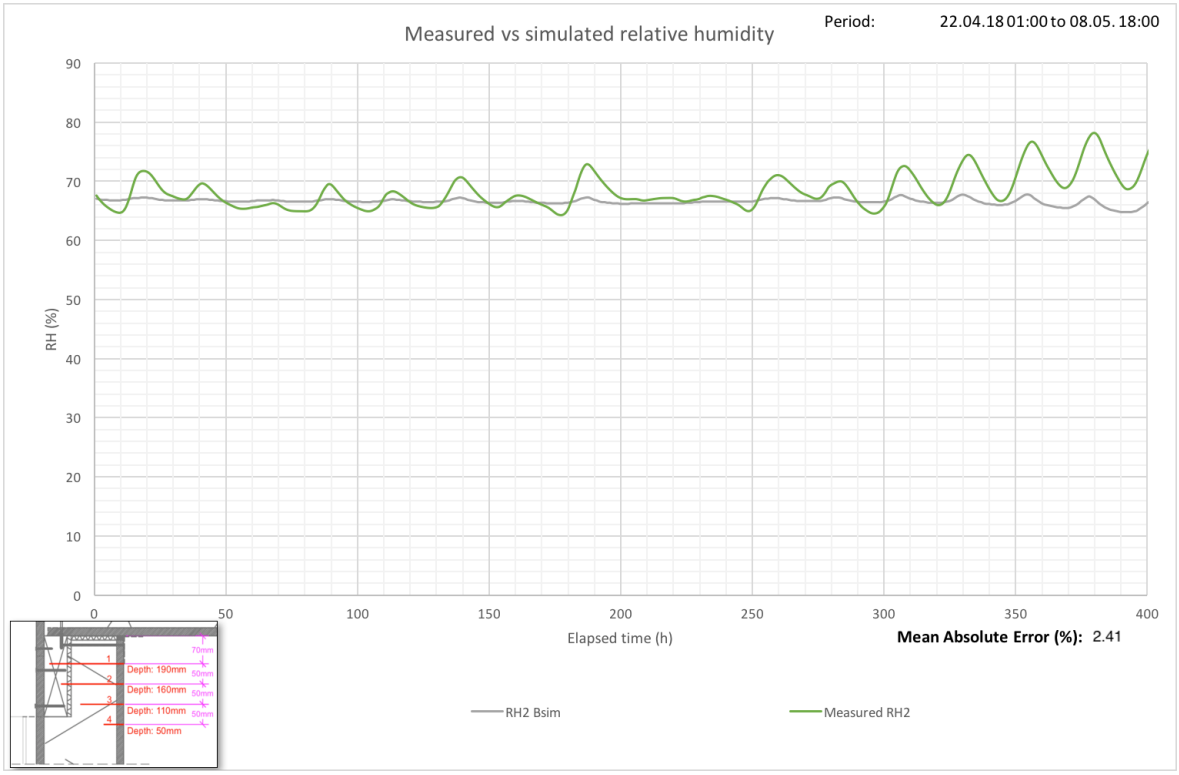

Figure H.17: Simulated vs measured relative humidity - sensor 2.

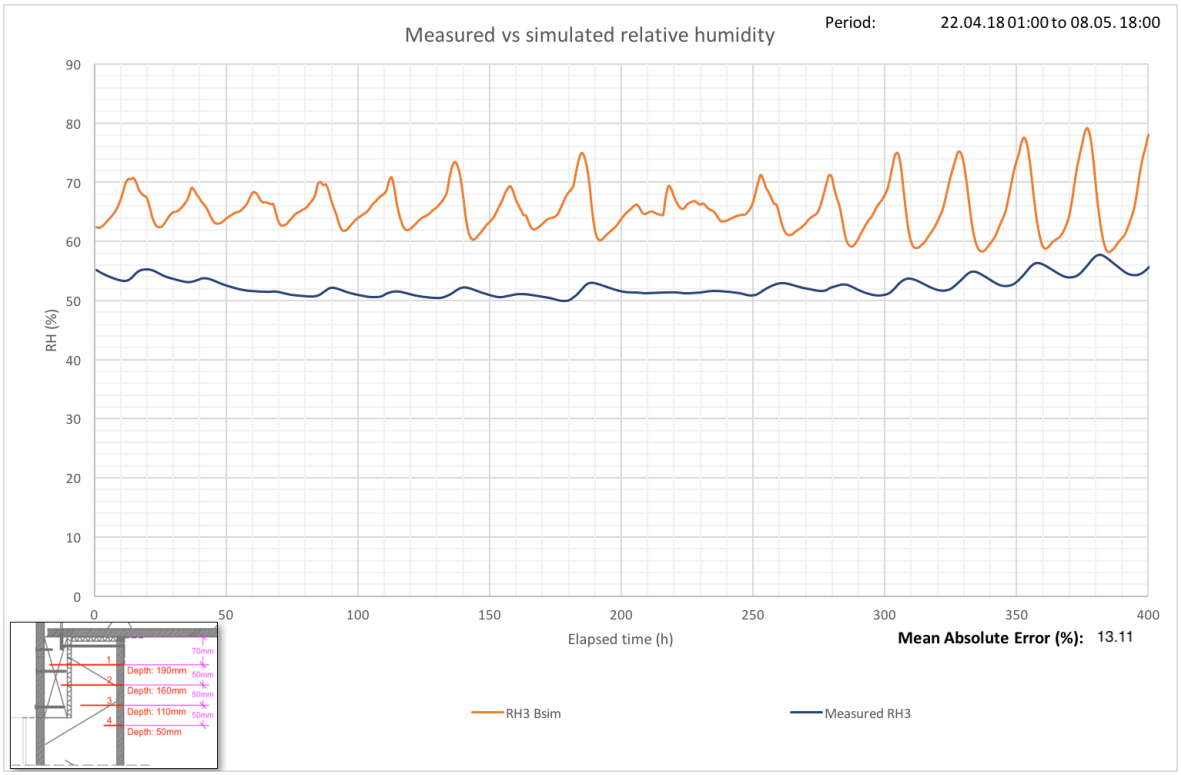

Figure H.18: Simulated vs measured relative humidity - sensor 3.

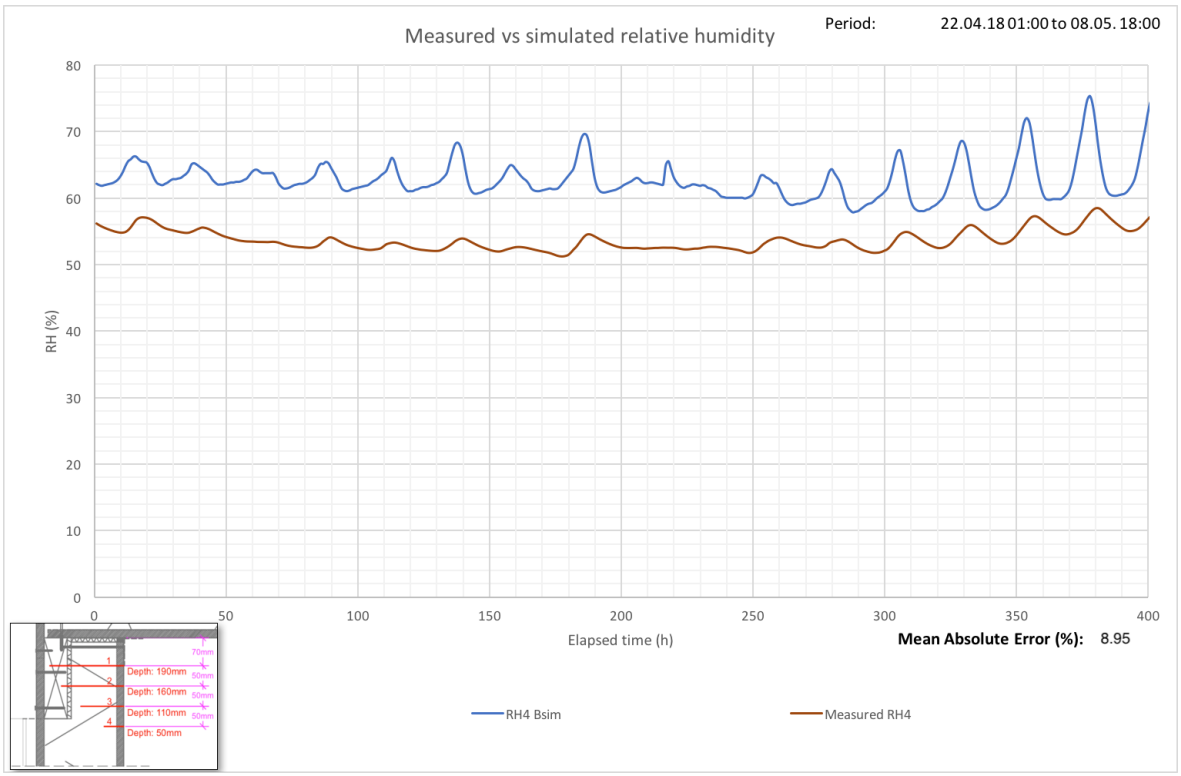

Figure H.19: Simulated vs measured relative humidity - sensor 4.

H.5 Wall structure - absolute water content plots

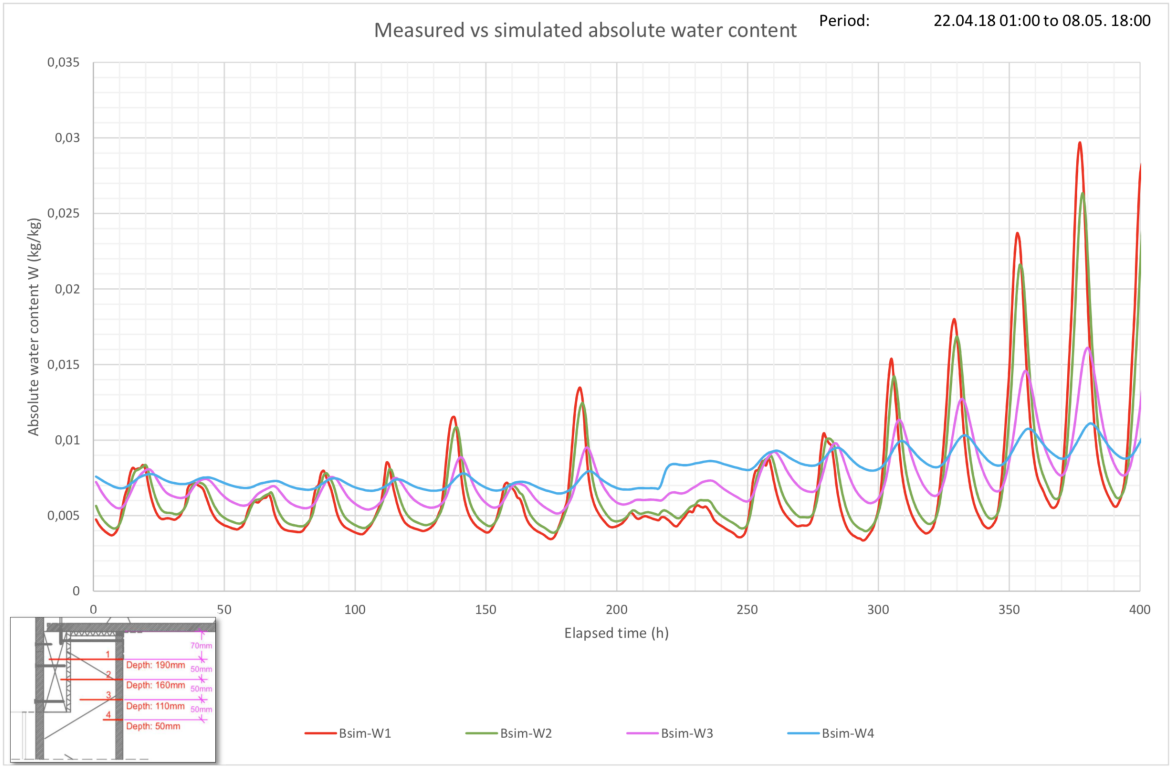

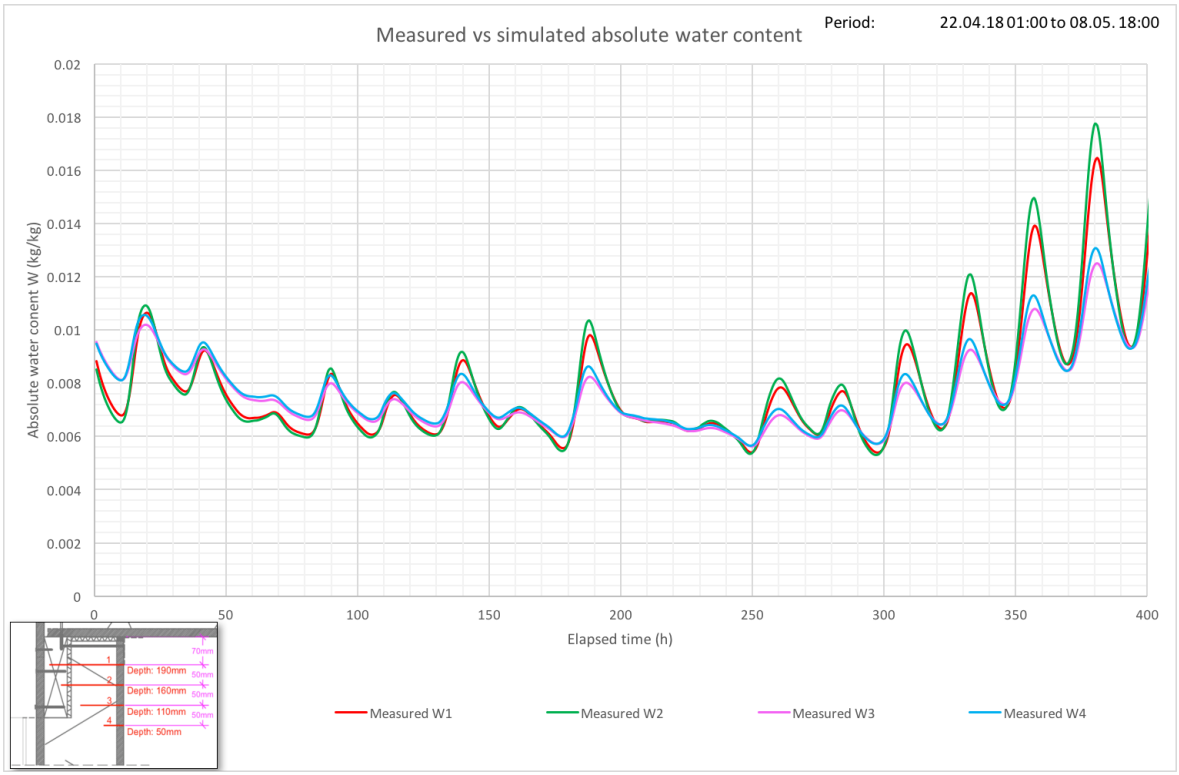

Figure H.21: Measured absolute water contents.

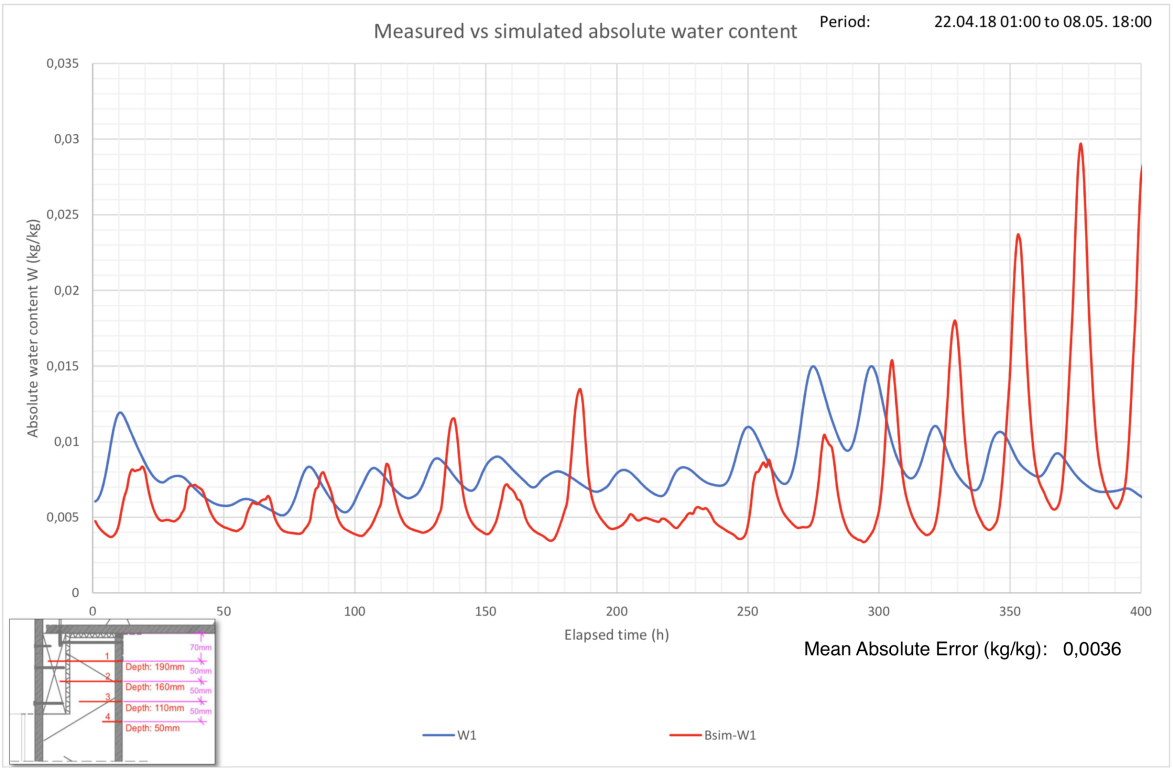

Figure H.22: Simulated vs measured absolute water content - sensor 1.

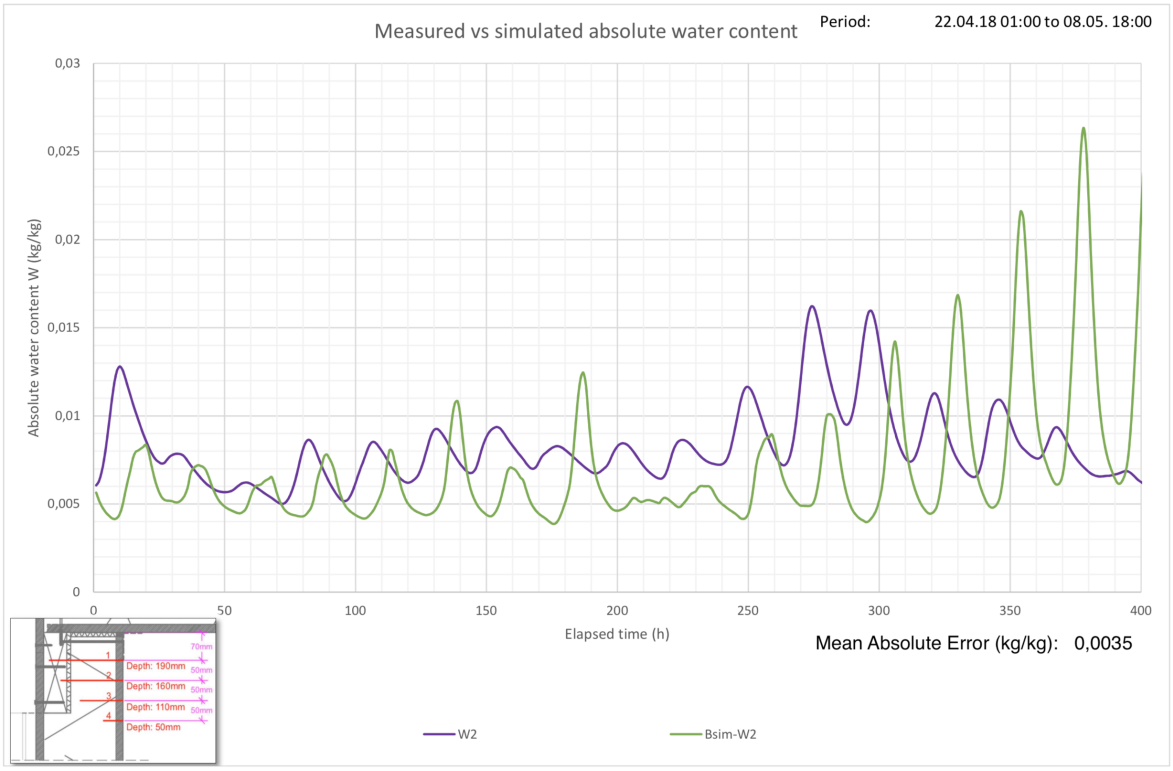

Figure H.23: Simulated vs measured absolute water content - sensor 2.

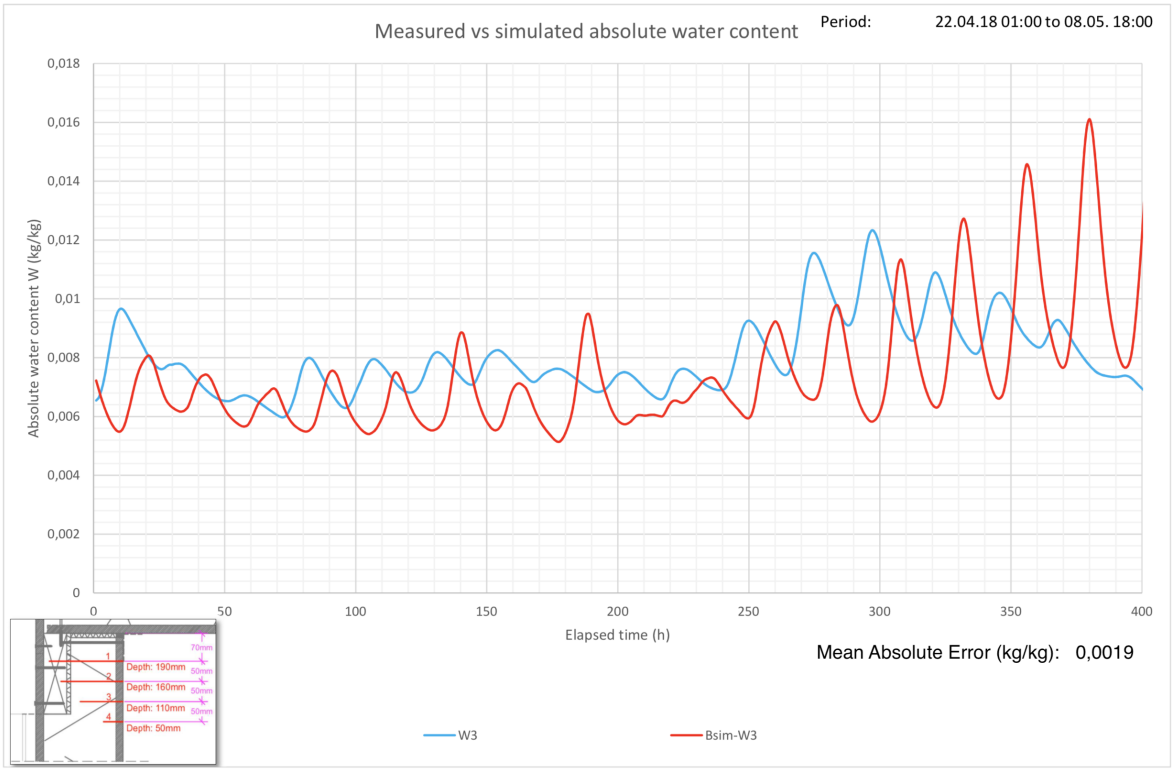

Figure H.24: Simulated vs measured absolute water content - sensor 3.

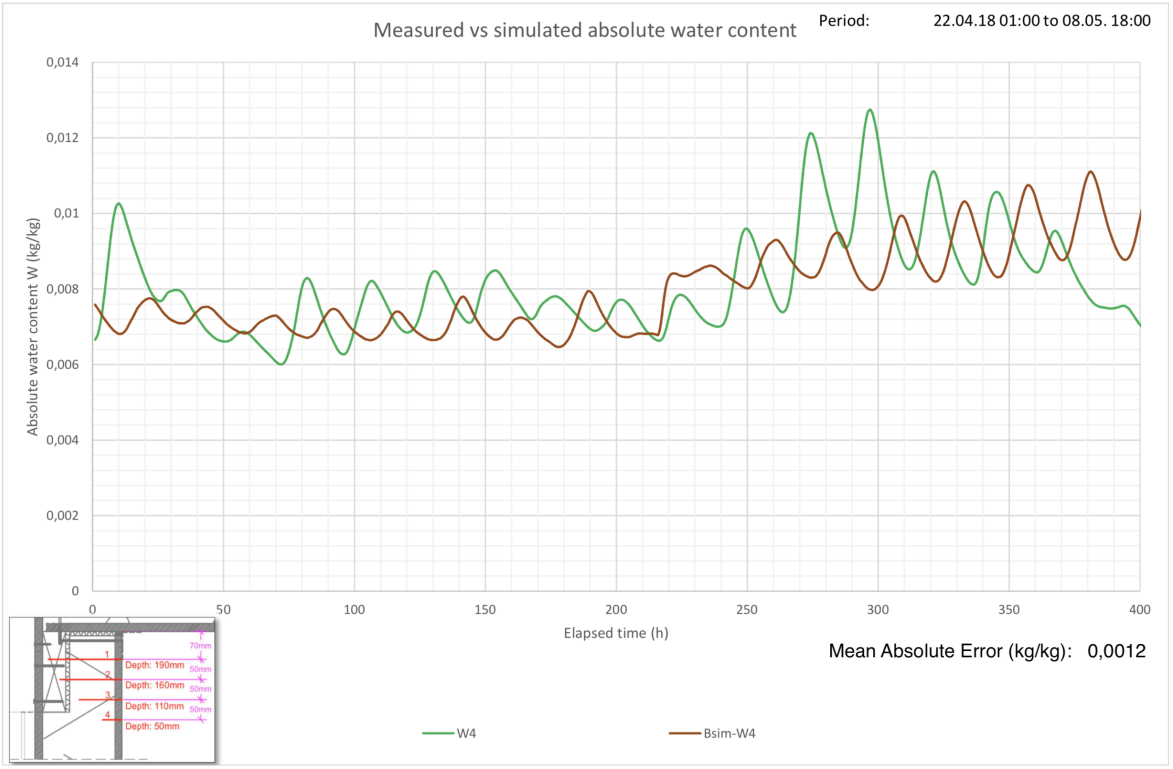

Figure H.25: Simulated vs measured absolute water content - sensor 4.